REACTIVITY OF CARBON CATHODE MATERIALS WITH ELECTROLYTE BASED ON PLANT AND LABORATORY DATA.

by

LEVY CHAUKE

Dissertation submitted in partial fulfilment of the requirements for the degree

MASTER OF SCIENCE: APPLIED SCIENCE (METALLURGY)

Department of Materials Science and Metallurgical Engineering, Faculty of Engineering, Built Environment and Information Technology, University of Pretoria, South Africa

2012

TITLE: REACTION OF CARBON CATHODE MATERIALS WITH ELECTROLYTE BASED ON PLANT AND LABORATORY DATA

REACTIVITY OF CARBON CATHODE MATERIALS WITH ELECTROLYTE BASED ON PLANT AND LABORATOTY DATA

STUDENT: LEVY CHAUKE

NUMBER: 26439965

DEGREE: MASTER OF SCIENCE (METALLURGY)

DEPARTMENT: DEPARTMENT OF MATERIALS SCIENCE AND METALLURGICAL ENGINEERING, FACULTY OF ENGINEERING, BUILT ENVIRONMENT AND INFORMATION TECHNOLOGY

UNIVERSITY: UNIVERSITY OF PRETORIA

SUPERVISOR: PROF ANDRIE M. GARBERS-CRAIG

STUDY YEAR: 2006-2012

Abstract

During the aluminium electrolysis process, pot linings determine the life span of the cell. As a result there has been considerable and ongoing research internationally on the penetrating chemical species and phases that form in the carbon cathode lining of the cell. The objective of the study is to identify phases that penetrate, react and cause expansion of carbon cathode during the electrolytic production of aluminium.

The study relied upon post-mortem carbon cathode samples from South African aluminium smelting plant and the development of a laboratory scale aluminium smelting cell. Samples were analysed using qualitative and quantitative x-ray powder diffraction and scanning electron microscopy, with energy dispersive spectroscopy. A sodium expansion test was done according to a test developed at the Council of Scientific and Industrial Research (CSIR), South Africa, based on the Samoilenko Rapoport method.

The following phases were identified in the post mortem carbon cathodes: Cryolite (Na_3AlF_6), Villiaumite (NaF), Fluorite (CaF_2), Alumina (Al_2O_3), Chiolite ($Na_5Al_3F_{14}$), Al-Nitride (AlN), Sodium-Cyanide (NaCN) and beta Diaoyudaoite ($NaAl_{11}O_{17}$). Cryolite (Na_3AlF_6), Villiaumite (NaF), Fluorite (CaF_2) and beta Diaoyudaoite ($NaAl_{11}O_{17}$) could be distinguished in the 30% and 100% graphitised carbon cathode samples after the laboratory scale electrolysis process. Chiolite ($Na_5Al_3F_{14}$) could only be distinguished in the 100% graphitised carbon cathode sample after the laboratory scale electrolysis test.

Wear due to reaction between sodium, the cathode, cryolite and nitrogen could not be confirmed in the laboratory scale samples, but could be inferred in the post mortem samples, according to the following reactions:

$3/2N_2(g) + 3C(s) + 3Na(\text{in } C) = 3NaCN(l)$

$1/2N_2(g) + Na_3AlF_6(l) + 3Na(\text{in } C) = AlN(s) + 6NaF(l)$

Sodium in the cathode was presumably present in the pores of the cathode, as the presence of intercalated sodium could not be confirmed by XRD analysis on the laboratory scale samples.

The electrolyte penetration depends on the degree of graphitisation (heat treatment temperature) of the carbon cathode. Carbon cathode that are heat treated at higher temperature (3000°C) has more graphitised and low porous structure as compared to the carbon cathode heat treated al low temperature (1200°). Therefore the 30% graphitised carbon cathode is more vulnerable to electrolyte penetration than the 100% graphitised carbon cathode.

The laboratory scale sodium expansion test confirmed that the degree of expansion of the carbon cathode decreases as the degree of graphitisation (30% graphitised > 100% graphitised) of the carbon cathode increases.

ACKNOWLEDGEMENTS

I would like to thank the following people and institution:

- Professor Andrie M. Garbers-Craig for her words of encouragement, mentorship and guidance.
- Professor J. Markgraaf for his guidance
- Council of Scientific and Industrial Research for the funding

I would also like to express my appreciation and gratitude to my family, friends, colleagues and Dawie van Vuuren for the support they offered during the course of this project, Dr Sabine Verryn and Wiebke Grote for doing the XRD analyses and Kalenda Mutombo, Sigqibo Camagu for the assistance in performing the SEM-EDS analyses. Dr S. Govender and Dr H. Moller for the discussion on the project.

Table of Contents

List of Figures

List of Tables

Abbreviations

Al - Aluminium

Al_2O_3 - Alumina

AlF_3 – Aluminium tri fluoride

AlN – Aluminium nitride

C – Carbon

CaF_2 – Calcium fluoride

EDS – Energy dispersive spectrometry

EMF - Electromotive force

F -Fluorine

N_2–Nitrogen gas

Na– Sodium

Na_3AlF_6 – Cryolite

NaCN – Sodium Cyanide

NaF –Sodium fluoride

O_2 -Oxygen gas

SEM –Scanning electron microscopy

XRD–X-ray diffraction

List of Symbols

γ	Henry's activity coefficient
T	Temperature (K)
R	Ideal Gas Constant (Pa m^3 K^{-1} mol^{-1})
λ	Wavelength (m)
d	Interplanar distance (Å)
θ	Angle of detection (degrees)

Chapter 1: Background to research

1.1. Introduction

Aluminium cannot be produced by the electrolysis of an aluminium salt dissolved in water because of the high reactivity of aluminium [1]. In 1886 an American chemist Charles Martin Hall and the Frenchman Paul Heroult independently discovered the process of producing aluminium electrolytically. They then called the process the Hall-Heroult process [2] [3]. An attempt to replace the process has not been successful [1][2]. The overall reaction of the Hall-Heroult process is given in equation 1.1 and a schematic drawing of a commercial cell is given in Figure 1[2] [3][4].

$$2Al_2O_3\ (dissolved) + 3C\ (s) = 4Al\ (l) + 3CO_2 \quad \ldots\ldots 1.1$$

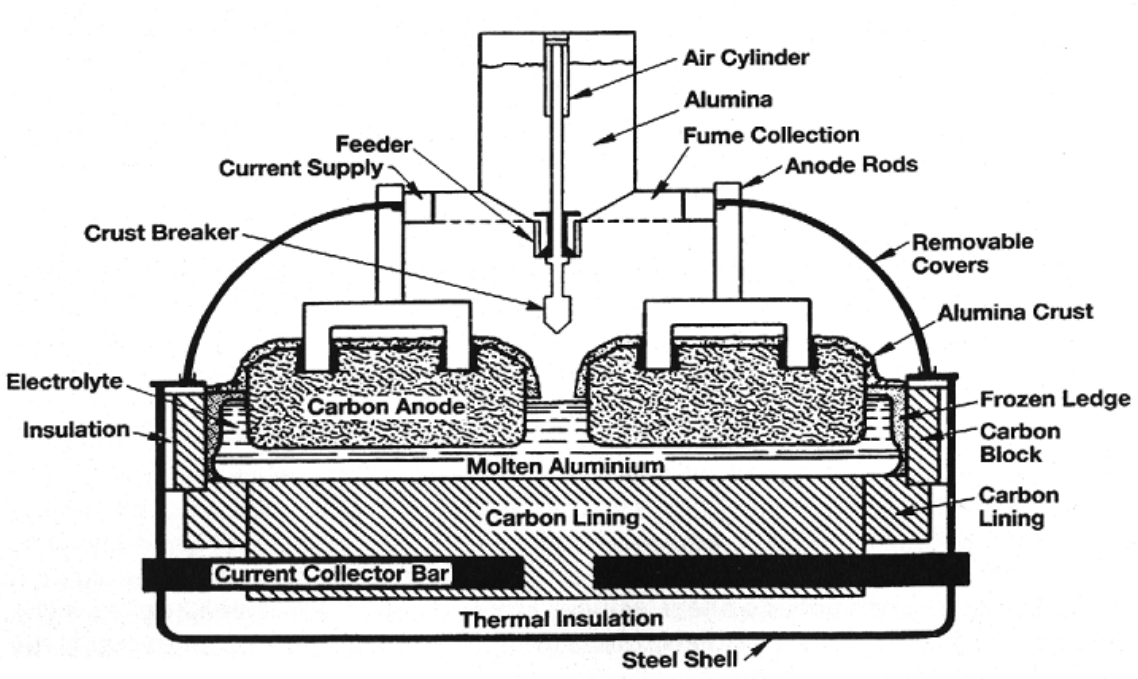

***Figure 1**: Schematic cross section drawing of an industrial Hall-Heroult cell with prebaked anodes [4].*

In the Hall-Heroult process, alumina (Al_2O_3) is dissolved in a carbon lined cell with a bath of molten cryolite (Na_3AlF_6) at a temperature of 960°C [1]. The electrolyte may have certain additives (mainly AlF_3 to lower the cryolite melting point from 1012°C to 960°C) [3].

The container of the cell is considered the cathode, but from an electrochemical point of view "cathode" is the interface between the aluminium metal and the electrolyte [2]. The carbon cathode conducts current to the cell and it has to withstand the corrosive environment, stress attributed to temperature fluctuations and chemical reactions [2]. The carbon cathode is often referred to as the most important part of the aluminium electrolysis cell, because it is mostly that component that provides the cell its life expectancy [2] [3].

1.2. Aim of the project

The cost related to delining and relining an electrolysis cell is substantial, therefore smelters would want to achieve the longest cell life possible. The material that fails first determines the life span of the cell.

The project investigated:

- Phases that form during the electrolysis process. The phases were qualitatively analysed using X-ray diffraction (XRD) method and quantified using Rietveld method.
- The expansion of different carbon grades when they were exposed to a sodium rich environment on a laboratory scale.
- Plant and laboratory scale carbon cathode samples with respect to wear mechanisms, and evaluated the usefulness of laboratory scale tests to forecast wear of carbon cathodes on a plant scale.

The primary aim of this study was to identify equilibrium phases that penetrate, react and cause expansion of carbon cathode materials during the electrolytic production of aluminium. The secondary aim is to evaluate the expansivity of the carbon cathode material when exposed to a sodium rich environment.

1.3. Hypothesis

During the aluminium electrolysis process, the bath (cryolite) constituents penetrate the carbon cathode lining.

- Penetration of electrolytes causes the carbon cathode lining to expand.
- Penetration of the electrolytes leads to the formation of unwanted phases and compounds within the carbon cathode lining, which causes additional wear.
- Laboratory scale tests are useful to potentially forecast wear of carbon cathodes on a plant scale.

Chapter 2: Literature Review

2.1. Introduction

2.1.1. Alumina production

Aluminium is the most abundant structural material in the earth's crust after oxygen and silicon. The mineable layer of earth's crust is composed of 8% aluminium [6]. Due to the high affinity of aluminium for oxygen, aluminium does not occur as a pure element in nature. Aluminium in the earth's crust is in the form of aluminium hydroxide [6], with bauxite as the most important ore for the production of aluminium [6].

The Bayer process was developed by Karl Josef Bayer hence it is called the Bayer process [6]. The Bayer process is used to produce alumina from its ore (Bauxite) in a continuous process. The digestion of the bauxite is attained by bringing about solubilisation of the alumina under pressure at a temperature of at least 140°C [6][7]. The bauxite is dissolved in a solution of sodium hydroxide (caustic soda) as illustrated by equations 2.1 and 2.2:

$$Al(OH)_3 + Na^+ + OH^- = Al(OH)_4^- + Na^+ \quad \ldots\ldots\ldots\ldots\ldots\ldots\ldots\ldots\ldots\ldots 2.1$$

$$AlOOH + OH^- + Na+ + H_2O = Al(OH)_4^- + Na^+ \quad \ldots\ldots\ldots\ldots\ldots\ldots\ldots\ldots 2.2$$

The Bayer process flow sheet is shown in Figure 2.1 [6]. The format of the diagram emphasizes the continuous flow of the Bayer process solution through the plant.

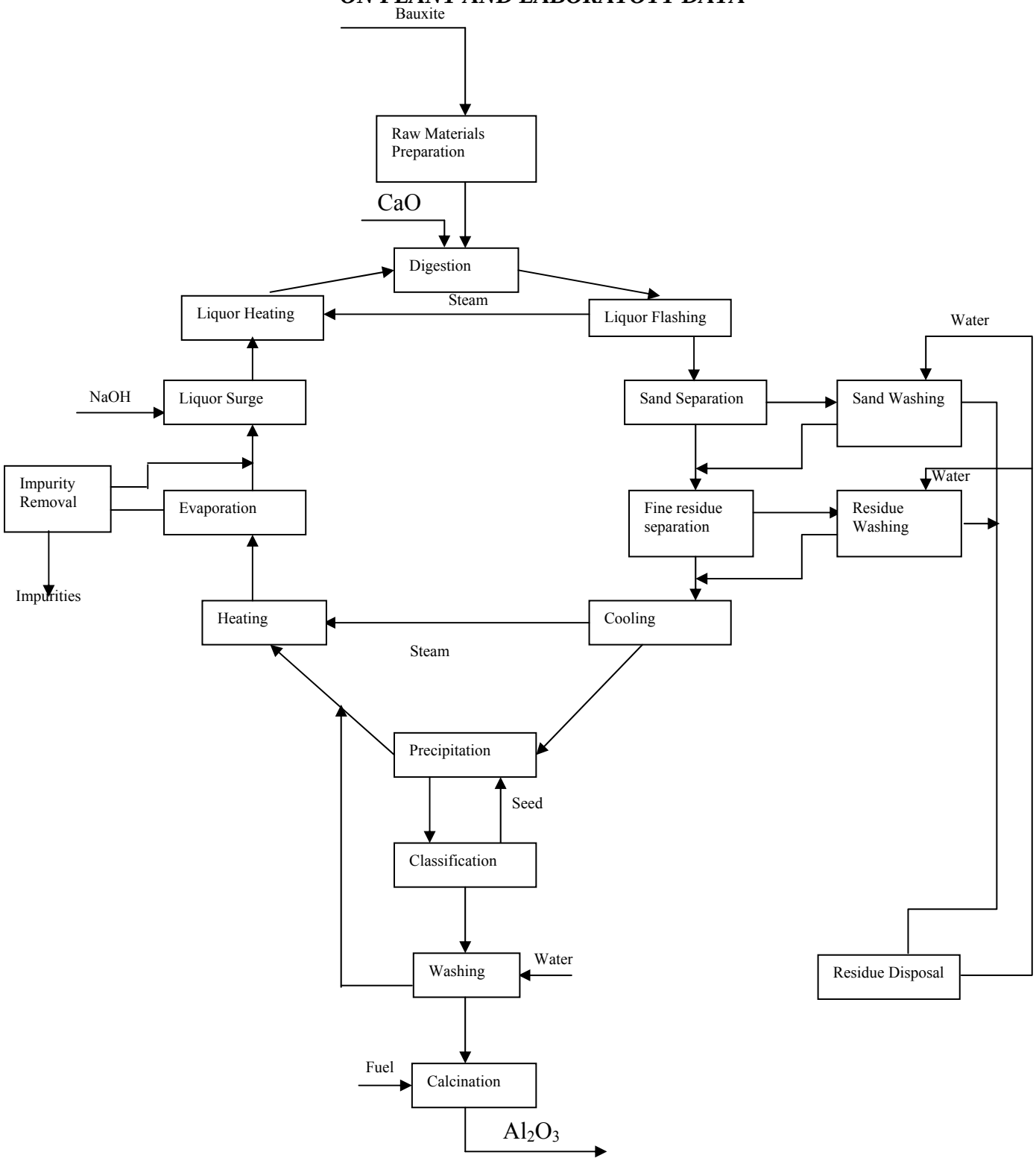

***Figure 2.1**: Bayer Process flow sheet [6].*

2.2. Aluminium Production

2.2.1. Aluminium electrolysis

The electrolytic production of aluminium is done in a steel pot (cell), lined with refractory, thermal insulators and carbon [4]. The overall reaction of aluminium electrolysis is given in equation 2.3 [8].

Al_2O_3 *(dissolved in* Na_3AlF_6, AlF_3, *and* CaF_2*)* + 3/2 C *(anode)* $\longrightarrow$ 2Al *(l)* + 3/2 CO_2 *(g)*..2.3

The bottom of the cell is lined with pre-baked carbon blocks. Carbon anodes are produced from carbon based materials such as coke and pitch binder [4]. The current electrolysis process uses pre-baked carbon blocks as the lining materials.

2.2.2. Electrolysis Cell

Normal operating cells consist of a rectangular steel shell lined with several layers of refractory materials. The cell is constructed in the following sequence: it has a steel shell followed by a castable refractory, then low-porosity semi insulating refractory and finally firebricks [9]. A significant amount of heat is lost through the sides of the cell wall, as the sides of the cell wall are less insulated [9]. Due to low temperatures associated with the side walls, the electrolyte that is in contact with the side walls solidifies to form the so called "frozen ledge". The "frozen ledge" protects the cell walls from the extremely corrosive molten cryolite [9].

This study will only focus on the carbon cathode of the electrolysis cell.

2.3. Carbon cathode lining (Cell lining)

The carbon cathode determines the life span of the cell and is at the base of the electrolysis cell. The use of the carbon cathode lining serves two purposes: it contains the molten metal and electrolyte and secondly it conducts electricity so that there can be a uniform current distribution along the bottom surface of the container [10]. The lining of the electrolysis cell has to be based on the following requirements, thus the choice of carbon-based materials.

- Chemical inertness and minimum permeability towards the chemical environment;
- Dimensional stability;
- Appropriate design to provide a vertically directed electric field towards the anode;
- Material properties and design features which will provide maximum service life at lowest cost [11].

2.3.1. Classification of carbon cathode blocks

Carbon cathode blocks are built based on the layered graphite structure (Figure 2.2). The graphene layers align themselves in the vertical direction. The coke is mixed with pitch and extruded or vibrated into a rectangular body, which is heat treated to a temperature between 1000°C to 3000°C [2].

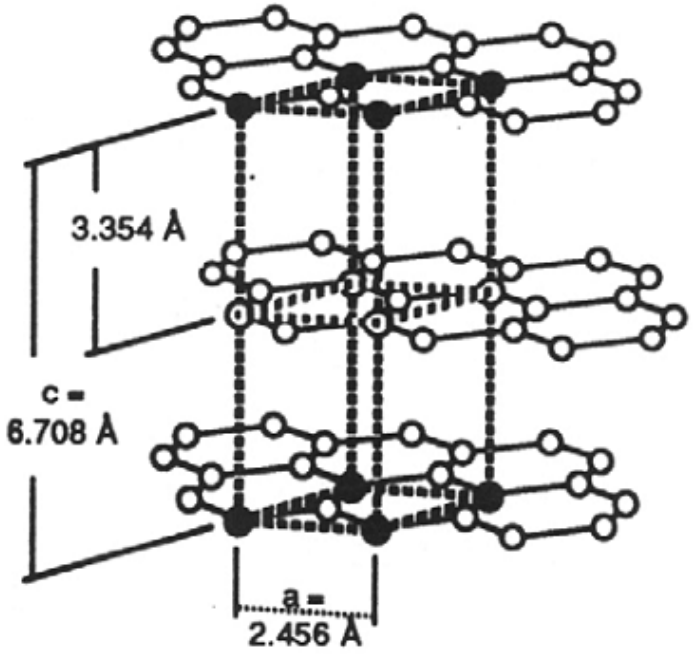

***Figure 2.2**: Unit cell of graphite [2]*

The carbon-carbon bonds in the a-direction are strong covalent bonds, while the bonds between layers (c-direction) are weak van der Waals bonds [2].

Four classes of carbon blocks are summarised depending on the heat treatment temperature of the block [2][12].

Graphitised cathode block: The whole block (aggregate and binder) consisting of graphitisable materials has been heat treated at 3000ºC, giving a graphitic material;

Semi-graphitised cathode block: The whole block (filler and binder) consisting of graphitisable materials, has been heat treated to about 2300ºC;

Semi-graphitic cathode block: The block has only been heat treated to normal baking temperatures (≈ 1200º C) but it has graphitised aggregates;

Amorphous cathode blocks: None or only part of the filler material is graphitised. The block is baked to ≈ 1200ºC [12].

During the forming process the particles tend to align parallel to the extrusion direction or perpendicular to the vibrating direction. As the heat treatment temperature of the material increases, the carbon structure becomes graphitic (crystalline) as shown in Figure 2.3. [2][12].

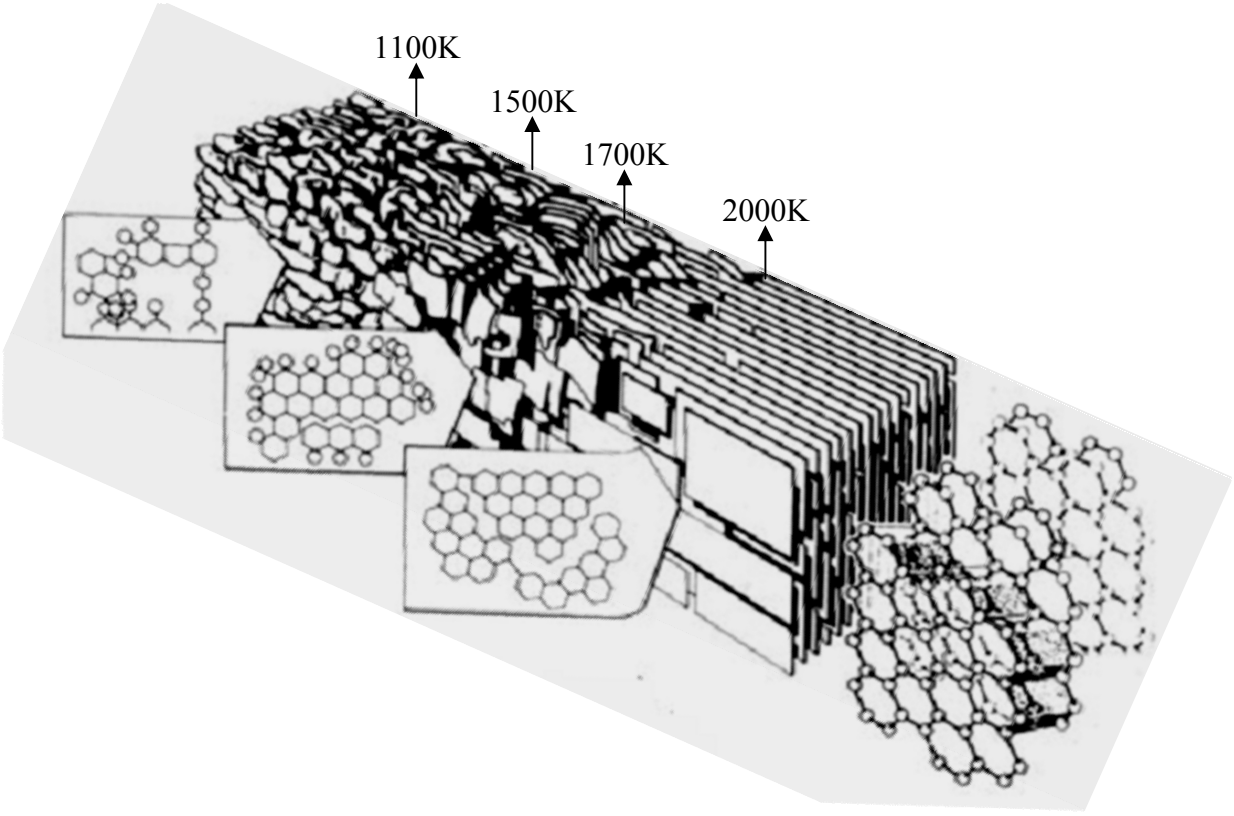

***Figure 2.3**: The carbon structure at different heat treatment temperature [2].*

The carbon cathode production process is designed so that it produces carbon blocks with properties listed in Table 2.1.

Table 2.1. *Selected properties of cathode blocks* [10].

Property	**Units**	**Type of block**			
		Amorphous	**Semi-graphitic**	**Semi-graphitised**	**Graphitised**
Real Density	g. cm^{-3}	1.85-1.95	2.05-2.15	2.05-2.18	2.2
Apparent Density	g. cm^{-3}	1.50-1.55	1.60-1.70	1.55-1.65	1.6-1.8
Total porosity	%	18-25	20-25	15-30	25
Open Porosity	%	15-18	15-20	Not available	Not available
Electrical Resistivity	μΩm	30-50	15-30	12-18	8-14
Thermal Conductivity	W/k.m	8-15	30-45	32	80-120
Crushing strength	MPa	25-30	25-30	Not available	15
Bending Strength	MPa	6-10	10-15	6-10	10-15
Rapoport Sodium expansion	%	0.6-1.5	0.3-0.5	0.3-0.5	0.05-0.15
Ash Content	Mass %	3-10	0.5-1.0	<1.5	<0.5

It is very important to have a carbon cathode that can withstand all the environmental challenges of the electrolysis process. In order to do a proper carbon cathode selection, the following properties are evaluated [13].

- Density
- Porosity
- Electrical resistivity
- Compressive strength
- Sodium expansion

Table 2.2 indicates the comparative view of three cathode blocks [13].

Table 2.2: *Comparative view of the three cathode block types* [13]

	Type of Cathode		
Comparative Properties	**Armophous**	**Semi-Graphitic**	**Graphitised**
Price	Low	moderate	High
Abrasion Resistance	Excellent	Good	Poor
Thermal shock Resistance	Acceptable	Very good	Excellent
Thermal Conductivity	Moderate	High	Very high
Electrical resistance • Room Temperature	High	Low	Very low
Crushing Strength	High	Adequate	Low
Swelling/Sodium	Adequate	Low	Very low

2.3.2. Carbon cathode deterioration

No carbon lining materials used in aluminium reduction cells are resistant to or fully inert to the corrosive molten salts under operational conditions [14]. Apart from the deterioration caused by temperature and external pressures, the expansion caused by the penetrating sodium/electrolyte is considered the driving force and the most significant cause of carbon cathode failure [15]. Mechanisms explaining observed wear in different parts of the carbon lining are summarised in Table 2.3 [14].

***Table 2.3**: Adverse effects on cathode linings [14].*

Main Mechanism	**Major Effect**	**Exemplified**	**Origin of species**	**Major area of attack**
Intercalation	Expansion of the carbon lining 0.1 to 8% linearly - Differential expansion by concentration gradients - Tension/ stresses in the carbon matrix	Alkali, alkaline earth or other strong electron donors entering basal plane positions	Co-deposition of species from the electrolyte. Secondary reactions in the lining	Cathode blocks
Chemical reactions A) – Primary reactions	Consumption of the lining materials	$C_{(s)} + O_{2\,(g)} \rightarrow CO_{2\,(g)} / CO_{\,(g)}$ $C_{(s)} + CO_2 \rightarrow 2CO_{\,(g)}$ $4Al_{\,(l)} + 3C \rightarrow Al_4C_{3\,(s)}$	Atmosphere Anodes gases, decomposed carbonates, air. Aluminium produced	Top and back side wall lining Al/C interface, particularly at the metal/electrolyte interface where dissolution/further reaction to Al_4C_3 takes place

***Table 2.3**: Adverse effects on cathode linings (continued)*

Main Mechanism	Major Effect	Exemplified	Origin of species	Major area of attack
B) – Secondary reactions	Molar volume expansion Tensions/Stress by differential thermal expansion between lining material and solid products formed	$FeS\,(s) + 2Na\,(l,g) \rightarrow Na_2S(s) + Fe(s)$	Block impurities/Electrolyte	Cathode lining
		$4Na_3AlF_6\,(l) + 12\,Na(l,g) + 3C(s) \rightarrow Al_4C_3\,(s) + 24NaF(s)$	Electrolyte/Atmosphere/Carbon lining	
		$4Na_3AlF_6\,(l) + 12\,Na(l,g) + 3O_2(g) \rightarrow 2Al_2O_3\,(s) + 24NaF(s)$	Electrolyte/Atmosphere	All parts of lining
		$2Na(l,g) + 2C(s) + N_2(g) \rightarrow 2NaCN(s)$	Electrolyte/Atmosphere	All parts of lining
		$2Na_3AlF_6\,(l) + 8Na(l,g) + 2O_2(g) \rightarrow 12NaF(s) + Na_2O.Al_2O_3(s)$	Electrolyte/Atmosphere,	Below the cathode carbon
		$8Na(l,g) + 2O_2 + 3Al_2O_3.2SiO(s) \rightarrow 3(Na_2O.Al_2O_3)(s) + Na_2O.2SiO_2(s)$	Refractory insulation	Below the cathode carbon

Sodium generation in the carbon cathode

Sodium in aluminium will be in equilibrium with species such as NaF and AlF_3 in the melt according to equation 2.3. It can react further in the carbon according to equation 2.4. [2].

Al (l) + 3NaF (in cryolite) = 3Na (in Al) + AlF_3 (in cryolite)……2.3.

Na (in Al) = Na (in C)……2.4.

Equation 2.5 indicates that some sodium could also be electrochemically reduced in carbon

$Na^+ + 1e^- = Na$ (in C) ……2.5

The electrochemical transport number for Na^+ in cryolite-alumina melts is close to one.

2.3.3. Main mechanisms for sodium penetration into the carbon cathode lining

The carbon cathode undergoes vast changes in its mechanical properties, due to sodium and bath penetration during the start-up stage and in regular operation [16][17]. The sodium penetration and diffusion methods in the carbon lining are still not fully understood. Three basic penetration mechanisms have been reported [17] [18]:

i. Following a typical interface mass transfer process, sodium may penetrate inside carbon under a chemical potential gradient[17];
ii. the direct reduction of sodium ions at the cathode interface and its "direct insertion" in carbon as shown in equation 2.5;
iii. The absorption of sodium from the vapour phase based on radioactive sodium experiment results [15] [17].

2.3.4. Reactions and compounds forming during the aluminium electrolysis process

To provide a fundamental thermodynamic understanding of what is going on within the cathode block during the electrolysis, a SOLGAS/Chemsage calculation program was carried out by Grjotheim and Kvande (Table 2.4) [10].

Table 2.4: *Chemical reactions and ΔG° at 1200K for the process described in the melt penetration model* [10]

Reaction	Chemical reactions	ΔG° KJ
1	$6NaF\ (l) + Al\ (l) = 3Na\ (in\ C) + Na_3AlF_6\ (l)$	+41.7
2	$0.5O_2\ (g) + C\ (s) = CO\ (g)$	-217.8
3	$1.5N_2\ (g) + 3C(s) + 3Na(in\ C) = 3NaCN\ (l)$	-165.8
4	$1.5\ Na_3AlF_6\ (l) + 1.53NaCN\ (l) + 3Na\ (in\ C) = 1.5AlN\ (s) + 9NaF\ (l) + 1.5\ (s)$	-262.2
5	$0.5N_2\ (g) + Na_3AlF_6\ (l) + 3Na\ (in\ C) = AlN\ (s) + 6NaF\ (l)$	-230.1
6	$1.5CO\ (g) + 0.75\ Na_3AlF_6\ (l) + 3Na\ (in\ C) = 0.75NaAlO_2\ (s) + 4.5NaF\ (l) + 1.5C\ (s)$	-355.3
7	$Na_3AlF_6\ (l) + 3Na\ (in\ C) + 0.75\ C\ (s) = 0.25\ Al_4C_3 + 6NaF\ (l)$	-79.4
8	$4.5\ CO\ (g) + 3Na\ (in\ C) = 1.5Na_2CO_3\ (l) + 3C\ (s)$	-225.8
9	$2.25Al_2O_3 + 0.75Na_2CO_3\ (l) + 3Na\ (in\ C) = 4.5\ NaAlO_2\ (s) + 0.75C\ (s)$	-387.2
10	$4.5AlN\ (s) + 3Na_2CO_3\ (l) + 3Na\ (in\ C) + 1.5C\ (s) = 4.5\ NaAlO_2(s) + 4.5NaCN\ (l)$	-893.4
11	$1.5NaCN\ (l) + 3Al_2O_3\ (s) + 3Na\ (in\ C) = 4.5\ NaAlO_2\ (s) + 1.5\ AlN + 1.5C\ (s)$	-218.5
12	$2Al_2O_3\ (s) + 0.75\ C\ (s) + 3Na\ (in\ C) = 3NaAlO_2\ (s) + 0.25\ Al_4C_3\ (s)$	-50.2
13	$4.5NaCN\ (l) + 3Al_2O_3\ (s) = 4.5\ NaAlO_2\ (s) + 1.5\ AlN\ (s) + 4.5\ C\ (s) + 1.5N_2\ (g)$	-52.7
14	$Na_2CO_3\ (l) + Al_2O_3\ (s) = 2NaAlO_2\ (s) + CO_2\ (g)$	-32.2
15	$Na_2CO_3\ (l) + C\ (s) + 0.5\ Na_3AlF_6\ (l) = 2CO\ (g) + 0.5NaAlO_2\ (s) + 3NaF\ (l)$	-86.3

Reaction 2 in Table 2.4 shows that oxygen is not stable in the presence of C, but reacts to form CO. Reaction 3 shows that if only Na, C and N_2 are present NaCN will be formed. In the presence of Na_3AlF_6, NaCN becomes unstable and reacts to form AlN(reaction 4). Na_3AlF_6 will react with N_2 to form AlN and with CO to form $NaAlO_2$ (Reactions 5 and 6). Al_4C_3 is not stable in the presence of N_2 or CO, and Al_4C_3 will only be formed from Na_3AlF_6 in argon atmosphere (reaction 7) [10].

Na_2CO_3 forms from CO and Na (in C) (reaction 8) but is not found in the bottom blocks, except sometimes near the lower part of the ends where the temperature in some cathode designs are too low for fluoride infiltration. Na_2CO_3 is unstable in the presence of Al_2O_3 (reaction 9 and 14), AlN(reaction 10) and Na_3AlF_6 (reaction 15). Na_2CO_3 will only be stable when all alumina has been converted to $NaAlO_2$. In an Al-F-O system α-Al_2O_3 is the stable oxide phase for cryolite ratio (CR) < 3.0 while $Na_2O.11Al_2O_3$ is stable for CR>3.0 and $NaAlO_2$ is stable in the presence of NaF [10].

2.3.5. Pore size distribution effect on bath penetration into the carbon cathode

The porous material structure of the carbon/graphite cathode is developing during the forming and baking stages. This material structure can naturally affect the degree of penetration of the bath (cryolite) species during the electrolysis process [19]. Internal porosity, pore size distribution, pore shape and orientation plays an important role in the penetration of bath species into the carbon cathode [19].

Total porosity, partial porosity with D_{mean} <600 µm, number of pores, pore size distribution, average pore diameter and total porosity of industrial carbon cathodes were characterised by Yuanling et al using image analysis [19]. The statistical results obtained by Yuanling et al, using image analysis, are given in Table 2.5 [19].

Table 2.5: *Statistical results of image analysis on the pores in cathode samples [19]*

Property	**Units**	**Type of block**		
		HC35	**HC100**	**SMH**
Total Porosity	%	21.05	15.35	25.48
Partial porosity with D_{mean} below 600µm	%	7.31	13.08	15.27
Number of pores		230	488	438
Average pore diameter	µm	186.61	135.97	182.31
Specific surface area of pore	$\mu m^2/ \mu m^3$	0.017	0.029	0.023

HC35 = Semi graphitic, HC100 = full graphitic and SMH = graphitised carbon

The fractional difference of pores in terms of pore size distribution is shown in Figure 2.4. Major fraction of pores in the region between 300µm and 900µm are mesopores in the HC35 and SMH cathode. Below 300µm the large part of the fraction is the micropores in the HC100 cathode [19]. In the HC100 cathode the largest proportion of pores are micropores with D_{mean} values smaller that 300µm.

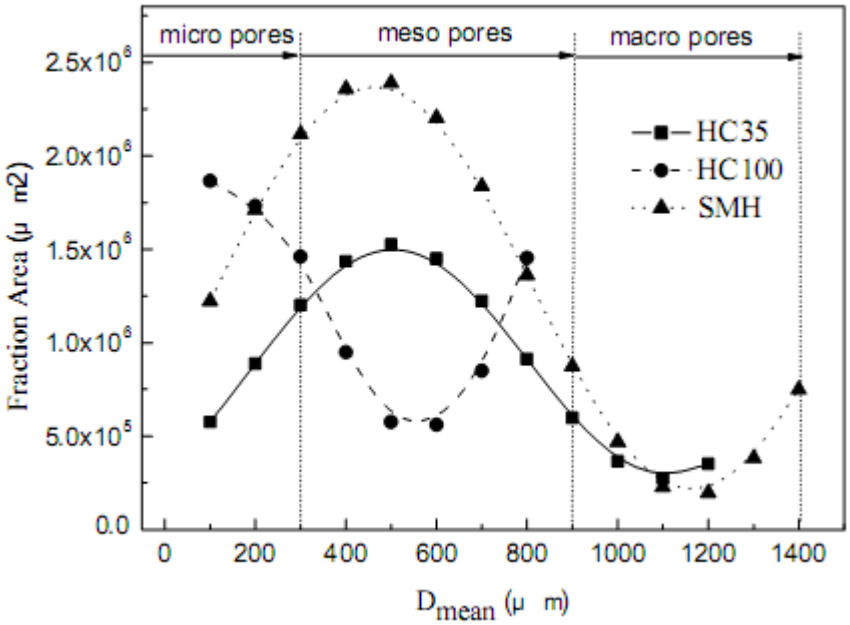

Figure 2.4: *Pore size distribution in carbon cathode at mean diameter* [19].

Penetration of bath constituents/element into the carbon cathode is therefore highly dependent on the degree of graphitisation of the cathode. During the electrolysis process the micropores provide penetration paths and capillary forces for the bath to penetrate the carbon cathode [19].

2.3.6. Reported phases that formed during the aluminium electrolysis process

Brilloit [20] identified and quantified phases that formed in spent carbon cathodes, using XRD. They reported the presence of $Na_5Al_3F_{14}$, Na_3AlF_6, NaF, CaF_2, $Na_2O.11Al_2O_3$, $NaAlO_2$, α-Al_2O_3, NaCN, AlN, Na_2CO_3, graphite and the possible presence of $NaCaAlF_6$ [18][20].

Dissolution of Na into Al and Na_3AlF_6

Extensive research has been done to determine the solubility of Na in liquid Al. The amount of Na that dissolves in Al depends on the thermodynamics and kinetics of the electrolysis process [16][21].

Scheuer [22] studied the Na solubility in liquid Al by heating Al with surplus Na under hydrogen until equilibrium was reached, after which the melt was quenched and the Na quantity was determined from the Al-rich layer [22]. The solubility results at different temperatures are given in Table 2.6 [22].

Table 2.6: *Solubility of Na in Al data as found by Scheuer in 1935* [22].

Temperature (K)	Solubility (at. % Na)
973	0.10
1023	0.115
1073	0.128

The results showed that the sodium solubility in liquid aluminium is temperature dependent. Increasing the temperature increases the sodium solubility.

Fink et al [23] used Scheuer's method to determine the boundary of the liquid miscibility gap. Fink's et al [23] performed their experiments under argon instead of hydrogen. They determined the monotectic temperature (temperature where on cooling the one liquid phase transforms into another liquid phase and a solid phase). Their results indicated that the monotectic temperature is at 932K with the one liquid containing 0.18 at % Na, and the solubility of Na decreased with increasing temperature. Due to decrease in solubility of Na with increasing temperature the results were doubtful, hence Ransley and Neufeld [24] investigated the amount of Na dissolved in liquid aluminium using the chemical analysis method. Ransley and Neufeld [24] found that the Na solubility increases with increasing temperature.

Ransley and Neufeld [24] studied the boundary of the miscibility gap and the solid solubility of Na in Al. The solubility of Na in liquid Al was found to be approximately 0.002 at. % in the temperature range 923-933K. Hansen and his team [25] used the electromotive force (EMF) technique and quench method to investigate the maximum solubility of Na in liquid Al. The results are indicated in Table 2.7.

Table 2.7: *Saturation composition of Na in liquid Al as obtained by Hansen* [25]

Temperature (K)	**Na in liquid Al (at. %)**
1023	1.348
1073	0.7639
1123	0.6610

Hansen's [25] results sparked controversy into the subject and this lead to further investigation by Fellner et al [26]. Fellner et al [26] further investigated the solubility of Na into Al at temperature 1023K and 1233K. The experiments were carried out by depositing Na into molten Al by the electrolysis of the molten mixture of 26.4% NaF + 73.6% NaCl. The results confirmed the work by Fink et al [23] and that of Ransley and Neufeld [24].

2.4. Solubility of metals in $NaF\text{-}AlF_3\text{-}Al_2O_3$

Thonstad [27] investigated the solubility of aluminium in $NaF\text{-}AlF_3\text{-}Al_2O_3$ melts. The analysis was done on quenched samples of the melts to determine the contents of metallic sodium and aluminium. The investigation was based on varying the molar ratio (NaF/AlF_3). It was found that the solubility of Al and Na at 1000°C decreases as the NaF/AlF_3 molar ratio is increased [27]. The change in solubility is due to Na content change as the molar ratio changes in the system. They further investigated the solubility of Na in liquid Al at constant cryolite ratio, but varying temperature. The solubility increases from 0.10 wt % Al at 1000°C to 0.14 wt % Al at 1060°C [27]. Graphic presentations of the results are given in Figures 2.5 and 2.6. Figure 2.5 is the graphic presentation of the effect of varying the NaF/AlF_3 ratio, saturated with Al_2O_3 on constant temperature [27]. The Na and Al metals have higher solubility when the NaF/AlF_3 ratio is high as shown in Figure 2.5.

Figure 2.6 shows the temperature effect on the solubility of metal in cryolite-alumina melts. It shows that the solubility increases with increasing temperature. Figure 2.5 and 2.6 show that when the bath is more basic (high cryolite ratio) at high temperature there is more metal that can penetrate the carbon cathode during electrolysis [27].

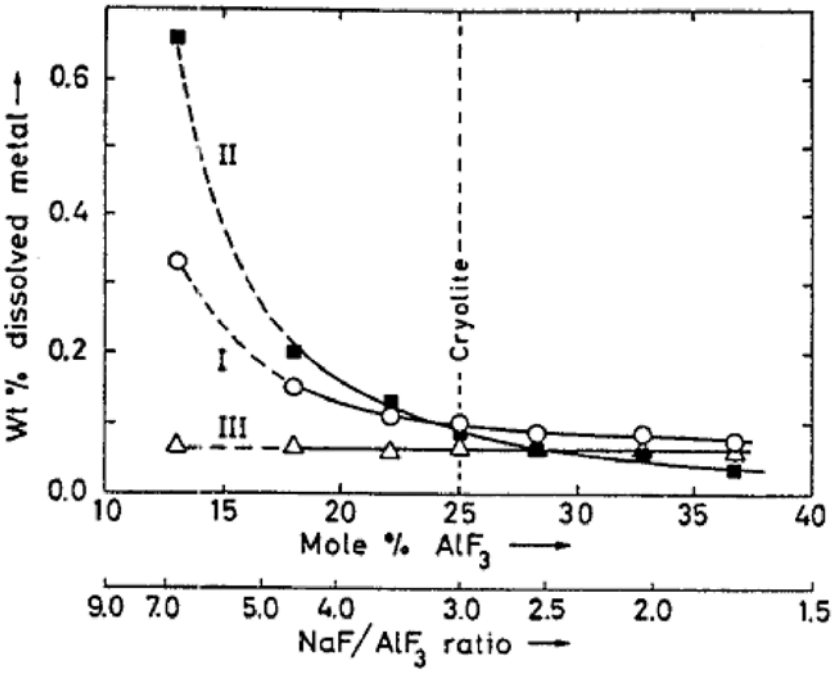

***Figure 2.5**: The solubility of metal in NaF-AlF3-Al2O3 melts at constant temperature of 1000°C. Curve I: Total solubility of sodium and aluminium as wt. % Al. Curve II: Sodium content in wt. % Na. Curve III: Aluminium content in wt. % Al [27].*

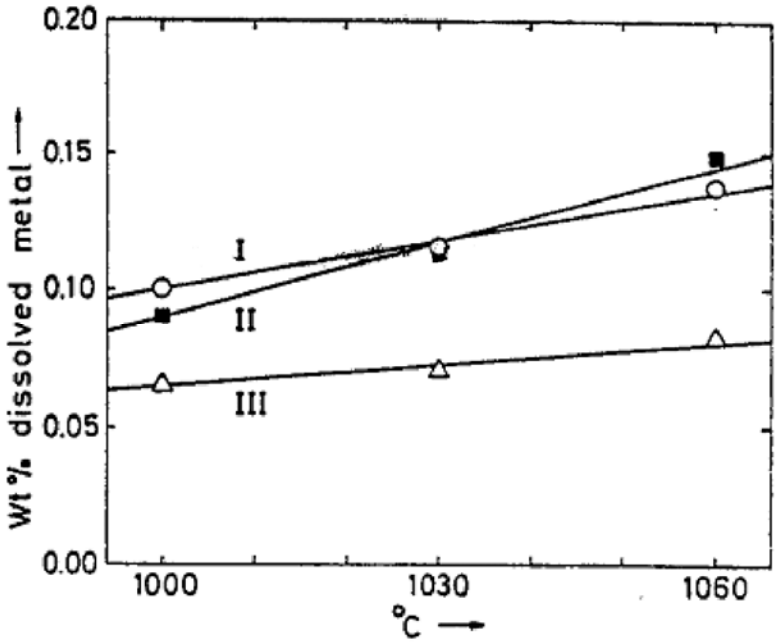

***Figure 2.6**: The solubility of metal in cryolite-alumina melts as a function of temperature [27]. Curve I is the total solubility of sodium and aluminium as wt% Al, Curve II is sodium concentration in wt% Na and Curve III is aluminium concentration in wt% Al [27].*

Sheng Jun Zhang et al [21] calculated the Al-rich section of the phase diagram and compared it to the work by Sheurer [22], Fink et al [23], Ransley and Neufeld [24], Hansen et al [25] and Fellner et al [26] and Murray [28] (Figure 2.7).

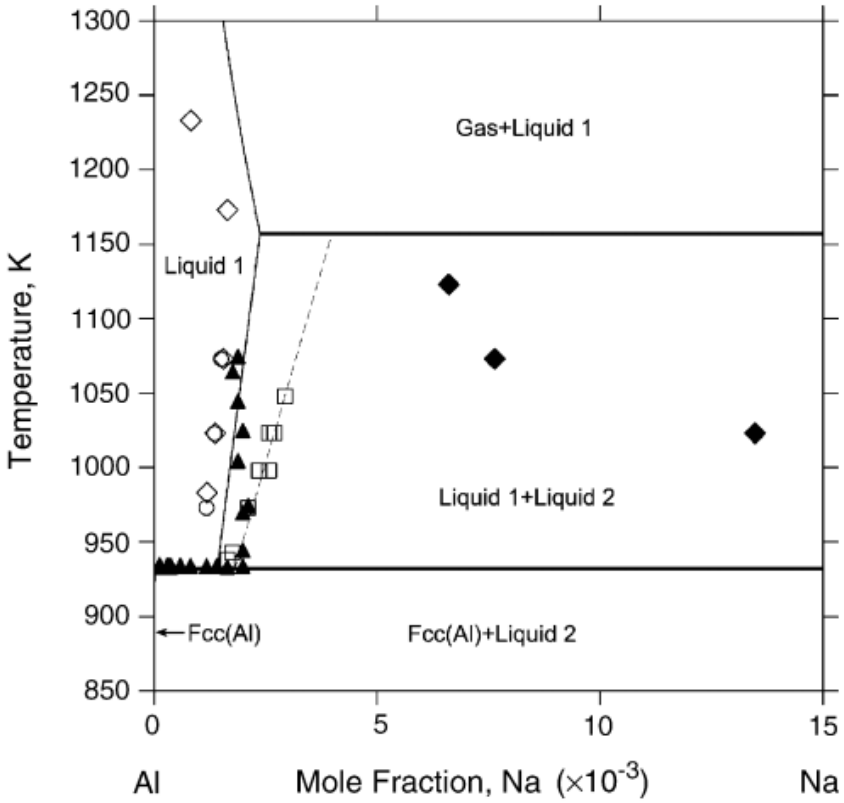

Figure 2.7: *Al rich side of calculated Al-Na phase diagram (solid lines) in comparison with data from Murray [28] (dashed lines) and Experimental data (O) by Scheuer [22]; (▲) by Fink et al [23]; (◊) by Ransley and Neufeld [24]; (□) by Hansen et al [25]; (♦) Fellner et al [26]*

The calculated phase diagram agrees with all the experimental data. However the work by Murray [28] does not agree with the recent data by Fellner et al [26]

2.5. Thermochemical investigation on the Al-Na system

Mitchel and Samis [29][30] concentrated on measuring the activities of Na in Al. The Na distribution in the melt was determined by quenching the samples and performing chemical analysis on the quenched samples [29][30]. Results of the work and those of other researchers are given in Figure 2.8 [29].

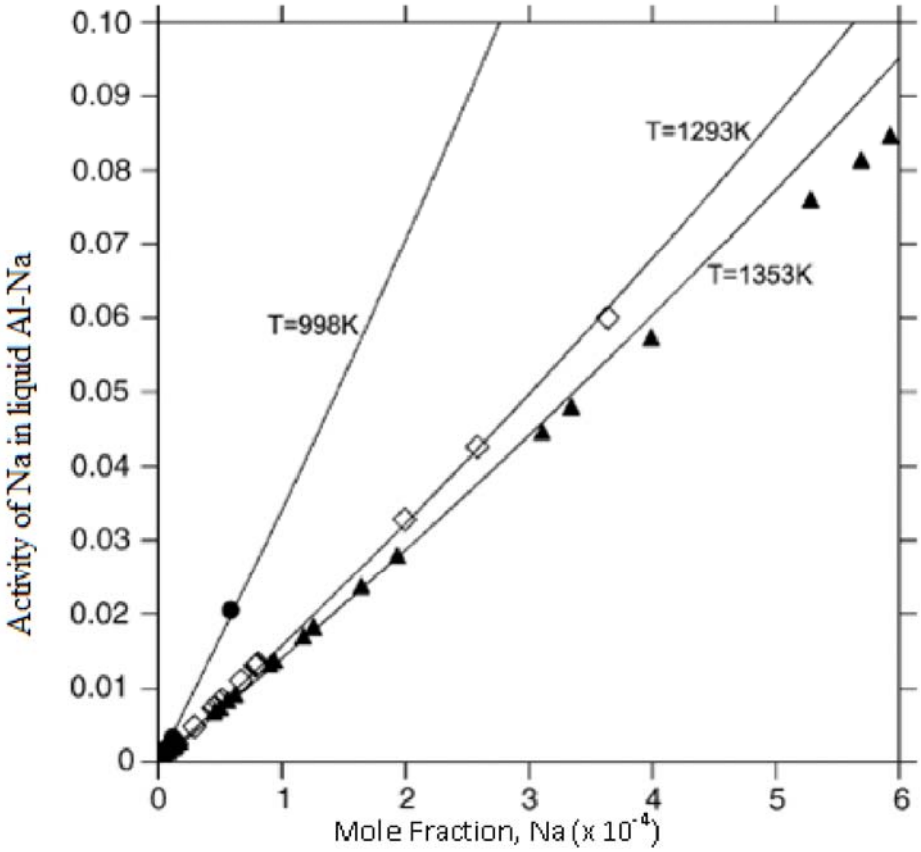

Figure 2.8: *The calculated activity of Na in liquid Al-Na in comparison with the experimental data (◊) at 1293K and (▲) at 1353K by Dewing [31] and (●) at 998K by Brisley and Fray [32].*

The calculated activity of Na in liquid Al-Na at different temperatures is shown in Figure 2.8. The activity increases with increasing the mole fraction Na, but the calculated values do not fit the experimental data at 1353K when the Na concentration is above 0.03 at. % [21].

Chapter 3: Experimental

3.1. Introduction

Carbon is used as cathode material in the aluminium smelting industry. Absorption and penetration of electrolyte or metallic sodium into the cathode lining might take days or years, depending on the start-up parameters and the quality of the cathode [33].

3.2. Literature

Significant research has been done on penetration of electrolyte into the carbon cathode lining and reactions that then take place between the electrolyte and carbon cathode. Different methods have been used:

i. The Y. Mikhalev and H.A. Oye method measures the absorption of metallic sodium in carbon cathode materials [34].
ii. The P. Brilloit, L.P. Lossius and H.A. Oye method studies the penetration and chemical reactions in carbon cathodes during electrolysis [18][20].

3.2.1. Y. Mikhalev and H.A. Oye method

Three commercial cathodes were used for the study. The properties of the different carbon cathodes that were studied by Y.Mikhalev and H.A.Oye are given in Table 3.1. [34].

Table 3.1: *Properties of carbon cathodes as studied by Y. Mikhalev and H.A. Oye* [34]

Material symbol	Material	Electrical Resistivity μΩm (20 ºC)	Thermal conductivity W/Km (35ºC)	Ash Content %	Porosity %
A	Gas-calcined anthracite filler with 30 % graphite added, baked to 1200 ºC	35	8	2.5	14
B	Graphite Filler, baked to 1200 ºC (Semi-graphitic)	17	35	0.35	21
C	Petroleum coke filler, calcined to 2300ºC (Semi-graphitised)	11	83	0.23	24
D	Graphite, Union Carbide, CS49	9	150	<0.05	22

Mikhalev and Oye performed their experiments under 99.99% argon. Their experimental setup is shown in Figure 3.1 [34].

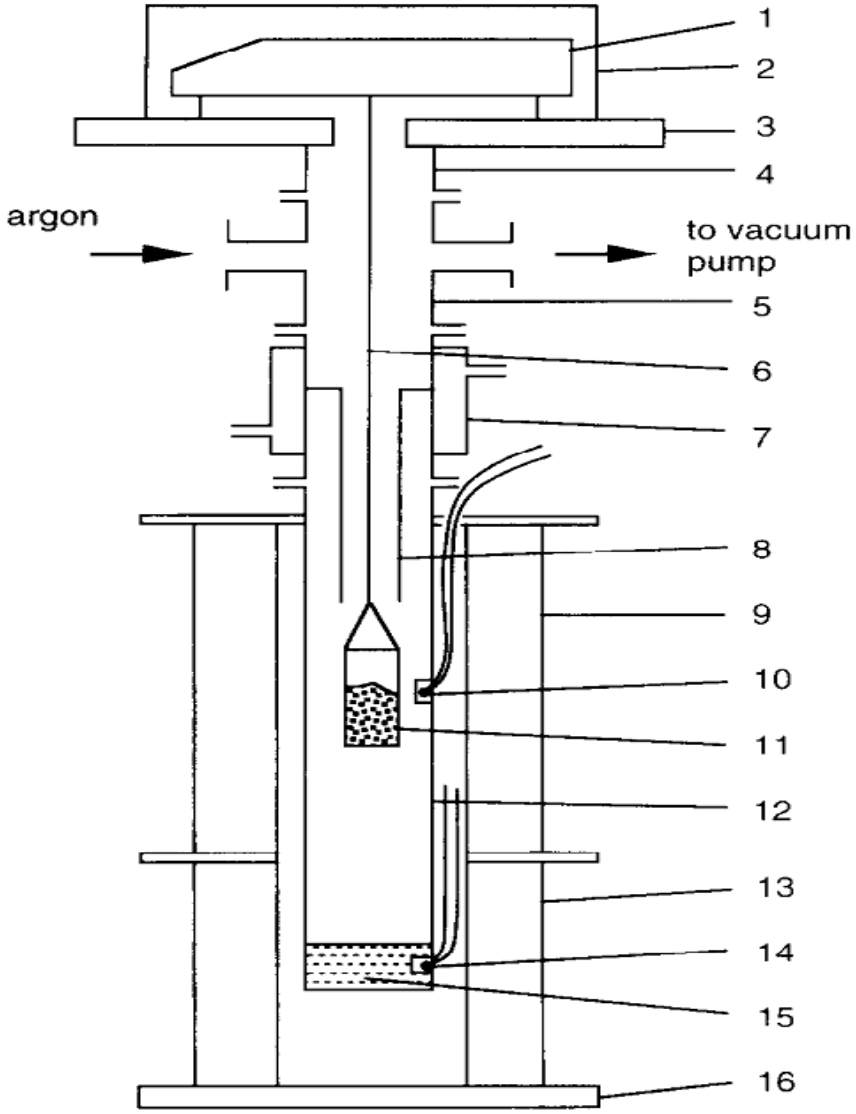

***Figure 3.1**: Schematic drawing of the equipment used by Y. Mikhalev and H.A. Oye during their electrolysis process (not to scale)* [34]*. (1) Electronic balance, (2) plexiglas cover, (3) steel plate, (4) fitting with flange, (5) cross piece, (6) nickel wire, (7) cooling jacket for water, (8) Alsint tube, (9) upper furnace, (10) Pt-10%Rh-Pt thermocouple, (11) nickel crucible with sample, (12) stainless steel reactor chamber, (13) lower furnace, (14) type K thermocouple, (15) molten sodium and (16) platform.*

The experimental work was carried out in two modes:

1. Isothermal: The sample temperature was kept constant while the vapour pressure of sodium was varied
2. Isobaric: Varying the sample temperature whilst keeping the sodium pressure constant [34].

Calculations of sodium pressure were carried out using equation 3.1:

$$lnP = 11.2916 – (12532.694/T)-0.3869\ lnT \quad \ldots\ldots\ldots\ldots\ldots\ldots\ldots\ldots\ldots 3.1$$

Where T is given in Kelvin and P in MPa. During the experiment the pressure (argon + sodium) was adjusted to 1 atm [34].

The experimental results are given and summarised in Figure 3.2 (Isothermal experiment) and Figure 3.3 (Isobaric experiment). The mass of the carbon samples increased relative to their original masses due to sodium absorption as the pressure increased at a constant temperature of 1227K [34].

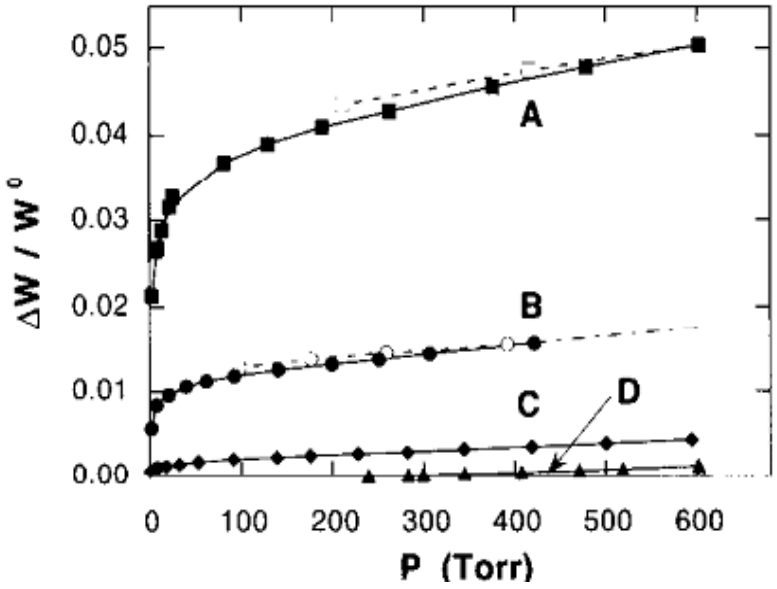

Figure 3.2: *Sodium absorption at constant temperature of 1227K [34].*

W^0 = Initial weight

ΔW = Change in weight

A- Is an amorphous graphite material

B- Is a semi-graphitic graphite material

C- Is a semi-graphitised graphite while

D- Is a fully graphitised graphite.

The isobaric experiment carried out under a pressure of 191 Torr for materials B and C are shown in Figure 3.3. The isobaric experiment showed an increase in absorption with decreasing temperature [34].

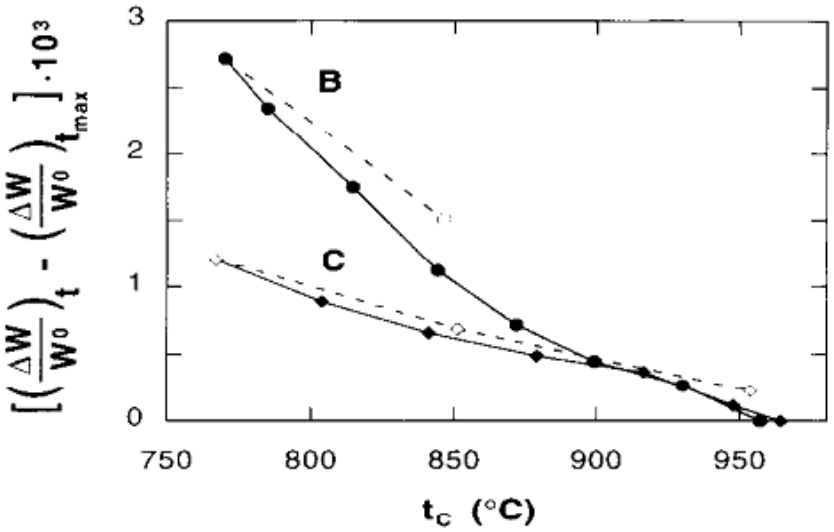

Figure 3.3: *Isobaric adsorption results of cathode samples B and C at 191 Torr [34].*

(t = Temperature; t_{max}= maximum temperature and t_c=critical temperature)

The maximum temperature at which maximum sodium absorption was observed was approximately 770°C for material B and approximately 762°C for material C, while the critical temperature (t_c = critical temperature) was observed at approximately 960°C for material B and approximately 970°C for material C.

The carbon materials used in these experiments were not fully graphitised. Sample A contained coal tar pitch with 30% graphitised and 30 % anthracite baked at about 1200°C, sample B contained coal tar pitch and graphite baked to 1200°C, while sample C contained coal tar pitch and petroleum coke and was graphitised at 2300°C [34]. Despite the differences in the three materials, their absorption isotherm behaviour was the same. The sodium absorption of these materials decreases with increasing the degree of graphitisation [34].

3.2.2. P.Brilloit et al method

P. Brilloit and co-workers studied the penetration of metallic sodium and molten salt into carbon cathode materials during aluminium electrolysis [18][20]. Laboratory equipment was constructed to simulate the industrial aluminium electrolysis process.

Three commercial cathode blocks were used in the study:

A. Gas calcined anthracite approximately 20% graphite added
B. Electro-calcined anthracite approximately 20% graphite added
C. Semi-graphitic 100% graphite approximately 100% graphite added

Samples 49.90 mm in diameter and 40 mm in height were drilled in the extrusion direction of the carbon blocks and dried at 80°C for 24hrs [18][20].

Before the start of each experiment, an electrolytic bath was prepared from 190 g of cryolite salt and 6% Al_2O_3 and 4% CaF_2. A graphite crucible of 75 mm external diameter, 50mm internal diameter and 150 mm height was used to contain the prepared bath (Na_3AlF_6, Al_2O_3 and CaF_2) and the sample [18][20]. The sample was forcefully inserted into the crucible. An alumina tube with the same external diameter as the sample was inserted and used as the insulator and prevented the crucible from acting as a cathode [18][20]. The prepared bath constituents were poured into the crucible. N_2 and Ar inlet and outlet holes were on the top lid and bottom of the crucible [18][20]. The complete experimental set-up is shown in Figure 3.4.

Experiments were run at a temperature of 1010°C, and current density of 0.75Acm^{-2}. The current and voltage were recorded during the experiments [18][20]. After each experiment the furnace was cooled, the crucible was removed from the furnace and broken in order to remove the sample. The sample was cut into two parts, one part was sectioned for XRD analysis. Metallic aluminium was observed on top of the sample not within the sample [20][21]. The XRD analysis detected several crystalline phases from the electrolysed carbon cathode samples. The detected phases were Na_3AlF_6, NaF, $Na_5Al_3F_{14}$, CaF_2, α-Al_2O_3, $Na_2O.11Al_2O_3$, $NaAlO_2$, AlN and NaCN [18][20].

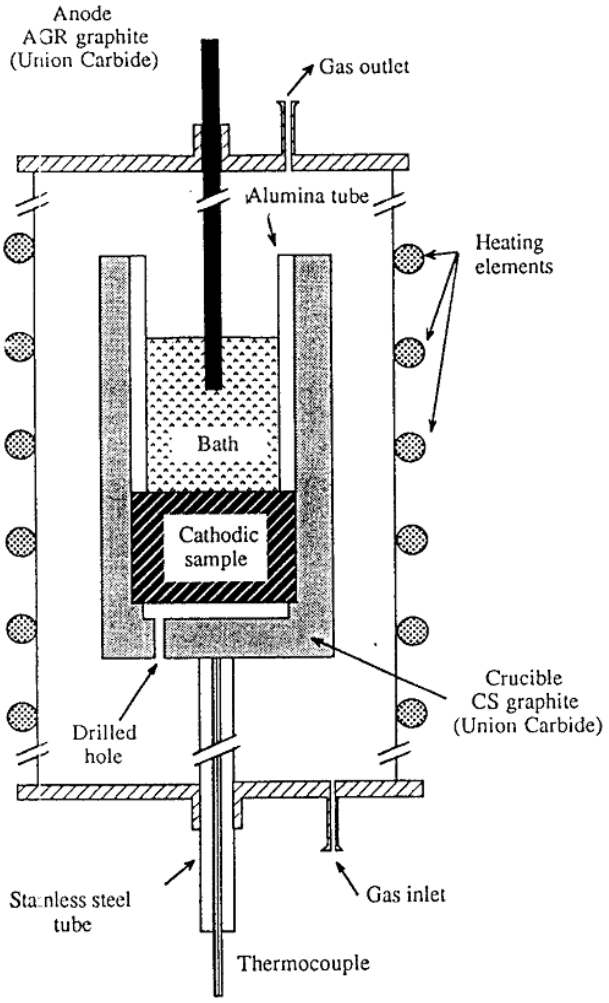

Figure 3.4: *Laboratory electrolysis setup from P.Brilloit et al [18][20]*

3.2.3. Sodium Expansion (Rapoport)

Though the mechanisms with which the sodium penetrate/diffuse into carbon cathode material has not yet been well defined, the sodium that is absorbed into the carbon structure results in carbon swelling, and this leads to the deterioration of the life span of the carbon cathode lining[5].

In 1957, Rapoport and Samoilenko [5] developed and published a simplified method for laboratory measurement of sodium expansion on carbon cathodes due to sodium penetration. The modified apparatus whereby the sodium expansion is measured at high temperature with zero and non-zero external pressure is given in Figure 3.5. A cylindrical carbon cathode sample of 30mm diameter and 60mm height was used for the study [5][35].

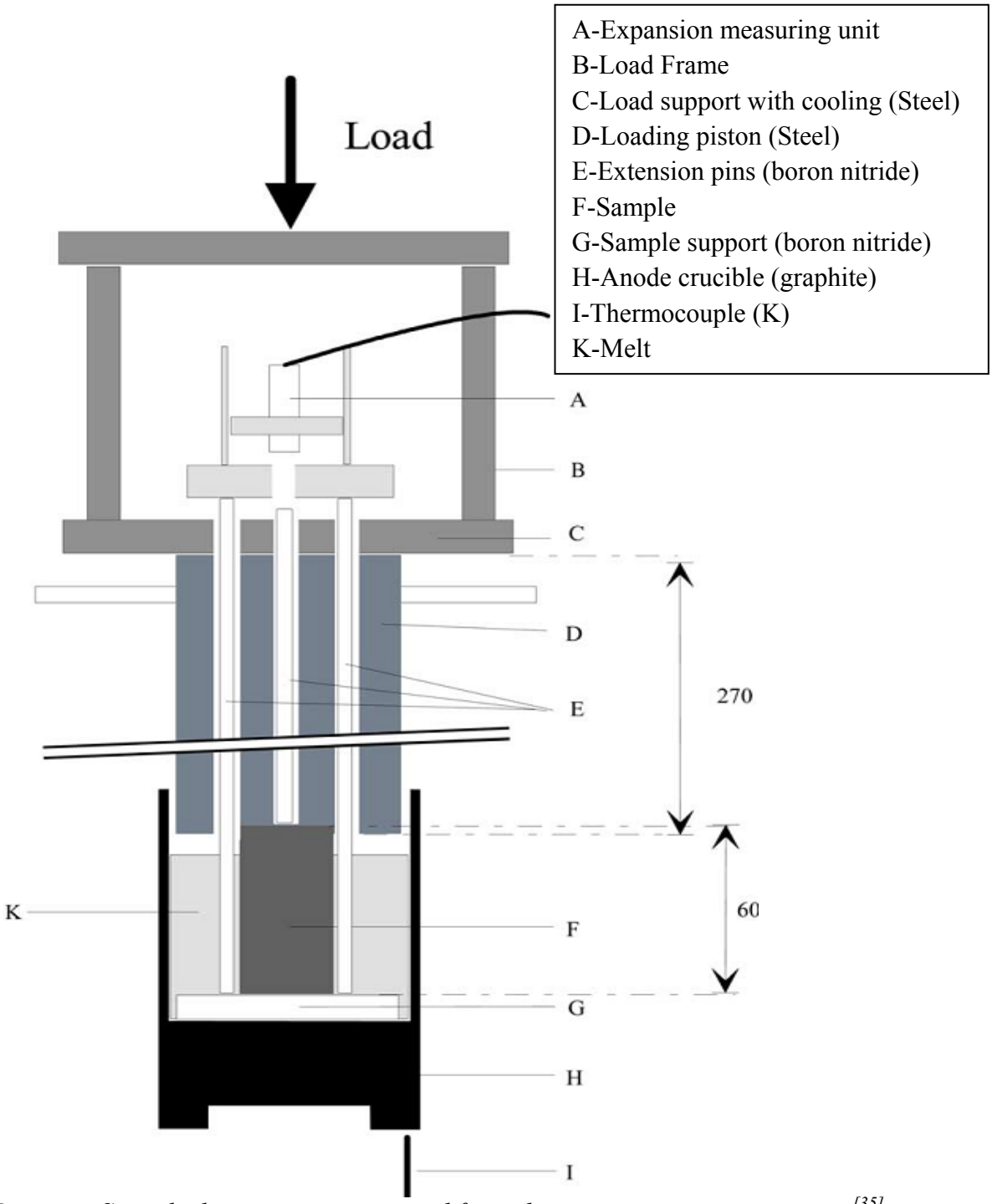

Figure 3.5: *Rapoport Samoilenko-type apparatus used for sodium expansion measurements* [35]

The bath (K) with cryolite ratio (NaF/AlF_3) of 3.89 was saturated with alumina and 5 wt% CaF_2. The total mass of the bath was 450g. The furnace was purged with argon (99.99%) to avoid oxidation. The experiment was run at 980°C, and 55mm of the height of the sample was immersed into the molten melt [5][35][36].

J.G. Hop [2] studied the different carbon materials using the same approach used by Samilenko [5][35]. The results obtained by Hop [2] are shown in from Figures 3.6 and 3.7.

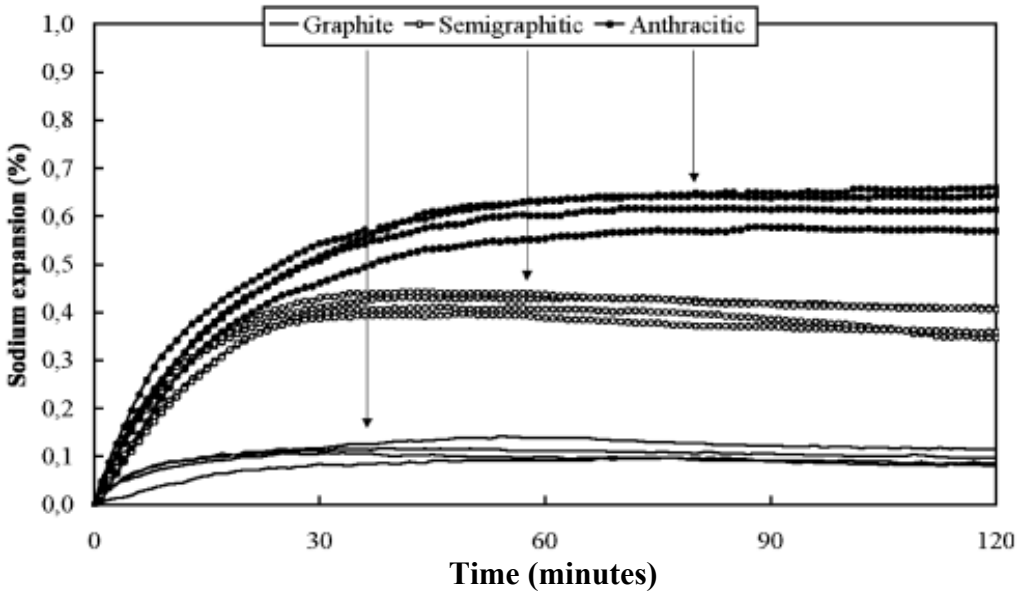

***Figure 3.6**: Sodium expansion for 3 different commercial carbon materials [2].*

The results showed an increase in sodium expansion as the degree of graphitisation decreases. J.G. Hop [2] further studied carbon materials that were produced from petroleum coke in his laboratory at different heat treatment temperatures. The results are given in Figure 3.7.

The significant outcome of the experiment is that expansion decreases with increasing heat-treatment temperature of the carbon [2]. This means the highly graphitised carbon material expands less due to sodium penetration as compared to less graphitised carbon materials.

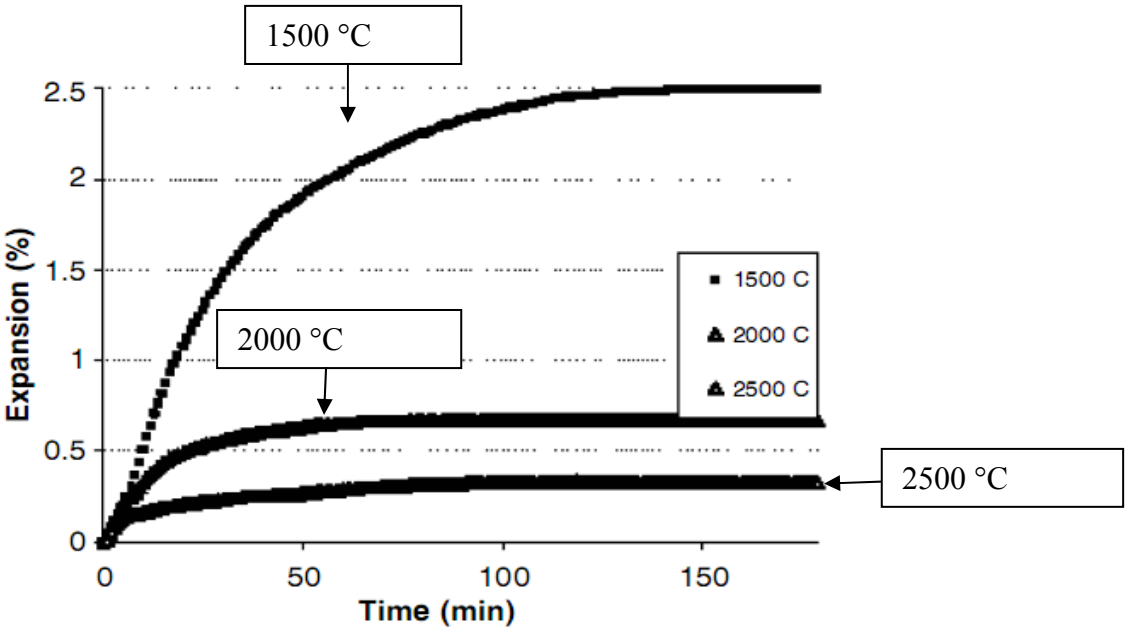

Figure 3.7: *Sodium expansion of the laboratory produced carbon materials at different heat treatment temperatures* [2].

3.3. Experimental procedure followed in this study

3.3.1. Introduction

The following section will outline the experimental procedures used to study the carbon cathode materials on a laboratory scale.

Two commercial carbon cathode grades were used for the study. The two carbon grades were 30% graphitised (C) and 100% graphitised (D) carbon. The two materials were chosen due to their availability, as they are materials that are currently used in the South African aluminium smelting industry.

The carbon cathodes were first characterised (Table 3.2), before they were used in the electrolysis and sodium expansion experiments.

Table 3.2: *Preparation, bulk density, total porosity and chemical analysis of the examined carbon grades* *(CSIR, High Temperature Laboratory)*.

Sample Name	Preparation	Bulk Density g/cm^3	Total Porosity %	Chemical analysis (mass %)					
				% Ash	C	S	N	H	O
C	Graphitised filler, whole block calcined above 2300ºC.	1.59	21.5	6.6	89.1	0.30	0.22	0.02	3.8
D	Graphitised cathode block: The whole block (aggregate and binder) consisting of graphitisable materials has been heat treated at 3000ºC, giving a graphitic material	1.7	19.6	1.6	97.8	0.13	0.47	0.14	0.13

3.3.2. Procedures

Two sets of experiments were done:

i. Electrolysis process
ii. Rapoport (sodium expansion) test

3.3.2.1. Electrolysis process

The experimental method of Brilliot et al [18][20] was used in this study with some modifications. The modifications are listed in Table 3.3.

Figure 3.8 illustrates the experimental setup that was taken into the furnace for the electrolysis process. The electrolysis experiment was performed in a graphite crucible of 75mm external diameter, 70 mm internal diameter, and height of 150mm. The cathodic carbon sample of approximately 70mm in diameter and 50mm height was force-fitted into the crucible. An alumina tube of approximately 70 mm external diameter was then fitted into the crucible above the sample to insulate the crucible and prevent it from acting as a cathode.

Table 3.3 *Modifications done to Brilloit et al [18][20] experimental approach*

P. Brilloit et al Method	Laboratory modifications
• Purged gas from the bottom of the furnace. • Two holes, one on the bottom and one on top lid, are used for N_2 or Ar inlet and outlet. • The graphite crucible screwed onto the stainless steel tube, fastened to the furnace bottom	• Purged gas from the top of the furnace. • Two holes, both on top lid for N_2 inlet and outlet. • Graphite crucible not screwed or fastened to the steel tube, but, was in the crucible holder.

A bath (cryolite) was prepared from 90% Na_3AlF_6, 6% Al_2O_3 and 4% CaF_2 giving a total mass of 400g. The crucible was filled with the total prepared bath. To ensure pressure equilibrium between the bottom of the sample and the rest of the furnace, a hole (10mm in diameter) was drilled in the bottom of the crucible. The crucible was inserted into the crucible holder and put into the furnace. The negative output of the DC power supply was connected to the handle of the crucible holder, and carried the current through the crucible to the carbon sample, thus, making it cathodic. An anode made from graphite was supported by a stainless steel rod fastened to the top lid. The anode supporter was connected to the positive output of the DC power supply.

The carbon granules between the crucible and the crucible holder were used to enhance the contact between the carbon graphite crucible and the high temperature resistant crucible holder. The graphite crucible material is used for its stability to withstand high temperatures and the salts used during electrolysis.

The furnace temperature was set at 1000 ºC. The K-type thermocouple was used to check the bath temperature. When the furnace temperature reached 600ºC nitrogen gas was purged into the system to prevent the oxidation of the carbon graphite crucible. After the bath has reached its melting temperature of 980 ºC, a power supply was connected to the setup as shown in Figure 3.8. After switching on the power supply, the anode was lowered 1mm into the bath. As the current started flowing, the electrolysis was timed. The anode was lowered every time when the current became unstable.

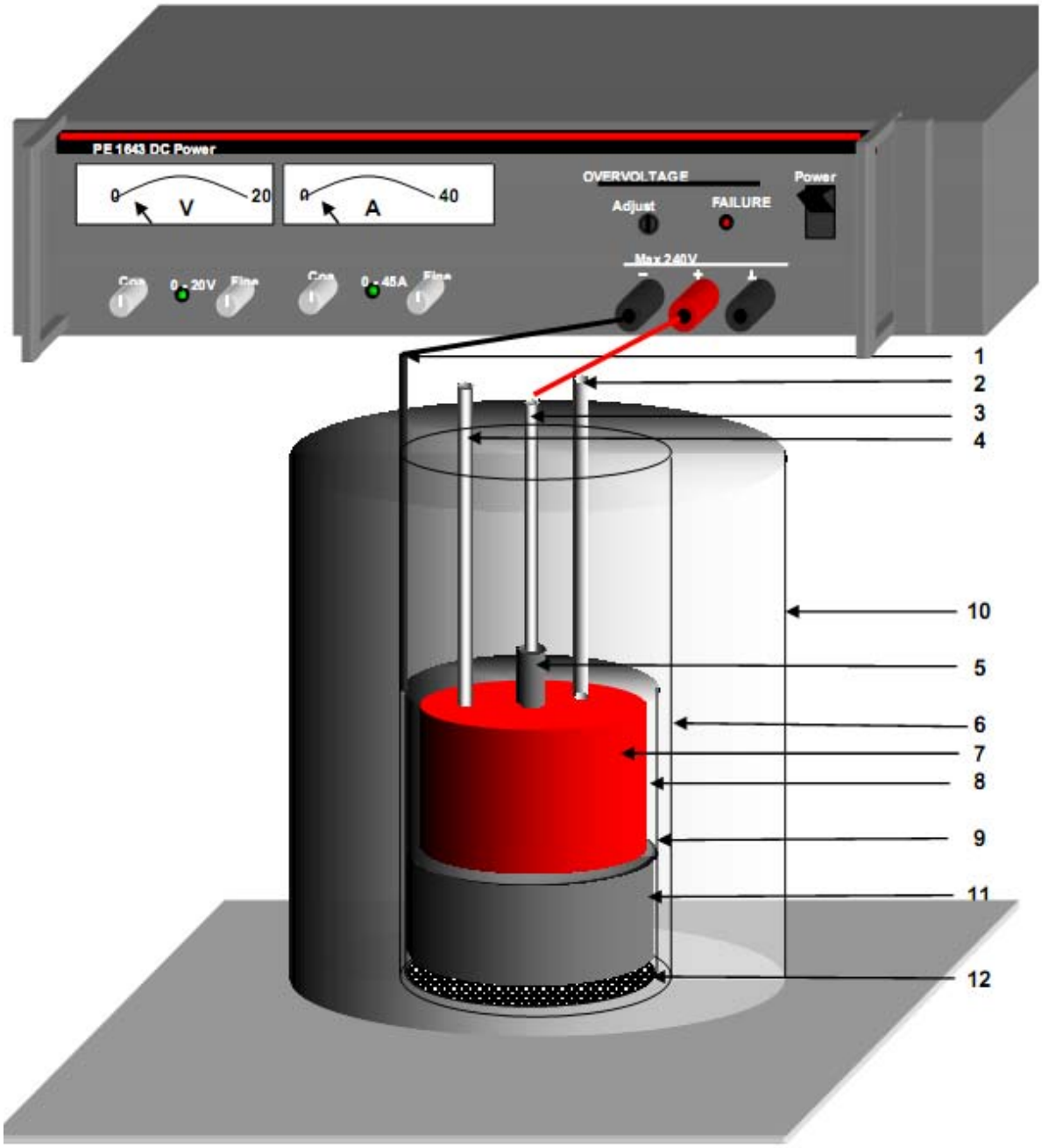

Figure 3.8: *Schematic drawing of the laboratory electrolysis process. (1) Cathode connection, (2) gas pipe, (3) anode connection, (4) thermocouple, (5) anode, (6) crucible holder, (7) molten cryolite, (8) alumina tube, (9) graphite crucible, (10) furnace, (11) carbon cathode sample, and (12) graphite granules.*

The electrolysis experiments on samples C_1 and D_1 were done for 1hr 30 min as shown in Table 3.4. After 1hr 30 min the furnace was cooled to 500ºC under nitrogen and the setup was removed from the furnace. The setup was allowed to cool for about 2 hours in air before removing the sample from the carbon graphite crucible. The same procedure was followed for samples C_2 and D_2, but changing the time of electrolysis to 3hours.

Table 3.4: *Cryolite Ratio, temperature, duration of electrolysis, current density and current for the electrolysis tests.*

Sample Name	Cryolite Ratio	Temp (ºC)	Time (hrs)	Current density (A/cm^2)	Current (A)
C_1	2.29	980	1hr 30min	0.75	28
D_1	2.29	980	1hr 30min	0.75	28
C_2	2.29	980	3hrs	0.75	28
D_2	2.29	980	3hrs	0.75	28

Duplication of the experimental work was done on the same carbon cathode grade under the same conditions.

3.3.2.2. Sodium expansion (Rapoport) test

The Rapoport test [5] was used to measure the expansive effect of sodium on the cathode carbon materials.

The Rapoport test (Sodium expansion test) was performed according to the CSIR High Temperature Laboratory Procedure. Cylindrical samples of 35 mm in diameter and 90 mm in height were drilled out of 30% graphitised (sample C) and 100 % graphitised (sample D) cathode blocks. These samples were drilled from the same blocks from which the samples for the electrolysis tests were drilled.

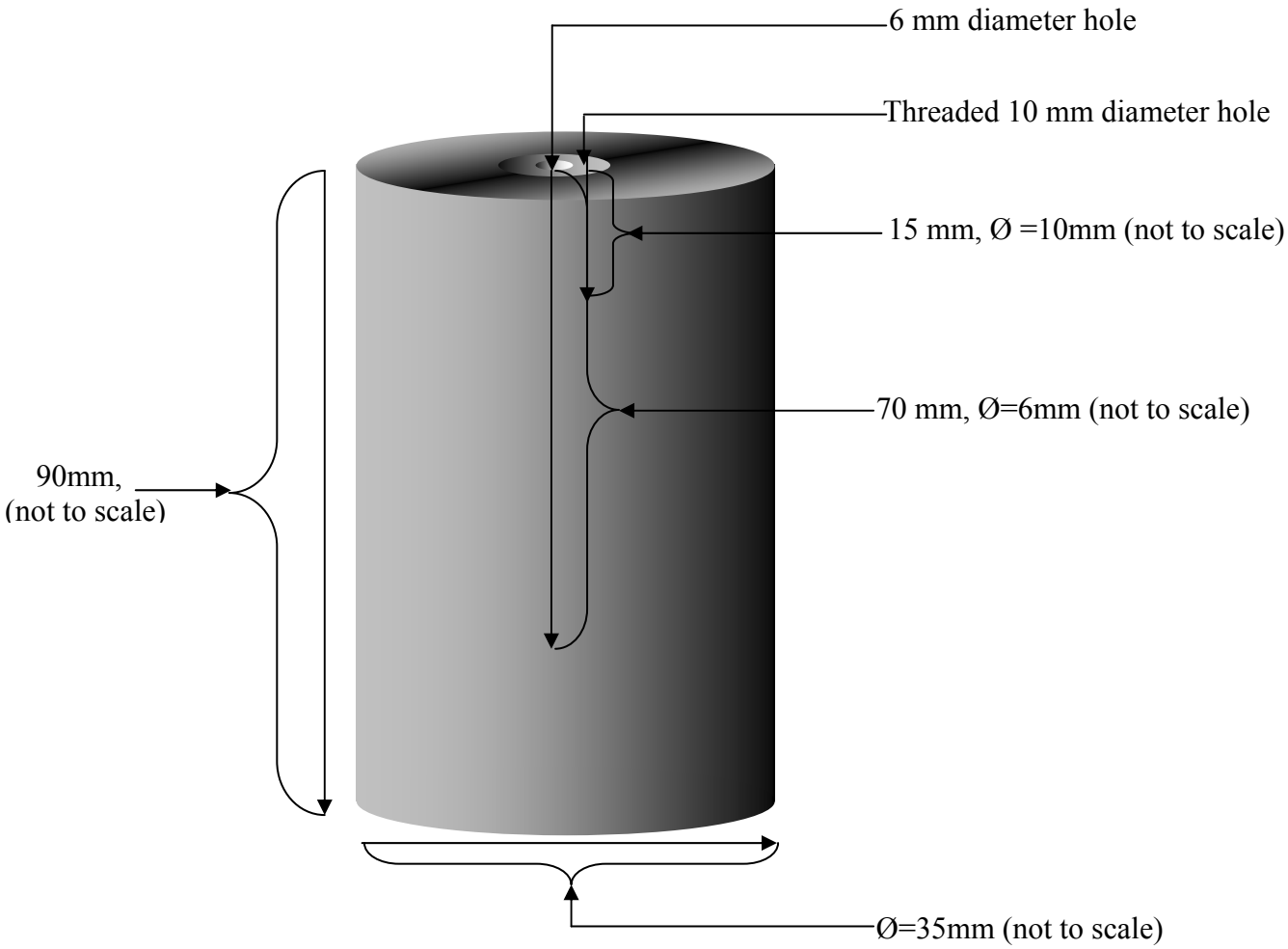

Figure 3.9: *Schematic drawing of the Rapoport (sodium expansion test) sample.*

i. A 35 mm diameter x 90 mm length sample was drilled from the block.
ii. A 10 mm diameter x 15 mm length hole was drilled in the middle of the specimen and 6mm x 70 mm length hole was drilled in the middle of the 10mm diameter hole as shown in Figure 3.10
iii. The 10mm diameter hole was threaded using an M12 die.
iv. The specimen was dried for 24hrs in a drying oven at 110ºC.

The bath (melt) of Na_3AlF_6 with a cryolite ratio of 2.29 was saturated with 10 % Al_2O_3 (70g) and 10% NaF (70g).

A graphite crucible of 75 mm external diameter and 70 mm internal diameter was used. The crucible was filled with the prepared bath. The crucible was put into the high temperature stainless steel crucible holder with two handles. The specimen was screwed onto the heat resistant steel tube which was also used for the anode connection and for positioning the heat resistant steel rod. The alumina tube was used to protect the specimen from being in contact with the steel lid. The steel lid prevented the bubbling electrolyte from spilling into the furnace. The carbon granules were used to enhance the contact between the carbon graphite crucible and the crucible holder.

The extensometer was then screwed on top of the tube as shown in Figure 3.10. The steel disc between the sample and the sintered alumina tube was used to avoid air access (burn-off of the graphite crucible) from entering into the melt and the loss of the melt by open evaporation. The sintered alumina tube was used to prevent short-circuit between the graphite sample and the steel rod. The sample was immersed 70 mm below the melt. When the temperature reached 1000ºC, the setup was equilibrated for 3 minutes without recording the expansion to avoid recording the thermal expansion of the steel rods.

As the specimen expands due to the penetration of the electrolyte, the heat resistant steel rod pushes against the extensometer and the needle on the extensometer moves, signalling the expansion of the sample.

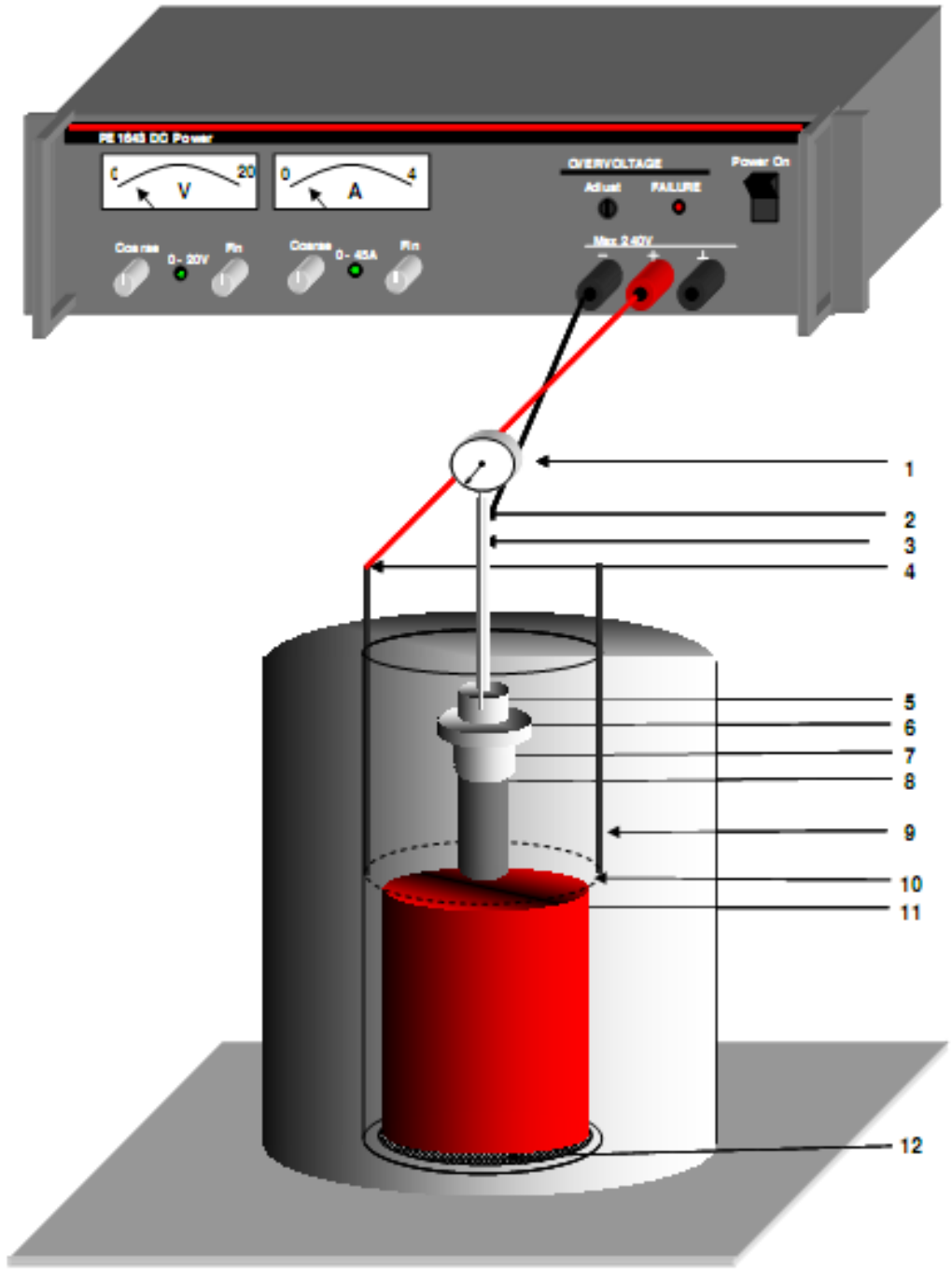

Figure 3.10: *Schematic drawing of the Rapoport setup. (1) Extensometer, (2) heat resistant steel tube, (3) heat resistant steel rod, (4) cathode connection, (5) sintered alumina tube, (6) circular steel lid, (7) alumina tube, (8) carbon cathode sample, (9) heat resistant steel crucible holder, (10) graphite crucible, (11) molten electrolyte, and (12) carbon granules.*

3.4. Analysis techniques

3.4.1. XRD analysis

X-ray diffraction (XRD) was used to identify and quantify the phases present in the carbon cathode samples. All samples were milled in a WC milling vessel and prepared for XRD analysis using a back loading preparation method. In the semi-quantitative XRD analysis, 15% Si (Aldrich 99%) was added to the samples. The samples were micronized in a McCrone micronising mill to ensure homogeneity in an ethanol liquid to ensure that the micronising does not have an influence in the crystal structure.

The samples were analysed using a PANalytical X'Pert PRO powder diffractometer with X'Celerator detector and variable divergence - and receiving slits with Fe filtered Co-K_α radiation. The phases were identified using X'Pert Highscore plus software. The relative phase amounts (weights %) were estimated using the Rietveld method (Autoquan Program). Normalised phase amounts are reported.

3.4.2. Optical microscopy analysis

A LEICA DM15000M reflected light microscope and a LEICA MZ16 stereo microscope were used. The microscopes were both fitted with digital cameras for capturing the micrographs. Only the stereo microscope micrographs are reported.

3.4.3. SEM-EDS analysis

SEM-EDS analysis was done using a JSM 6510 Jeol Scanning Electron Microscope (SEM), with an energy-dispersive X-ray spectroscopy (EDS) facility.

Chapter 4: Post-Mortem analysis of the cathode samples removed from a South African aluminium smelter

4.1. Introduction

SGL Carbon Group is the producer and provider of the carbon cathode blocks for the South African aluminium smelting industry. The carbon cathode block manufacturing process is given in Figure 4.1, as given by the SGL Carbon Group.

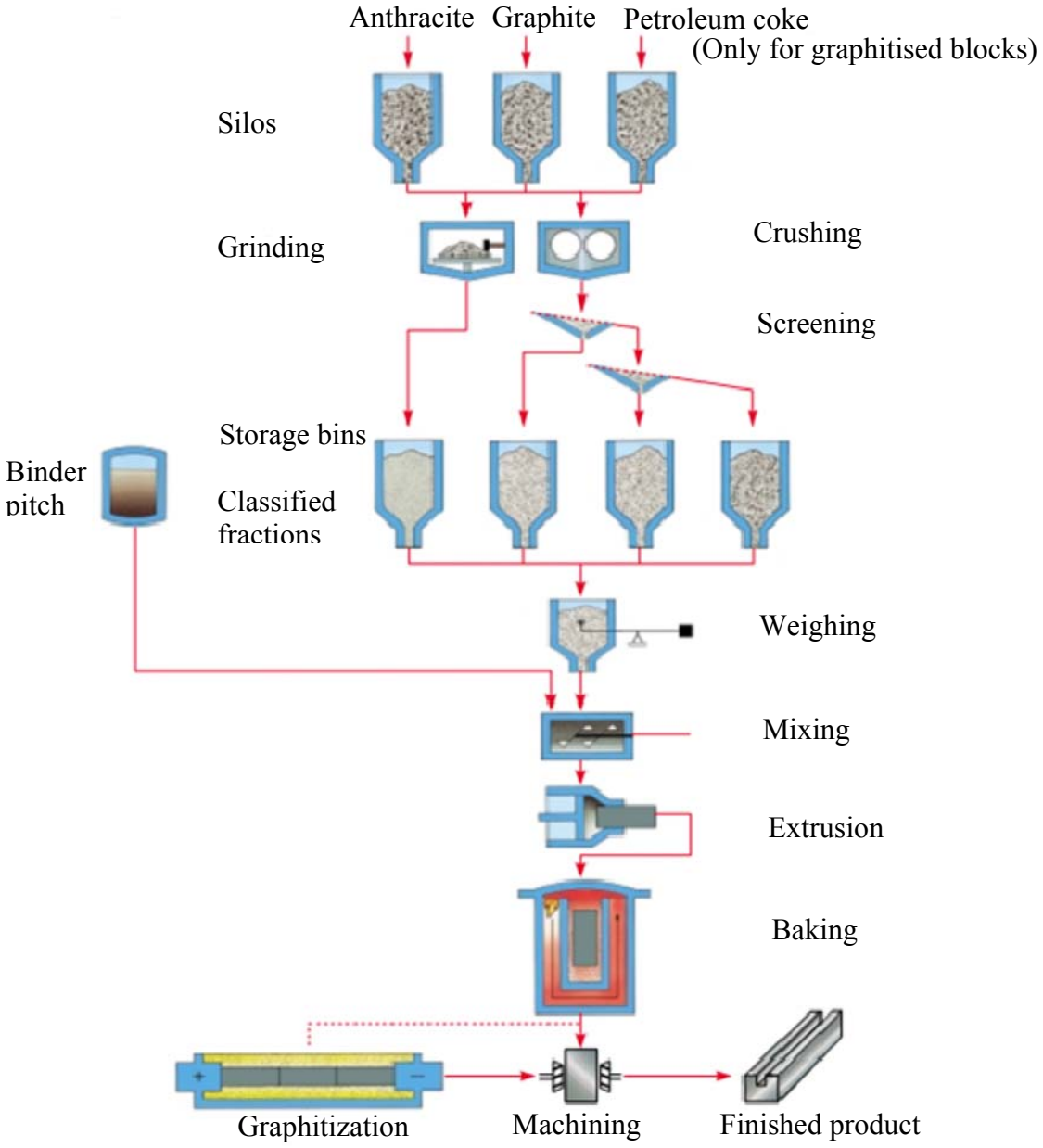

Figure 4.1: *Flow process for the manufacturing of the carbon cathode blocks* [37]

Graphite cathode blocks are produced by a technologically advanced process, using advanced equipment and high quality electrically calcined anthracite as raw material. They are formed by extrusion or by vibrocompaction after mixing the raw materials (either a mixture of pitch, calcined anthracite and/or graphite in case of semi-graphitic and graphitic materials). These materials are then fired at approximately 1200°C [37].

4.1.1. Properties of the carbon cathode from SGL Carbon Group.

The physical and thermal properties of the extruded blocks from the SGL Carbon Group were determined in the High Temperature (HT) Laboratory at the Council for Scientific and Industrial Research (CSIR) before the electrolysis process. The results are given in Table 4.1. The carbon blocks were heat treated between 2400°C-3000°C.

Table 4.1: *Characteristics of the carbon cathode block, as determined by the CSIR HT laboratory*

SGL CARBON			
EXTRUDED BLOCKS			
Physical properties	**Unit**	**Graphitic**	**Semi-graphitic**
Real Density	g/cm^3	2.02	2.09
Apparent Density	g/cm^3	1.77	1.62
Open Porosity	%	11.2	21.2
Total Porosity	%	12.4	23.2
Cold Crushing Strength	MPa	22.5	18.9
Flexural Strength	MPa	13.6	12.2
Electrical Resistivity at room temperature	μΩm	11.9	10.8
Electrical Resistivity (1000°C)	μΩm	8.27	9.1
Thermal Expansion (<1000°C) First run	K^{-1}	5.40E-06	3.9E-06
PLC (12hrs @ 950°C) (BS1902:5.10)	%	0.02	0.02
Sodium Expansion after 2 hours	%	0.23	0.68

4.2. Post-mortem Samples

4.2.1. Solidified bath analysis

After the electrolysis cell has reached the end of its life, the bath is left to solidify, the solidified bath is removed from the cell, and the cell is re-lined.

A sample of a solidified electrolyte was obtained from a South African aluminium smelter for characterisation. The phase composition of the electrolyte was then compared to the phases that were distinguished in the spent cathode plant samples. This analysis was done by using XRD and SEM-EDS analyses.

The following phases were identified from the XRD (appendix A) analysis of the solidified bath: Corundum (Al_2O_3), Cryolite (Na_3AlF_6), NaF (Villiaumite), $NaAl_{11}O_{17}$ (Diaoyudaoite) and Fluorite (CaF_2). Bulk SEM-EDS analysis of the solidified electrolyte confirmed the presence of all five of these phases (Table 4.2).

Table 4.2: *SEM-EDS data and phases of the solidified bath.*

Detected elements in at%							
Carbon (C)	Nitrogen (N)	Oxygen (O)	Fluorine (F)	Sodium (Na)	Aluminium (Al)	Calcium (Ca)	Phase or Phases
N/d	N/d	N/d	50.52	49.46	0.02	N/d	NaF
0.31	N/d	53.08	4.06	6.43	36.07	0.05	NaF and $NaAl_{11}O_{17}$
1.32	N/d	0.25	59.63	29.33	9.47	N/d	Na_3AlF_6
2.63	N/d	0.74	60.25	19.86	7.53	8.99	CaF_2 and Na_3AlF_6
1.32	0.01	59.83	1.67	3.43	33.70	0.04	$NaAl_{11}O_{17}$
N/d	N/d	59.30	0.14	0.52	39.72	0.32	Al_2O_3

N/d = Not detected

4.2.2. Carbon cathode samples

Two carbon cathode (SGL products) samples from two failed aluminium cells were received from a South African aluminium smelter. The two samples had different virgin graphite content (sample "A" had 96.82 while sample "B" had 92.93 wt%). These two samples were used to determine the phase chemical profile through the carbon cathodes. The two samples were taken from similar positions (40cm from the sidewall) but from different cells (Figure 4.2).

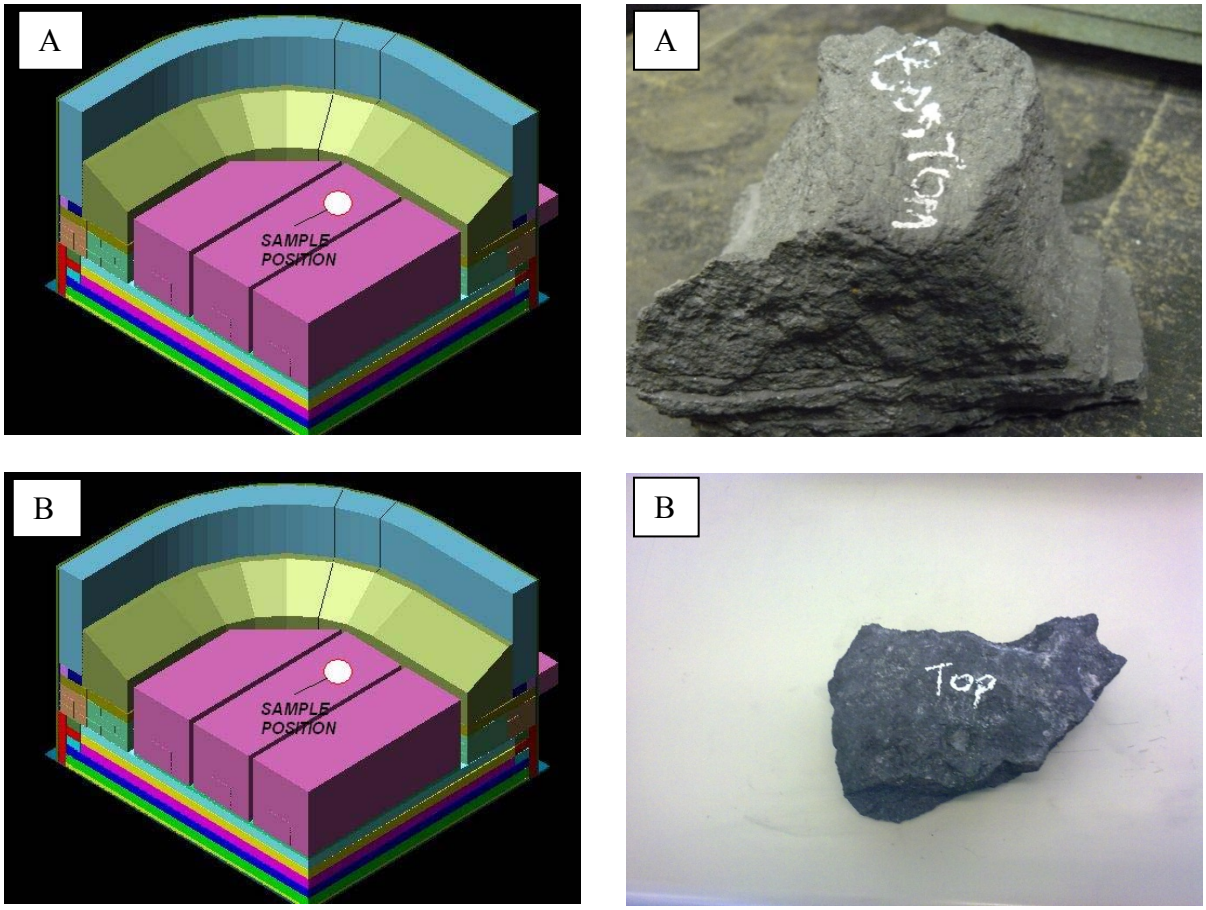

***Figure 4.2**: Positions from where the post-mortem samples were taken and the samples that were used for analysis (not to scale).*

The pot life of sample "A" was 1944 days while that of sample "B" was 1644 days. The samples were cut into slices, up to 33.77mm (sample A) and 26.81mm (sample B) below the electrolyte-carbon cathode interface. The sections were subsequently analysed by x-ray diffraction (XRD) and scanning electron microscope (SEM). The sections are labelled A_1-A_5

and B_1-B_5 depending on the distance from the carbon cathode-electrolyte interface (Table 4.3).

Table 4.3 shows the sample thicknesses and their distances from the carbon cathode-electrolyte interface. It also shows that A_1 and B_1 are samples closest to the carbon cathode-electrolyte interface while samples A_5 and B_5 are the furthest removed from this interface.

The received samples were co-drilled without lubricant (water) to 35 mm diameter and 60 mm height. To ensure that bath penetration is determined at its possible high level the sampling was stopped at approximately 35 mm for sample "A" and approximately 27 mm for sample "B". Specimens of sizes given in Table 4.3 were cut without lubricant using the ATM Brillant 250X wet abrasive cut-off machine. To ensure the sample distance from the hot zone (HZ), after each specimen cut the height of the sample and thickness of the specimen was measured using a calliper.

***Table 4.3**: Section thickness and distance from carbon cathode-electrolyte interface.*

Sample	Sections				
A, 1644 days	A_1	A_2	A_3	A_4	A_5
Thickness (mm)	5.49	6.75	6.83	8	6.7
Distance from HZ (mm)	5.49	12.24	19.07	27.07	33.77
B, 1323 days	B_1	B_2	B_3	B_4	B_5
Thickness (mm)	2.52	4.86	4.88	6.33	8.22
Distance from HZ (mm)	2.52	7.38	12.26	18.59	26.81

HZ = Hot zone

4.3. Microstructural analysis results

4.3.1. Introduction

Microstructural analyses of both sample "A" and sample "B" were done using reflected light microscopy.

4.3.2. Sample "A" section images

Figure 4.3 shows the stereo microscope images of Sample "A" sections. Three regions were distinguished in all the sample sections, namely the carbon substrate, pores and the bath penetrated sections. Section A_1 shows a high degree of bath penetration while sample A_5 shows a high degree of porosity. This confirms that most pores in sample A_1 were filled with the electrolyte. Since sample A_5 was the furthest removed from the carbon-electrolyte interface, its pores were not fully penetrated by the electrolyte.

4.3.3. Sample "B" section images

Electrolyte could easily be distinguished in all "B" sample sections (Figure 4.4). The amount of electrolyte decreased with increasing distance from the cathode-electrolyte interface. The pores are more visible in section B_5, as was expected. This is due to the fact that section B_5 was the furthest removed from the cathode-electrolyte interface.

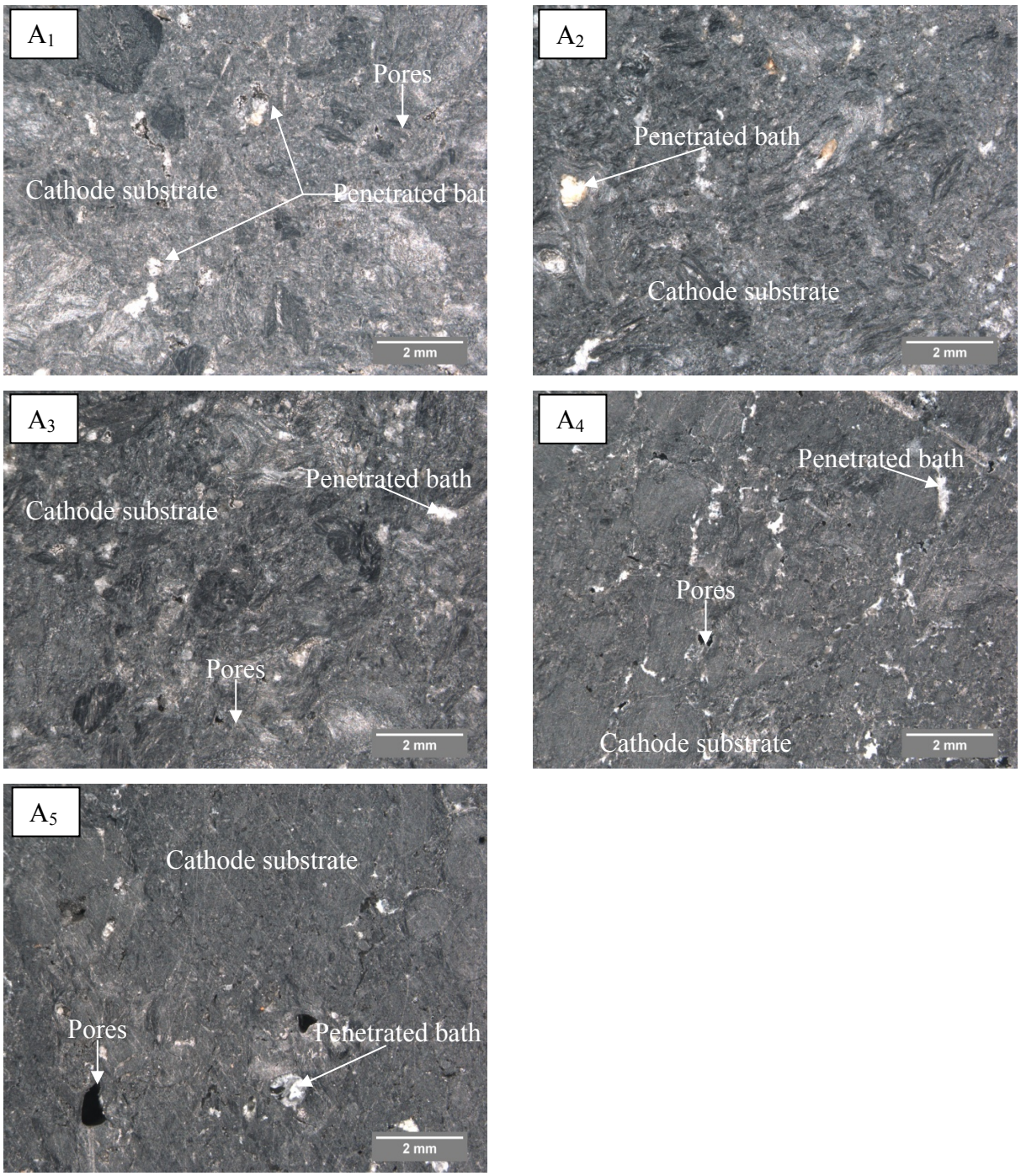

Figure 4.3: *Stereo microscope images of cathode sample "A" (in operation for 1944 days)*

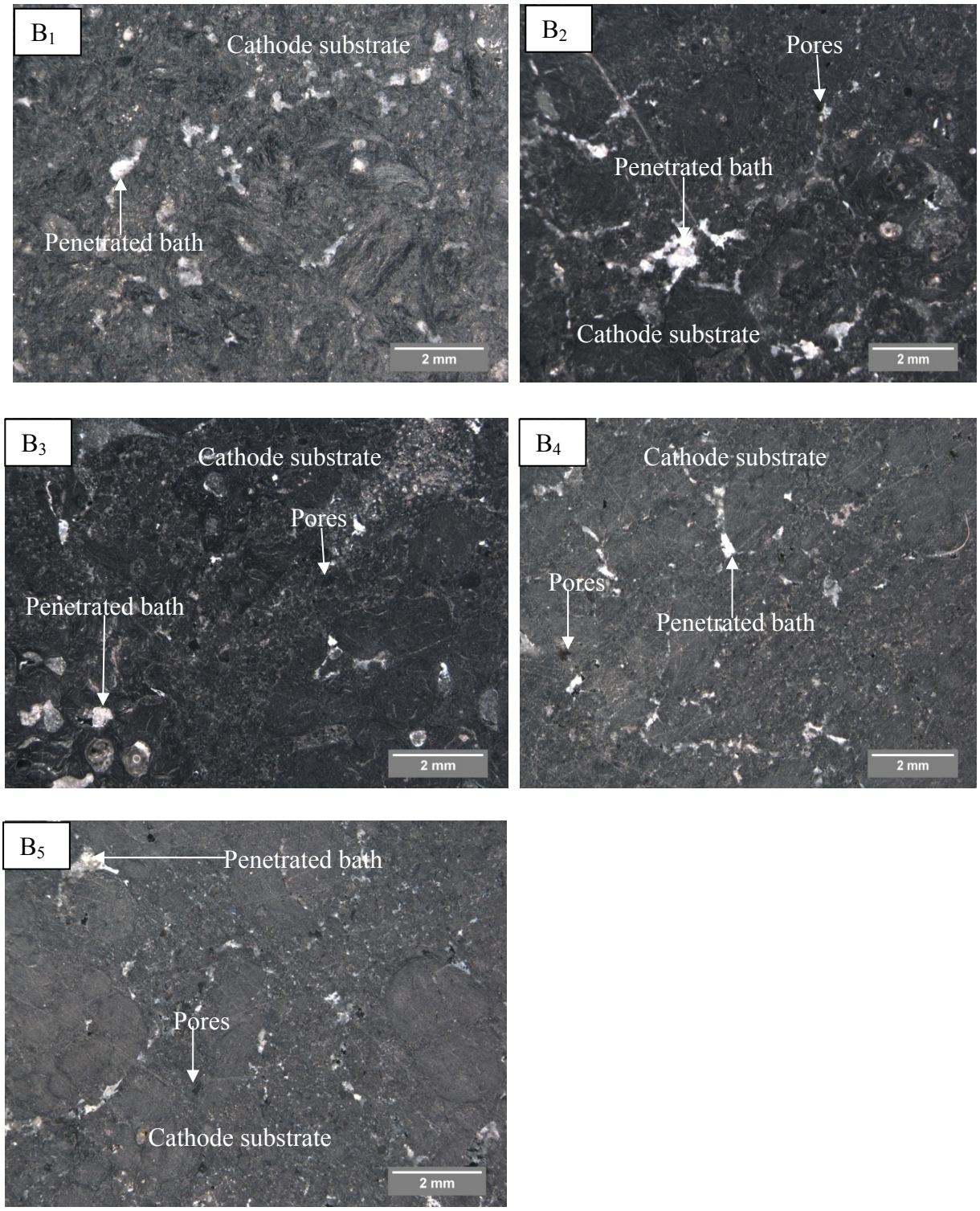

Figure 4.4: *Stereo microscope images of the sample "B" electrolysed for 1644 days*

4.3.4. Comparison between sections of sample "A" and sample "B"

Bath penetration and pores could be distinguished in both sample "A" and sample "B". There is a higher degree of bath penetration in sample "A" sections than in sample "B"

sections. The high degree of penetration in sample "A" can be attributed to the longer electrolysis period (1944 days) as compared to 1644 days of sample "B".

Section A_2 was compared to section B_3 as they were the same distance from the cathode-electrolyte interface. Similarly could sections A_4 and B_5 be compared. There are no pores visible in A_2 as compared to B_3. The degree of bath penetration is higher in A_2 than in B_3. The penetrated electrolyte is concentrated in certain areas of section B_3 while it is distributed throughout section A_2.

Comparing section A_4 to section B_5, it is clear that pores in B_5 are more visible than the pores in A_4. There was more bath penetration in section A_4 than in section B_5.

4.4. Quantitative XRD analysis results using the Rietveld method

In both sample sections (A and B) six common phases were identified by XRD. These phases are Al-Nitride (AlN), Cryolite (Na_3AlF_6), Fluorite (CaF_2), beta Diaoyudaoite ($NaAl_{11}O_{17}$), Villiaumite (NaF) and Graphite (C). Sodium cyanide (NaCN) was identified in the "A" sample sections but not in the "B" sample sections. Chiolite ($Na_5Al_3F_{14}$) and Corundum (Al_2O_3) were only identified in the "B" sample sections. All diffractograms are given in Appendixes B and C.

The relative phase amounts (weight %) were estimated using the Rietveld method (Autoquan Program) and are given in Tables 4.4 and 4.5. Amorphous phases, if present were not taken into consideration in the quantification.

The sampling was taken and stopped on the depth where the penetration was assumed to be at its high level, this was to ensure that phases and chemical species that penetrate the carbon lining can be identified and evaluated.

Table 4.4: *Quantitative XRD results of sample sections A_1-A_5*

Sample A	Distance from HZ (mm)	Phase Quantity in wt %							
		Al-Nitride (AlN)	**Chiolite ($Na_5Al_3F_{14}$)**	**Cryolite (Na_3AlF_6)**	**Fluorite (CaF_2)**	**Graphite 2H_**	**beta Diaoyudaoite ($NaAl_{11}O_{17}$)**	**Sodium CN (NaCN)**	**Villiaumite (NaF)**
A1	**5.49**	N/d	N/d	3.79±0.69	2.12±0.14	76.78±3.28	6.94±0.82	0.27±0.002	10.11±0.14
A2	**12.24**	1±0.02	N/d	3.41±0.45	1.48±0.57	81.71±3.71	2.82±0.16	0.6±0.001	8.97±0.22
A3	**19.07**	0.8±0.001	N/d	5.41±0.56	1.57±0.47	80.46±3.69	3.18±0.62	0.59±0.01	7.99±0.56
A4	**27.07**	N/d	N/d	7.68±0.6	1.53±0.13	79.92±3.52	2.66±0.52	N/d	8.21±0.78
A5	**33.77**	0.77±0.002	N/d	5.81±0.47	1.44±0.21	80.54±3.73	3.47±0.68	0.71±0.01	7.26±0.63

Table 4.5: *Quantitative XRD results of sample sections B_1-B_5*

Sample B	Distance from HZ (mm)	Phase Quantity wt%							
		Al-Nitride (AlN)	Chiolite ($Na_5Al_3F_{14}$)	Cryolite (Na_3AlF_6)	Fluorite (CaF_2)	Graphite 2H_	beta Diaoyudaoite $NaAl_{11}O_{17}$	Corundum (Al_2O_3)	Villiaumite (NaF)
B1	**2.52**	0.62±0.03	2.16±0.02	21.22±1.63	2.39±0.81	66.35±1.28	4.5±0.23	1.78±0.10	0.98±0.006
B2	**7.38**	1.73±0.01	1.3±0.01	23.05±2.07	1.89±0.22	66.2±1.33	3.86±0.33	1.41±0.12	0.56±0..008
B3	**12.26**	1.75±0.02	0.04±0.01	21±1.52	2.46±0.18	67.36±1.43	4±0.48	0.79±0.02	2.56±0.61
B4	**18.59**	N/d	1.15±0.02	25.77±2.16	2.4±0.11	63.78±1.57	3.96±0.85	0.7±0.01	2.24±0.78
B5	**26.81**	N/d	0.65±0.02	20.6±1.43	2.57±0.10	67.63±1.39	3.69±0.95	0.55±0.001	4.32±0.59

The profile data in Tables 4.4 and 4.5 was used to construct graphs (Figures 4.5 - 4.13) to determine the trend in phase concentration in relation to distance from the cathode-electrolyte interface at different life spans (days of operation). Phases common to both sample sections were drawn on the same graph to compare their concentrations with distance from the cathode-electrolyte interface and to compare their phase compositions with the time they were in operation.

In sample "B" Al-Nitride (AlN, Figure 4.5) was only identified in the first three sections (B_1, B_2 and B_3) and B_1 has a lower concentration than the other sections, while in sample "A" Al-Nitride was identified in A_2, A_3 and A_5. The "B" samples have higher concentrations of Al-Nitride as compared to the "A" samples.

Comparing sections taken from the same distance from the cathode-electrolyte interface: B_3 has a higher AlN concentration than A_2. AlN was not identified in either of the A_4, B_4 and B_5 sample sections.

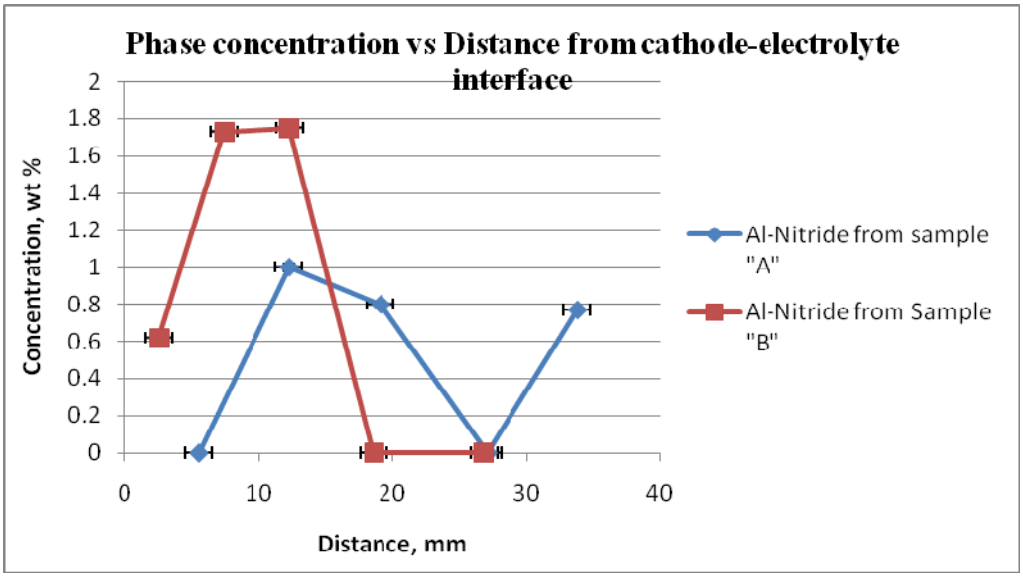

Figure 4.5: *Comparison of the Al-Nitride phase profiles of the two samples (A and B)*

Cryolite (Na_3AlF_6, Figure 4.6) was identified in both the "B" and "A" sample sections. The cryolite content in samples "B" is throughout higher than the "A" sample sections. The "A" sample sections showed a slight increase in cryolite content with increasing distance from the cathode-electrolyte interface while the "B" sample series does not have a distinct trend.

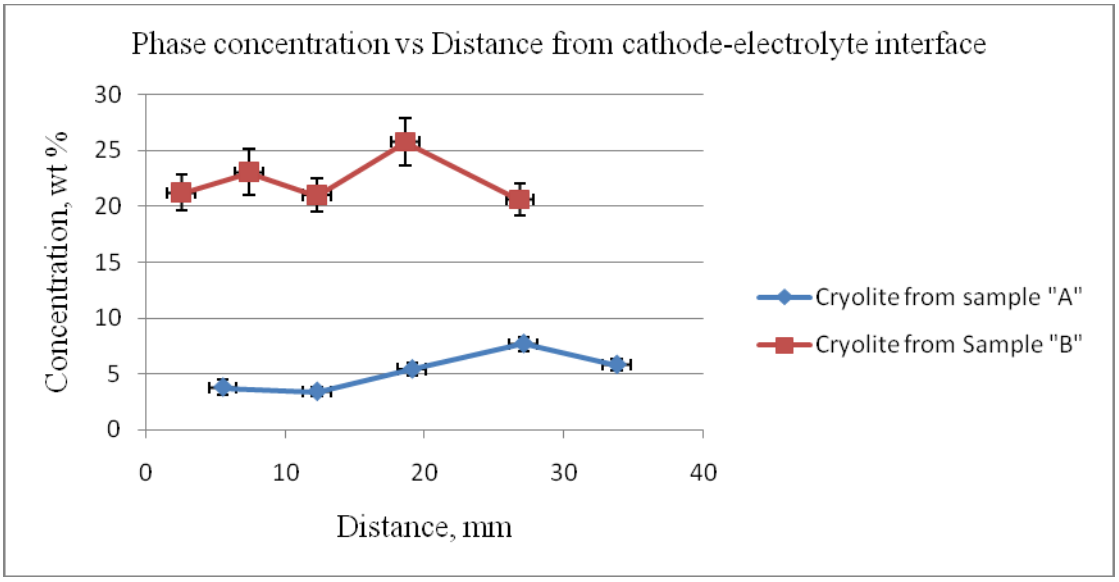

Figure 4.6: *Comparison of the cryolite phase profiles the two samples (A and B)*

Comparing the fluorite content (CaF_2, Figure 4.7) of both samples shows that the "B" sections contain higher concentrations of CaF_2 as compared to the "A" sections. The A_1 section (closest to the carbon cathode-electrolyte interface) has a high fluorite concentration, but with increasing distance from the carbon-electrolyte interface the fluorite content decreases drastically and then remains constant.

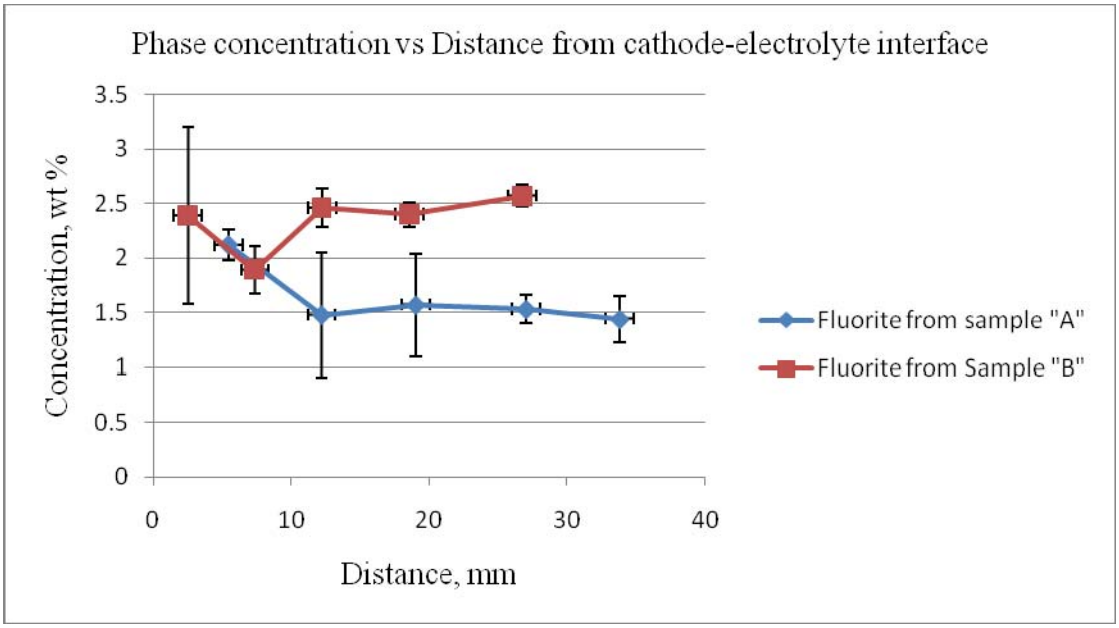

Figure 4.7: *Comparison of the fluorite phase profiles of the two samples (A and B)*

Sample section A_2 (1.48 wt %) has a lower fluorite concentration as compared to sample section B_3 (2.46 wt %). Section B_5 (2.57 wt %) also has a higher fluorite concentration than A_4 (1.53 wt %).

$NaAl_{11}O_{17}$ (Figure 4.8) was identified in both samples (A and B). Sample "B" sections have higher $NaAl_{11}O_{17}$ concentrations as compared to the "A" sample sections. Only the $NaAl_{11}O_{17}$ concentration in sample A_1 exceeded those found in all samples "B" sections.

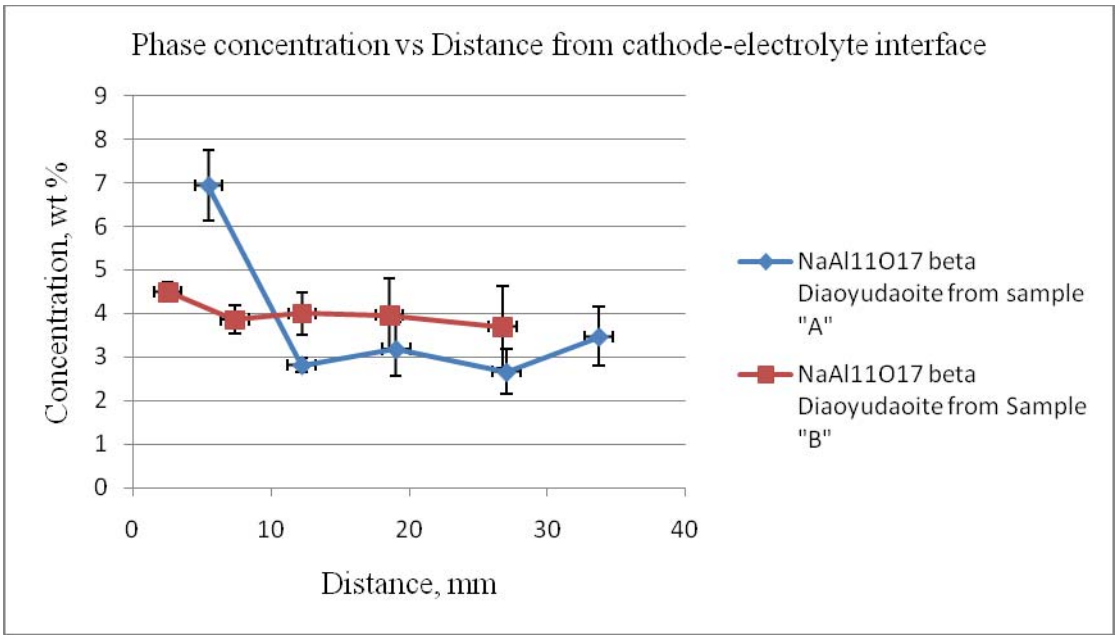

Figure 4.8: *Comparison of the beta Diaoyudaoite phase profiles of the two samples (A and B)*

Villiaumite (NaF, Figure 4.9) concentrations in sample "A" sections are higher than in any of the sample "B" sections. Villiaumite concentration increased with increasing distance from the carbon-electrolyte interface in the sample "B" sections, while sample "A" sections showed a decrease in concentration of villiaumite with increasing distance from the carbon-electrolyte interface.

NaCN, Al_2O_3 and $Na_5Al_3F_{14}$ were not common to both sample "A" or "B" sections. Sodium cyanide (NaCN, Figure 4.10) was identified only in the sample "A" sections. A distinct trend could not be observed.

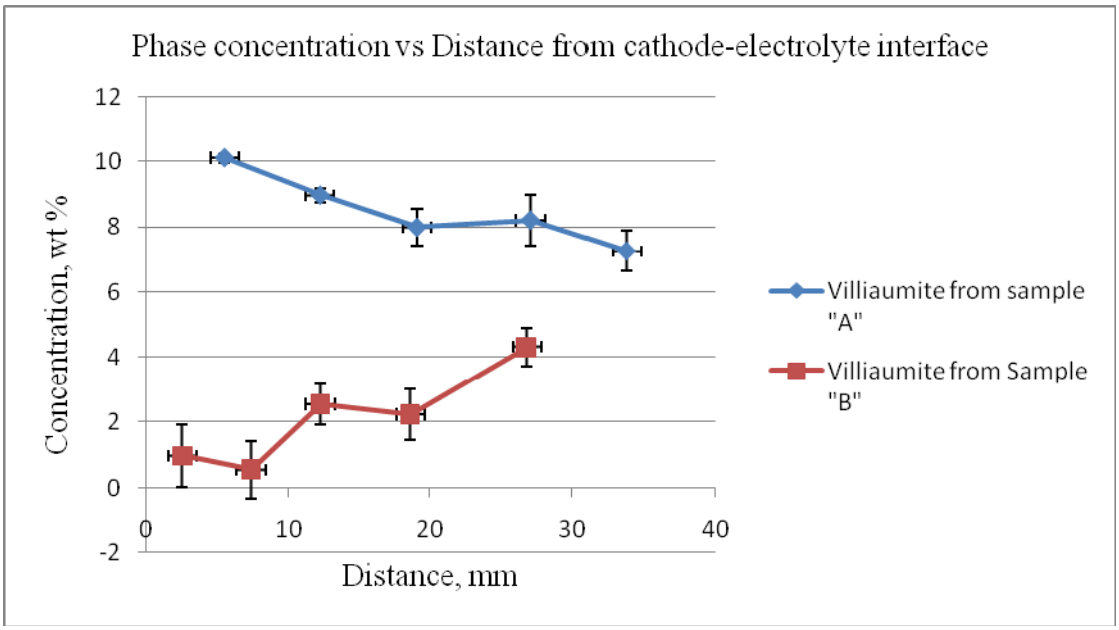

***Figure 4.9**: Comparison of the villiaumite phase profiles of the two samples (A and B)*

.

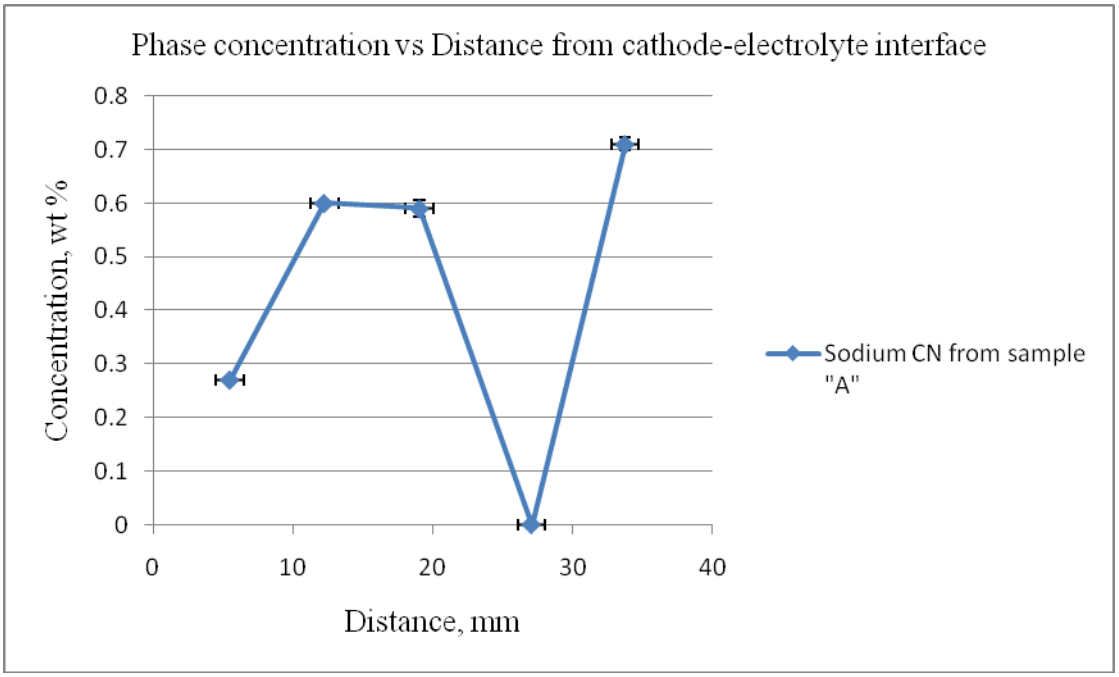

***Figure 4.10**: Sodium cyanide phase profile of "A" samples*

Corundum (Al_2O_3, Figure 4.11) and Chiolite ($Na_5Al_3F_{14}$, Figure 5.12) could only be indentified in sample "B" slices. The concentration of both corundum and chiolite decreases with increasing distance from the cathode-electrolyte interface.

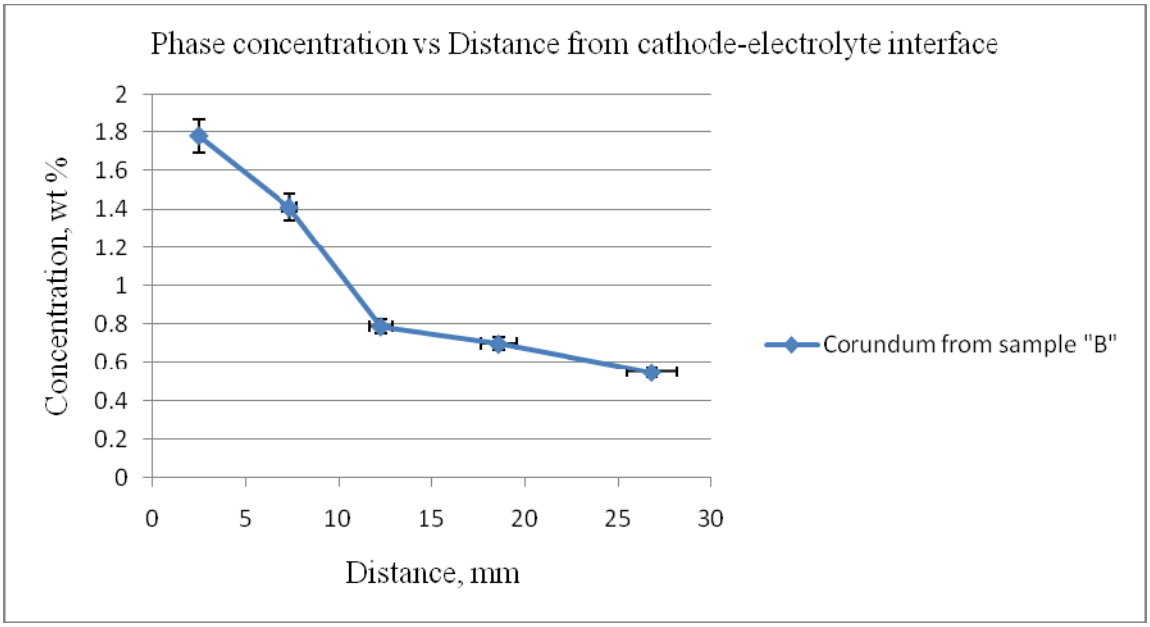

***Figure 4.11**: Corundum phase profile of B samples*

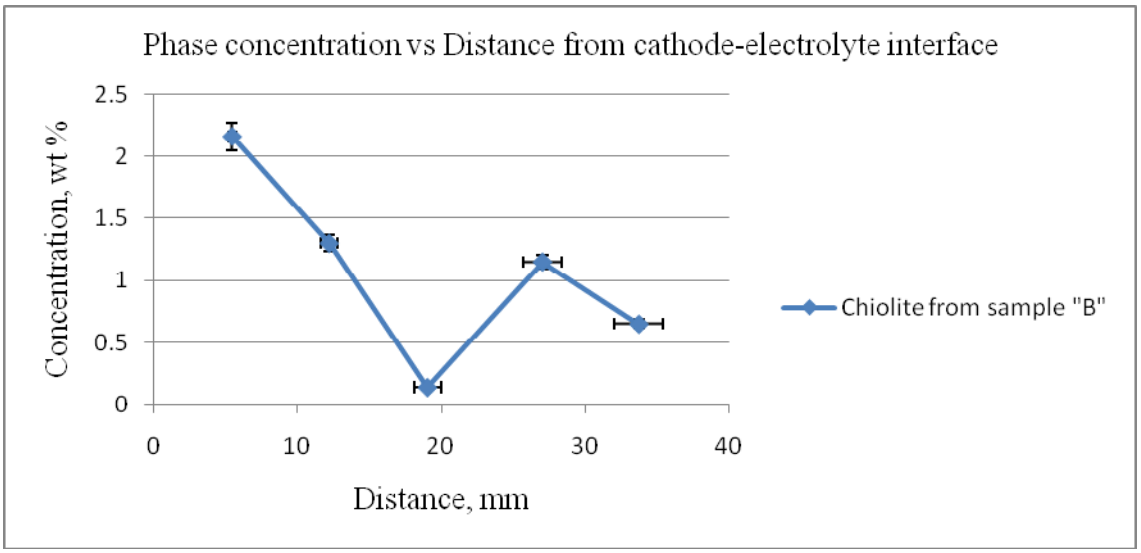

***Figure 4.12**: Chiolite phase profile of B samples*

The graphite concentrations (Figure 4.13) of sample “A” sections are all higher than those in the sample “B” sections. The more non-graphitic phases present in a sample, the lower the concentration of graphite.

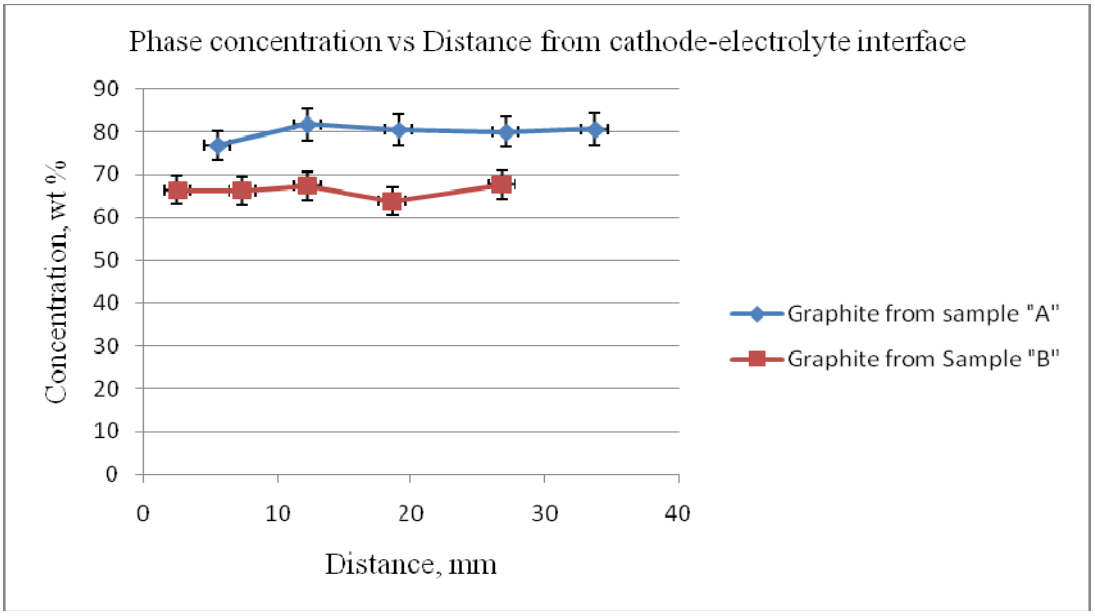

Figure 4.13: *Comparison of the graphite phase profiles of the two samples (A and B)*

4.4.1. Summary of XRD results of post mortem carbon cathode samples

It is observed that the phases were still measurable at the analysed sample depth, this serves the purpose of this study, because the main purpose was to identify and evaluate phases penetrating the carbon lining, hence within this depth penetrated phases can be identified and evaluated.

In both samples “A” and “B” the following phases were identified AlN, Na_3AlF_6, CaF_2, $NaAl_{11}O_{17}$, NaF and graphite phase. NaCN was only identified in sample “A”, while $Na_5Al_3F_{14}$ and Al_2O_3 were only identified in sample “B”.

The sample “B” sections contained more cryolite, fluorite, diaoyudaoite than the “A” sample sections, while the “A” sample sections were more enriched in villiaumite. Cryolite, villiaumite, fluorite and diaoydaoite were identified in the solidified electrolyte, as well as in sample sections “A” and “B”. AlN could be found in both sample sections “A” and “B”, while sample sections “A” also contained NaCN, and sample sections “B” also contained $Na_5Al_3F_{14}$. Al_2O_3 could be found in both the solidified electrolyte and sample sections ”B”.

The emphasis was put on the graphite peak to determine whether it broadens or shifts due to electrolyte penetration or sodium intercalation. Full width at half maximum (FWHM) data was obtained from using the X’Pert Data Viewer software and results are given in Table 4.6.

It could therefore be concluded from Table 4.6 there is no peak broadening and position change as it is shown by the 2θ values and d-spacing values not changing from one sample to the other. The phase and electrolyte penetration does not affect the peak position.

Further sample analysis showed that the analysed post-mortem sample is a hexagonal structure that consists of hexagonal arrays of carbon. The lattice parameters were a=2.39Å and C=6.72Å.

***Table 4.6**: The effect of electrolyte penetration on the graphite peak.*

	Sample number				
Sample	1	2	3	4	5
Virgin carbon cathode					
Position (2θ)	31.00	31.00	31.00	31.00	31.00
d-spacing (Å)	3.37	3.37	3.37	3.37	3.37
FWHM [2θ]	0.220	0.221	0.220	0.220	0.221
A					
Position (2θ)	30.99	30.99	30.99	30.99	30.99
d-spacing (Å)	3.37	3.37	3.37	3.37	3.37
FWHM [2θ]	0.221	0.221	0.220	0.220	0.221
B					
Position (2θ)	31.01	31.01	31.01	31.01	31.01
d-spacing (Å)	3.37	3.37	3.37	3.37	3.37
FWHM [2θ]	0.220	0.220	0.220	0.220	0.221

4.5. SEM analysis results

4.5.1. Introduction

The different slices of samples “A” and “B” were individually hot mounted in Bakelite black resin and polished. Bulk chemical analyses were performed on the two samples “A” and “B”. Arbitrary points were chosen on the polished sections and analysed.

4.5.2. SEM results of sample "A"

Figure 4.14 is the SEM-EDS backscattered electron image used for the bulk elemental analysis of the "A" sample. The chemical elements present in the bulk "A" samples are given in the same Figure 4.14. It also shows the quantity of each element present in the bulk sample.

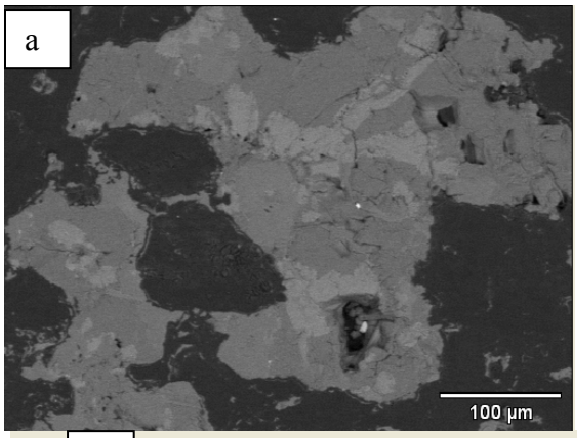

Element Line	Wt%	Wt% error
C K	43.61	±0.21
O K	2.80	±0.21
F K	24.70	±0.51
Na K	7.91	±0.05
Al K	8.62	±0.04
Ca K	1.45	±0.05
N K	1.91	±0.01

b

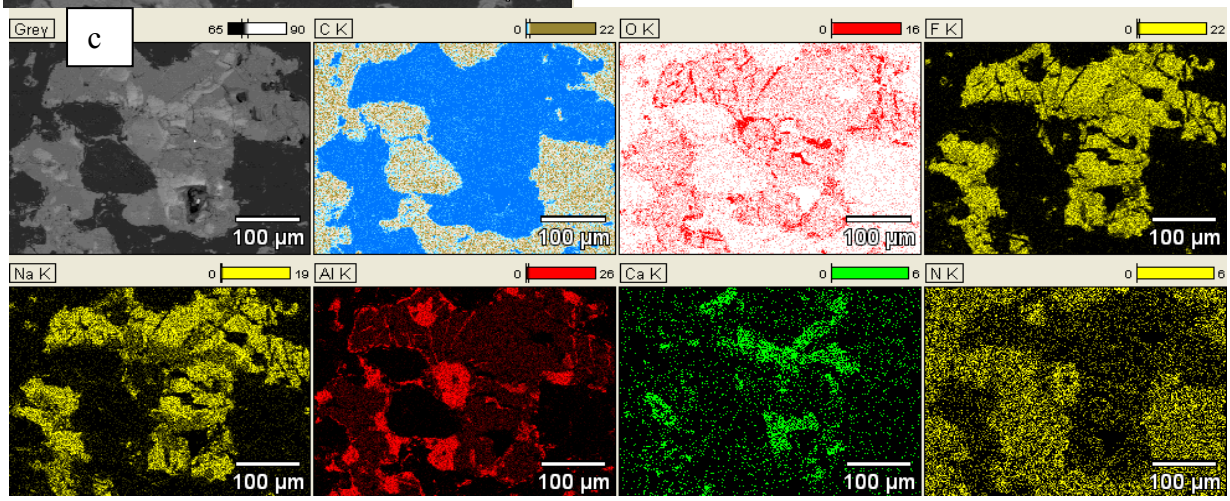

Figure 4.14: *SEM-EDS backscattered elemental analysis of sample "A" (a) Backscattered electron image, (b) concentration of each element and (c)EDS X-ray maps.*

In Figure 4.14 (a) is the sample used for bulk elemental analysis, (b) shows the semi-quantitative concentrations of each detected element using the EDS quantification method, and (c) shows the elemental mapping of the bulk sample.

Electron backscattered images of all sample sections are given in Figures 4.15 – 4.19. Points are marked on these images where EDS analyses of the different phases were performed. From the EDS analyses the stoichiometries of the phases were calculated. The elemental analysis data, as well as the calculated stoichiometries are given in Tables 4.7.-4.11.

The phases NaF, $NaAl_{11}O_{17}$, Na_3AlF_6, CaF_2 and NaCN could be detected in sample section A_1 (Figure 4.15 and Table 4.7). Of these phases NaCN was not found in the solidified electrolyte.

In Table 4.7-4.11, there traces of Na and F on the graphite particle section, is seen as well that in some they appear as NaF phase (Table 4.8). The presence of Na and F could not necessary mean intercalation, but it means they penetrated the carbon cathode through the porous sections of the carbon cathode.

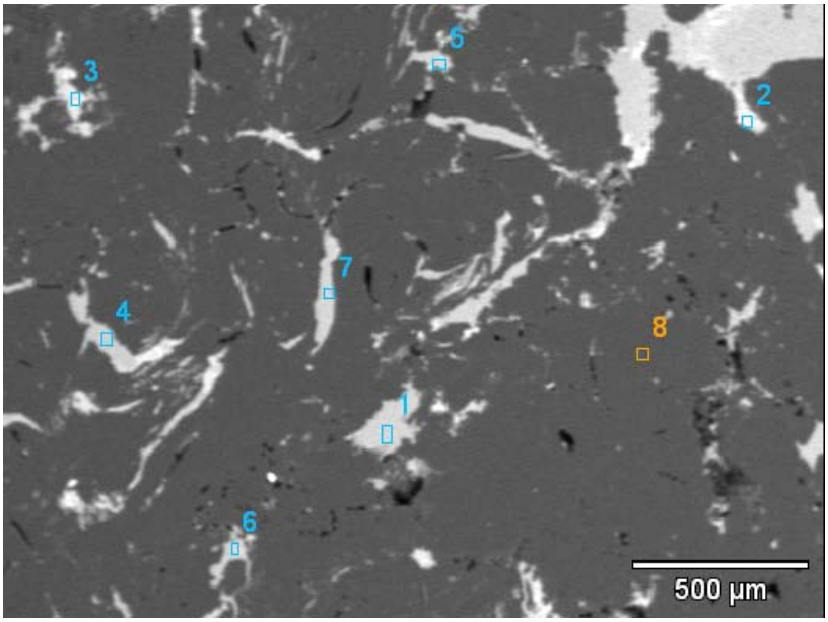

Figure 4.15: *Backscattered electron image of sample A_1 showing penetrated electrolyte and the analysed points*

Table 4.7: *EDS results of possible phases that could be distinguished in sample A_1 (at %)*

Point	**Detected elements in at%**							
	Carbon (C)	Nitrogen (N)	Oxygen (O)	Fluorine (F)	Sodium (Na)	Aluminium (Al)	Calcium (Ca)	Phase or Phases
1	N/d	N/d	N/d	50.52	49.46	0.02	N/d	NaF
2	0.31	N/d	53.08	4.06	6.43	36.07	0.05	NaF and $NaAl_{11}O_{17}$
3	1.32	N/d	0.25	59.63	29.33	9.47	N/d	Na_3AlF_6
4	2.63	N/d	0.74	60.25	19.86	7.53	8.99	CaF_2 and Na_3AlF_6
5	1.32	0.01	59.83	1.67	3.43	33.70	0.04	$NaAl_{11}O_{17}$
6	98.82	N/d	N/d	N/d	0.26	0.81	0.11	Graphite
7	0.16	0.06	0.68	57.24	32.14	9.72	N/d	Na_3AlF_6
8	4.61	4.78	47.79	N/d	7.86	34.72	0.24	$NaAl_{11}O_{17}$ and NaCN

N/d = Not detected

The phases NaF, Na_3AlF_6, $NaAl_{11}O_{17}$, NaCN, CaF_2 and AlN could be detected in sample A_2 (Figure 4.16 and Table 4.8). The presence of both the Na and F in the graphite region possible confirms the intercalation. Of these phases AlN and NaCN were not found in the solidified electrolyte.

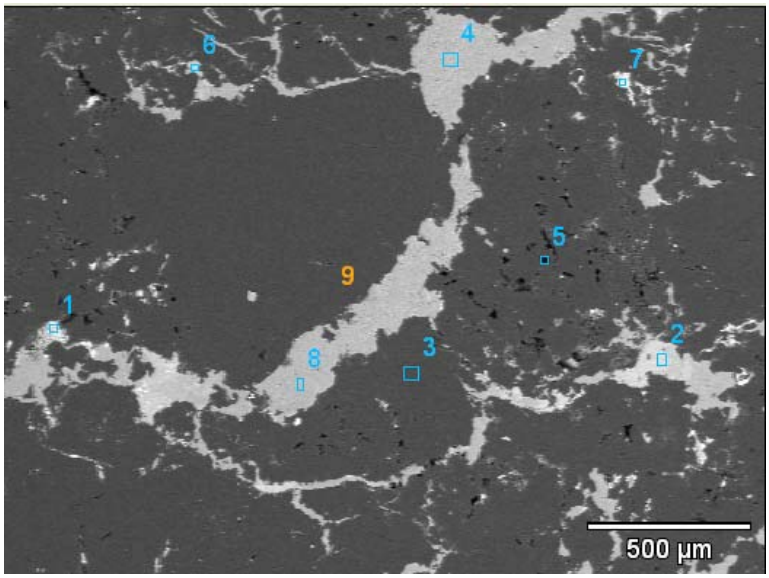

***Figure 4.16**: Backscattered electron image of sample A_2 showing penetrated electrolyte and analysed points*

***Table 4.8**. EDS results of possible phases that could be distinguished in Sample A_2 (at %)*

Point	Detected elements in at %							
	Carbon (C)	Nitrogen (N)	Oxygen (O)	Fluorine (F)	Sodium (Na)	Aluminium (Al)	Calcium (Ca)	Phase or Phases
1	3.93	N/d	0.92	51.91	43.24	N/d	N/d	NaF
2	0.46	0.26	N/d	59.88	29.79	9.61	N/d	Na_3AlF_6
3	0.14	N/d	59.78	1.62	32.98	4.62	0.86	$NaAl_{11}O_{17}$
4	21.34	22.68	0.65	19.29	35.93	N/d	0.11	NaF and NaCN
5	N/d	N/d	0.26	59.78	20.68	0.81	18.47	NaF and CaF_2
6	0.53	25.61	0.18	26.28	22.36	24.72	0.30	AlN and NaF
7	98.03	N/d	N/d	0.86	0.87	0.24	N/d	Gaphite and NaF
8	0.04	N/d	N/d	61.73	28.71	9.52	N/d	Na_3AlF_6

N/d = Not detected

Although sample A_3 has a very low nitrogen concentration, two nitrogen-containing phases, namely NaCN and AlN, could be distinguished. Other phases that could be detected are NaF, Na_3AlF_6, $NaAl_{11}O_{17}$ and CaF_2.

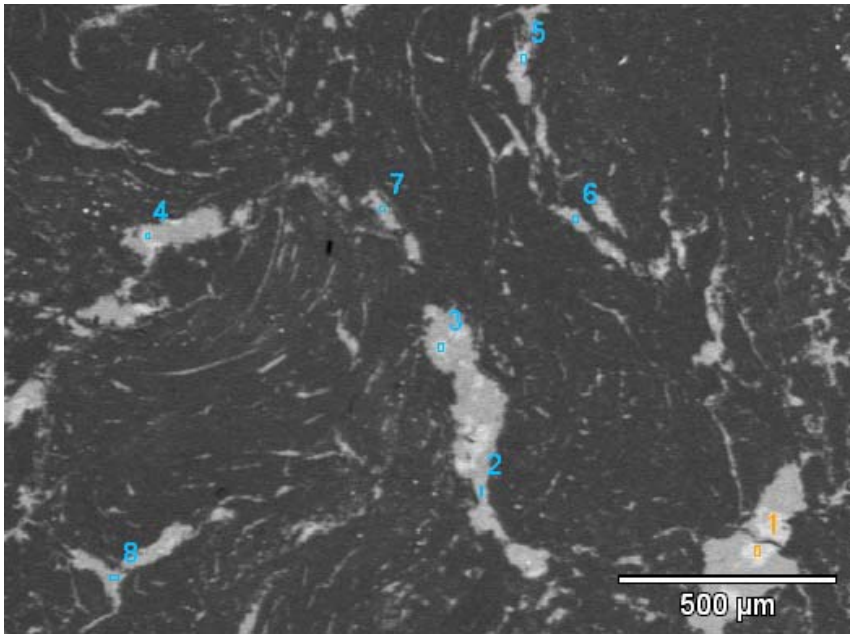

***Figure 4.17**. Backscattered electron image of sample A_3, showing penetrated electrolyte and the analysed points*

***Table 4.9:** EDS results of possible phases that could be distinguished in Sample A_3 (at %)*

Point	**Detected elements in at %**							
	Carbon (C)	Nitrogen (N)	Oxygen (O)	Fluorine (F)	Sodium (Na)	Aluminium (Al)	Calcium (Ca)	Phase or Phases
1	0.39	N/d	58.10	0.11	4.82	35.62	0.96	$NaAl_{11}O_{17}$
2	0.05	N/d	0.08	48.89	50.26	0.72	N/d	NaF
3	19.15	44.67	N/d	0.36	19.78	18.82	0.22	NaCN and AlN
4	0.18	N/d	N/d	59.78	30.06	9.98	N/d	Na_3AlF_6
5	N/d	N/d	0.19	66.80	0.39	N/d	32.81	CaF_2
6	0.81	N/d	N/d	58.30	32.41	8.16	0.13	Na_3AlF_6 and NaF
7	96.87	N/d	0.02	0.33	2.62	0.16	N/d	Graphite
8	0.03	N/d	0.06	48.28	50.81	0.82	N/d	NaF

N/d = Not detected

In sample A_4 only the electrolyte reaction product $NaAl_{11}O_{17}$, together with cryolite (Na_3AlF_6), NaF and CaF_2 could be distinguished (Figure 4.18 and Table 4.10).

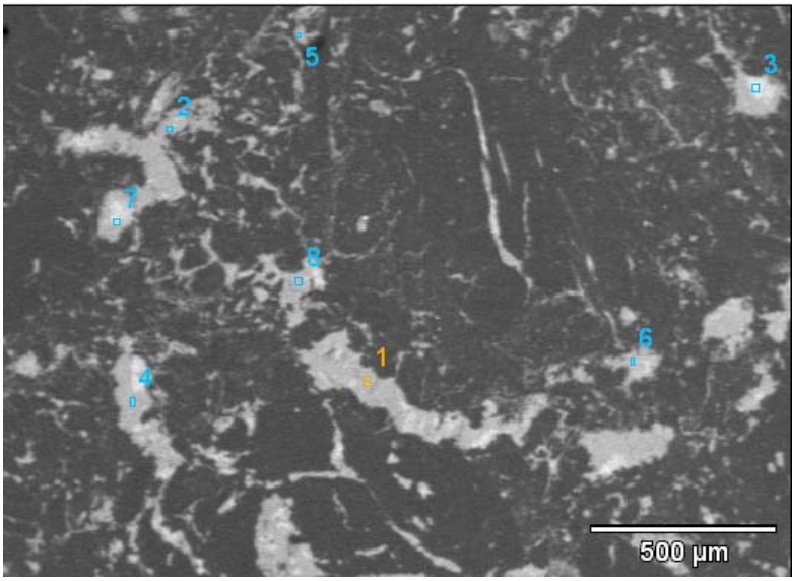

***Figure 4.18**. Backscattered electron image of sample A_4, showing penetrated electrolyte and the analysed points*

***Table 4.10**: EDS results of possible phases that could be distinguished in Sample A_4 (at %)*

Point	**Detected elements in at %**							
	Carbon (C)	Nitrogen (N)	Oxygen (O)	Fluorine (F)	Sodium (Na)	Aluminium (Al)	Calcium (Ca)	Phase or Phases
1	0.07	N/d	N/d	61.45	28.78	9.62	0.08	Na_3AlF_6
2	1.62	0.02	57.14	0.58	3.12	37.52	N/d	$NaAl_{11}O_{17}$
3	98.72	N/d	N/d	N/d	1.16	0.12	N/d	Graphite
4	0.79	0.03	0.19	65.16	1.68	N/d	32.15	CaF_2
5	0.72	N/d	0.21	49.19	49.42	0.46	N/d	NaF
6	0.81	N/d	0.46	48.10	49.86	0.73	0.04	NaF
7	1.24	N/d	N/d	61.35	27.13	10.28	N/d	Na_3AlF_6
8	0.26	N/d	N/d	58.81	31.71	9.17	0.05	Na_3AlF_6 and NaF

N/d = Not detected

Two phases that contain nitrogen (points 3, 4 and 7 in Figure 4.19 and Table 4.11) could be detected in sample A_5, namely NaCN and AlN. These are reaction products that formed in the carbon cathode. The phases Na_3AlF_6, NaF, $NaAl_{11}O_{17}$ and CaF_2 resulted from electrolyte that penetrated the carbon cathode.

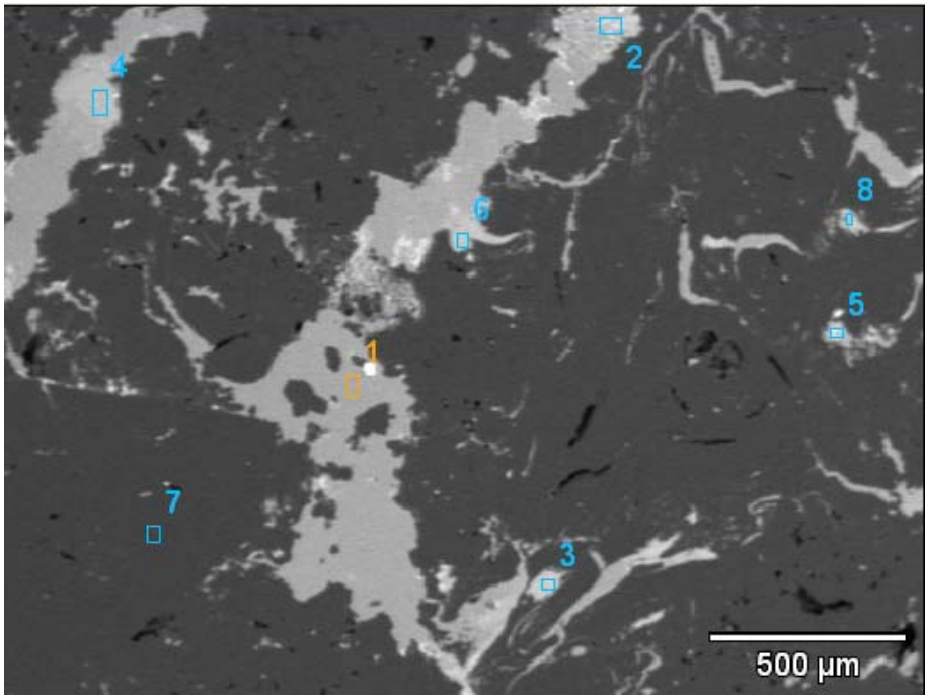

***Figure 4.19**. Backscattered electron image of sample A_5, showing penetrated electrolyte and the analysed points*

Table 4.11: *EDS results of possible phases that could be distinguished in Sample A_5 (at %)*

Point	**Detected elements in at %**							
	Carbon (C)	Nitrogen (N)	Oxygen (O)	Fluorine (F)	Sodium (Na)	Aluminium (Al)	Calcium (Ca)	Phase or Phase
1	0.48	0.01	N/d	62.72	24.95	11.78	0.06	Na_3AlF_6
2	1.06	N/d	N/d	45.58	51.63	1.73	N/d	NaF
3	8.28	7.86	0.06	46.84	28.74	8.22	N/d	Na_3AlF_6 and NaCN
4	0.42	25.67	N/d	24.29	24.28	25.02	0.26	NaF and AlN
5	0.36	N/d	58.74	0.28	4.69	35.93	N/d	$NaAl_{11}O_{17}$
6	1.63	N/d	N/d	33.05	0.16	N/d	65.16	CaF_2
7	0.21	26.72	0.32	26.51	23.46	22.78	N/d	NaF and AlN
8	97.86	N/d	N/d	0.51	1.29	0.34	N/d	Graphite

N/d = Not detected

4.5.3. SEM results of "B" samples

Figure 4.20 is the SEM-EDS backscattered electron image used for the bulk chemical analysis of the "B" sample. The chemical elements present in the bulk "B" samples are given in the same Figure 4.20. It also shows the quantity of each element present in the bulk sample

a

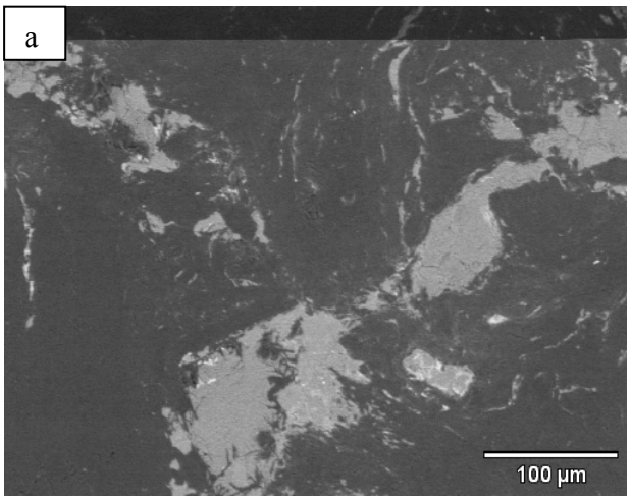

b

Element Line	Wt%	Wt% error
C K	45.97	±0.53
O K	3.62	±0.73
F K	21.01	±0.59
Na K	8.63	±0.16
Al K	9.52	±0.11
Ca K	2.02	±0.27
N K	1.23	±0.03

c

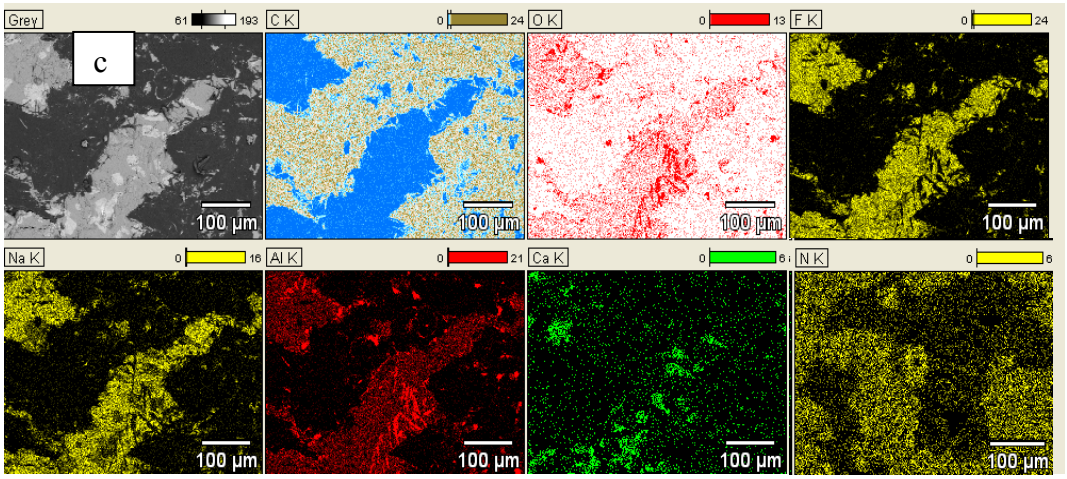

Figure 4.20: *SEM-EDS backscattered elemental analysis of sample "B" (a) Backscattered electron image, (b) concentration of each element and (c) EDS X-ray maps.*

The bulk elemental analysis of sample "B" showed all the possible elements that could be identified from the electrolysed sample. In Figure 4.20 (c) elemental mapping shows the position of each element in the bulk sample.

The only nitrogen-containing phase that could be identified in sample B_1 is AlN (point 4, Figure 4.21 and Table 4.12). Na_3AlF_6, NaF, CaF_2, Al_2O_3 and $NaAl_{11}O_{17}$ could also be distinguished in this sample, which are all phases that originated from the electrolyte. $Na_5Al_3F_{14}$ was also found in sample B_1, which could not be found in the electrolyte.

The same observation from samples "A" analysis was seen on sample "B" where Na and F are seen on the graphite particle sections.

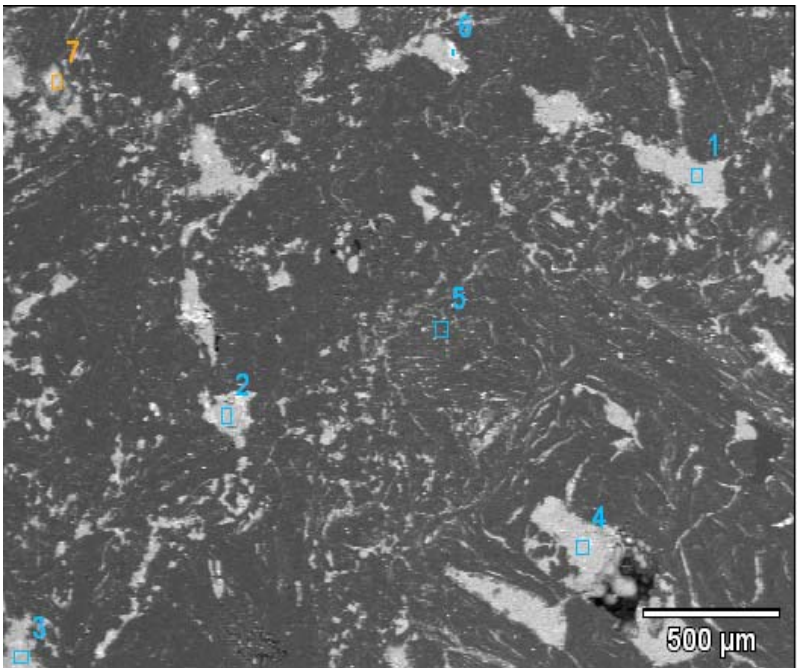

***Figure 4.21**: Backscattered electron image of sample B_1, showing penetrated electrolyte and the analysed points*

***Table 4.12:** EDS results of possible phases that could be distinguished in Sample B_1 (at %)*

Point	**Detected elements in at %**							
	Carbon (C)	Nitrogen (N)	Oxygen (O)	Fluorine (F)	Sodium (Na)	Aluminium (Al)	Calcium (Ca)	Phase or Phases
1	N/d	N/d	N/d	60	26.67	6.54	6.63	Na_3AlF_6, NaF and CaF_2
2	0.23	N/d	0.14	63.63	20	12	4	$Na_5Al_3F_{14}$ and CaF_2
3	0.03	N/d	44.83	12.26	12.26	30.61	0.01	NaF and Al_2O_3
4	0.06	25.17	0.02	23.09	23.81	26.94	N/d	NaF and AlN
5	N/d	N/d	52.69	0.06	13.45	33.80	N/d	$NaAl_{11}O_{17}$
6	96.98	N/d	N/d	0.88	1.62	0.52	N/d	Graphite
7	N/d	N/d	N/d	61.53	31.33	7.10	0.04	Na_3AlF_6 and NaF

N/d = Not detected

The phases AlN and $Na_5Al_3F_{14}$ were detected in sample B_2, which did not originate from the electrolyte (Point 6, Figure 4.22 and Table 4.13). Na_3AlF_6, Al_2O_3, CaF_2, NaF and $NaAl_{11}O_{17}$ could also be distinguished in sample B_2, which are all associated with the electrolyte.

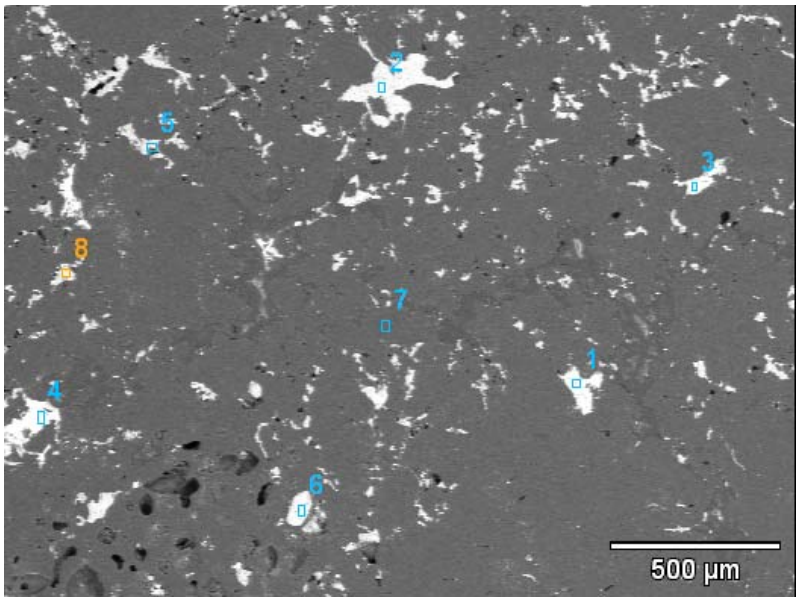

***Figure 4.22**: Backscattered electron image of sample B_2, showing penetrated electrolyte and the analysed points*

***Table 4.13**: EDS results of possible phases that could be distinguished in Sample B_2 (at %)*

Point	**Detected elements in at %**							
	Carbon (C)	Nitrogen (N)	Oxygen (O)	Fluorine (F)	Sodium (Na)	Aluminium (Al)	Calcium (Ca)	Phase or Phases
1	N/d	N/d	21.82	37.06	21.64	19.64	N/d	Na_3AlF_6 and Al_2O_3
2	0.26	N/d	0.50	59.83	30.38	9.03	N/d	Na_3AlF_6
3	0.03	N/d	0.025	62	21.42	12.03	4.5	$Na_5Al_3F_{14}$ and CaF_2
4	0.01	N/d	54.86	3.22	6.95	34.96	N/d	NaF and $NaAl_{11}O_{17}$
5	94.24	N/d	N/d	4.02	0.90	0.65	0.20	Graphite
6	N/d	4.17	N/d	58.33	20.83	16.67	N/d	$Na_5Al_3F_{14}$ and AlN
7	0.36	0.03	N/d	59.12	31.01	9.48	N/d	Na_3AlF_6 and NaF
8	N/d	4.14	N/d	57.34	21.73	16.79	N/d	$Na_5Al_3F_{14}$ and AlN

N/d = Not detected

Signs of bath penetration and phase formation could only be observed in certain areas of sample B_3. All the phases that are associated with the electrolyte could be distinguished

(Na_3AlF_6, $NaAl_{11}O_{17}$, Al_2O_3, CaF_2 and NaF), as well as reaction products $Na_5Al_3F_{14}$ and AlN (Figure 4.23 and Table 4.14).

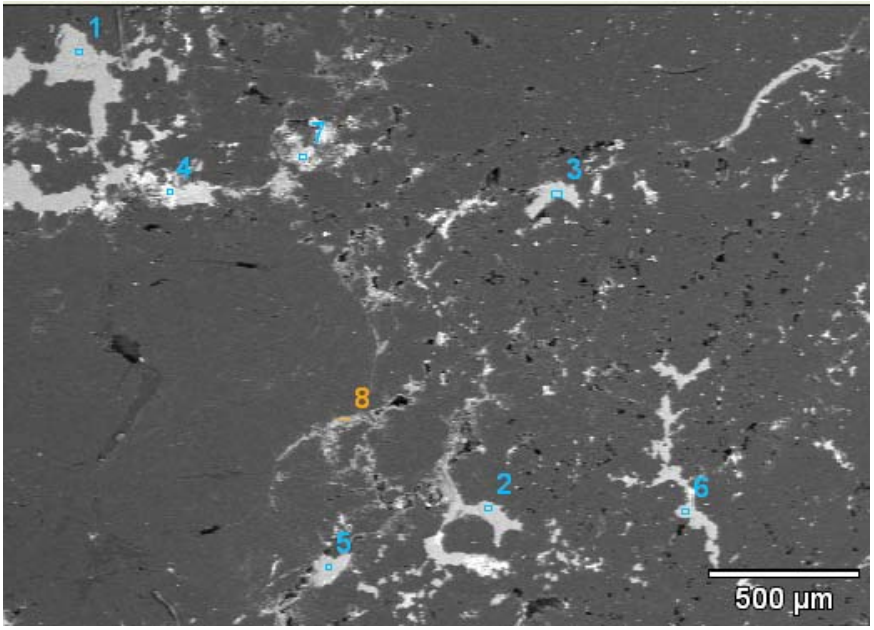

***Figure 4.23**: Backscattered electron image of sample B_3, showing penetrated electrolyte and the analysed points*

***Table 4.14**: EDS results of possible phases that could be distinguished in Sample B_3 (at %)*

Point	**Detected elements in at %**							
	Carbon (C)	Nitrogen (N)	Oxygen (O)	Fluorine (F)	Sodium (Na)	Aluminium (Al)	Calcium (Ca)	Phase or Phases
1	N/d	N/d	0.74	64.24	18.97	16.03	0.02	Na_3AlF_6 and $Na_5Al_3F_{14}$
2	0.13	N/d	51.68	0.45	32.92	14.68	0.14	$NaAl_{11}O_{17}$
3	0.56	16.63	33.86	0.89	0.82	46.86	0.38	Al_2O_3 and AlN
4	0.2	19.6	N/d	39.92	0.77	20.08	19.07	AlN and CaF_2
5	0.58	N/d	N/d	68.76	0.23	N/d	30.43	CaF_2
6	0.27	N/d	N/d	59.81	28.68	11.24	N/d	Na_3AlF_6
7	1.17	N/d	N/d	52.61	46.22	N/d	N/d	NaF
8	98.26	N/d	N/d	0.16	1.58	N/d	N/d	Graphite

N/d = Not detected

A very low concentration of reaction products was found in sample B_4. There is a higher degree of bath penetration (associated with the phases CaF_2, Na_3AlF_6, $NaAl_{11}O_{17}$ and NaF) than reaction products (associated with $Na_5Al_3F_{14}$) in this section (Figure 4.24 and Table 4.15).

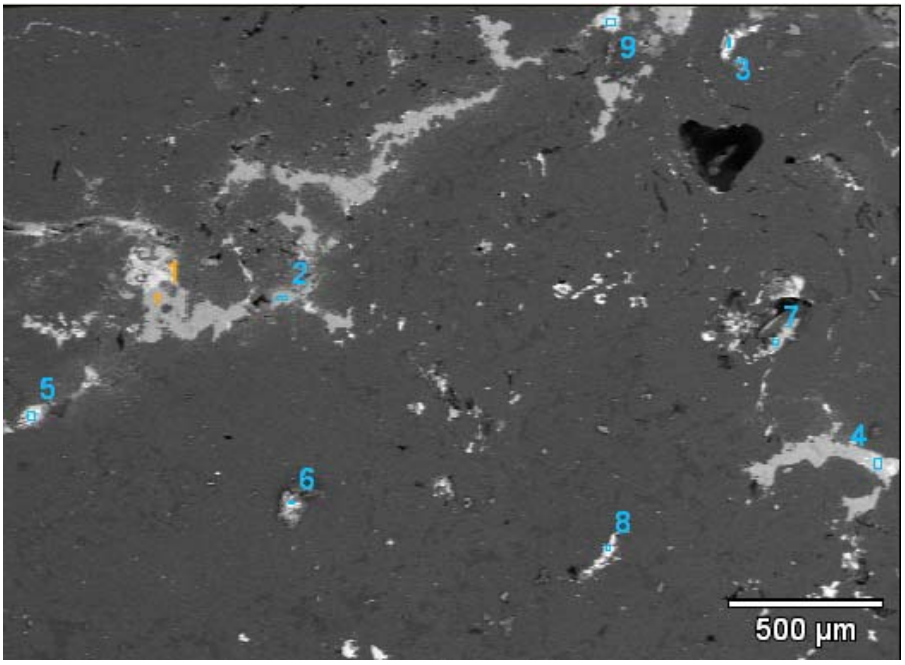

Figure 4.24: *Backscattered electron image of sample B_4, showing penetrated electrolyte and analysed points.*

***Table 4.15**: EDS results of possible phases that could be distinguished in Sample B_4 (at %)*

Point		**Detected elements in at %**						
	Carbon (C)	Nitrogen (N)	Oxygen (O)	Fluorine (F)	Sodium (Na)	Aluminium (Al)	Calcium (Ca)	Phase or Phases
1	0.21	N/d	N/d	65.48	0.88	0.63	32.80	CaF_2
2	N/d	N/d	0.10	58.16	31.21	10.53	N/d	Na_3AlF_6
3	N/d	N/d	59.29	0.41	3.61	36.69	N/d	$NaAl_{11}O_{17}$
4	0.11	N/d	0.61	62.38	21.68	14.24	0.98	$Na_5Al_3F_{14}$
5	0.06	N/d	N/d	50.16	49.21	0.57	N/d	NaF
6	N/d	N/d	N/d	59.46	32.64	7.90	N/d	Na_3AlF_6 and NaF
7	0.62	N/d	0.17	62.58	22.17	6.50	7.96	Na_3AlF_6 and CaF_2
8	98.71	0.02	N/d	N/d	1.17	0.10	N/d	Graphite
9	N/d	N/d	58.20	0.32	4.38	37.10	N/d	$NaAl_{11}O_{17}$

N/d = Not detected

Only the reaction product $Na_5Al_3F_{14}$ could be identified in sample B_5 (Figure 4.25 and Tale 4.16). The phases NaF, $NaAl_{11}O_{17}$, Na_3AlF_6, CaF_2 and Al_2O_3 could also be found in this sample, due to electrolyte that penetrated the cathode.

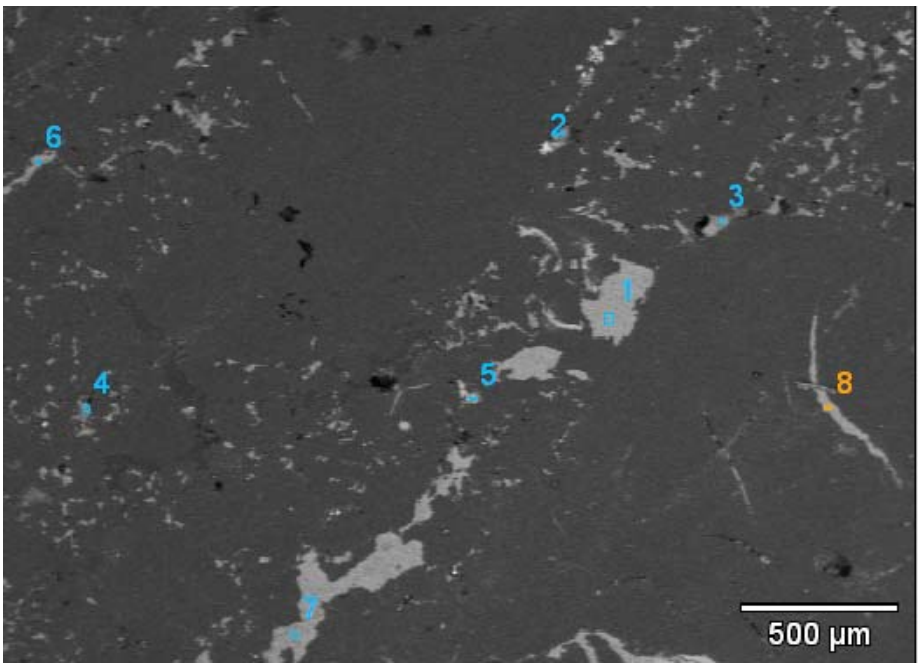

***Figure 4.25**: Backscattered electron image of sample B_5, showing penetrated electrolyte and the analysed points*

***Table 4.16:** EDS results of possible phases that could be distinguished in Sample B_5 (at %)*

Point	**Detected elements in at %**							
	Carbon (C)	Nitrogen (N)	Oxygen (O)	Fluorine (F)	Sodium (Na)	Aluminium (Al)	Calcium (Ca)	Phase or Phases
1	0.14	N/d	N/d	63.67	23.20	12.81	0.18	$Na_5Al_3F_{14}$
2	2.24	N/d	N/d	49.87	46.21	1.68	N/d	NaF
3	N/d	0.01	0.36	68.72	18.42	11.63	0.86	$Na_5Al_3F_{14}$
4	1.19	N/d	60.18	N/d	4.68	33.95	N/d	$NaAl_{11}O_{17}$
5	2.16	0.03	N/d	63.23	17.93	7.69	8.96	Na_3AlF_6 and CaF_2
6	1.68	N/d	N/d	57.48	30.89	7.32	2.63	Na_3AlF_6 and NaF
7	0.17	N/d	61.62	0.78	1.29	36.14	N/d	Al_2O_3
8	98.16	N/d	N/d	0.30	0.68	0.42	0.44	Graphite

N/d = Not detected

4.6. Summary and conclusions

Stereo microscopic results showed that there is a higher degree of alteration of the cathode material "B" than cathode material "A" although cathode "B" had a shorter life than cathode "A". Larger open pores could be distinguished in cathode "A" than in cathode "B", although more wear is associated with cathode sample "B",

The bath constituents penetrated both carbon linings "A" and "B". The phases cryolite (Na_3AlF_6), villiaumite (NaF), fluorite (CaF_2) and diaoyudaiote ($NaAl_{11}O_{17}$) could be distinguished in the solidified electrolyte, as well as in cathode samples "A" and "B". Al_2O_3 could only be distinguished in the solidified electrolyte and in cathode sample "B". XRD analysis indicated that sample "B" has higher concentration of Na_3AlF_6 than sample "A", and also contained $Na_5Al_3F_{14}$, which could not be identified in the solidified electrolyte and in sample "A". Chiolite ($Na_5Al_3F_{14}$) is formed according to equation 4.1, when cryolite (Na_3AlF_6) is heated above 734°C with liquid aluminium fluoride (AlF_3) [38] :

$$5Na_3AlF_6 + 4AlF_3 = 3Na_5Al_3F_{14} \qquad 4.1$$

It can therefore be assumed that the temperature associated with cathode sample "B" exceeded 734°C.

Both cathode samples "A" and "B" contain the reaction product AlN, while NaCN could only be found in sample "A". These two reaction products form according to the following reactions [10]:

$3/2N_2(g) + 3C(s) + 3Na(\text{in } C) = 3NaCN(l)$……4.2

$1/2N_2(g) + Na_3AlF_6(l) + 3Na(\text{in } C) = AlN(s) + 6NaF(l)$……4.3

Wear of the industrial carbon cathode samples proceeded mainly through penetration of electrolyte into the carbon cathode, but also through the formation of the reaction products NaCN and AlN.

Chapter 5: Results of laboratory scale experiments

This chapter is comprised of experimental observations and results of the laboratory electrolysis experiments. It also includes the pore size distribution results obtained using the ImageJ tool analysis tool.

5.1. Pore size distribution analysis

Every carbon cathode material has a degree of porosity depending on the particle size distribution, firing temperature and degree of graphitisation. The structure of the carbon cathode is developed during the forming and baking stages [19]. The porosity and pore size distribution of the carbon cathode have a direct influence on the penetration of sodium and electrolyte into the cathode lining during the electrolysis of aluminium.

To determine the pore size distribution of the carbon cathode material, two carbon grades (30% graphitised and 100 % graphitised) were examined.

5.1.1. Method of analysis

Two specimens were cut from each of the carbon grades. The specimen sizes were 5mm thick and 25mm in diameter. The specimens were cold mounted in resin and allowed to set for 24 hours. The mounted specimens were ground and polished using 600µm – 2400µm grinding paper.

Thirty arbitrary micrographs of each specimen were analysed at the same magnification. The images were analysed using the ImageJ software (Java-based image processing programme developed at the National Institute of Health). The image analyses were conducted at different pore sizes.

5.1.2. Results

The results of the two carbon grade samples are given in Figure 5.1. The graph illustrates cumulative data of pore size that occupy certain area within the carbon cathode. The arbitrary chosen ranges were 1-5µm, 5-10µm, 10-20µm, 20-50µm, 50-100µm, 100-200µm,

and 200-400µm and +400µm. The results of the pores with +400µm diameters were not included because they occupy a very small area (about 0.0005%) of the surface.

5.1.3. Comparison of the results

100% graphitised carbon cathode material has a greater fraction of pores within the 1-5µm, 5-10µm size ranges than the 30% graphitised carbon. The two cathode materials have the same fraction of pores in the 10-20µm size range. The 30% graphitised carbon has more pores in the ranges 20-50µm, 50-100µm, 100-200µm and 200-400µm size range, than the 100% graphitised carbon. The 100% graphitised carbon mostly contains small pores (1-5µm) while in the 30% graphitised carbon most of the pores are within the diameter range of 200-400µm.

5.1.4. Conclusion

The 30% graphitised carbon provides larger penetration channels for the electrolyte and sodium to penetrate the carbon cathode than the 100% graphitised carbon. Cumulatively, the 30% graphitised has more pores than the 100% graphitised carbon.

5.2. Experimental Results

Aluminium electrolysis and sodium expansion experiments were performed in the laboratory on 30% graphitised (Sample C) and 100% graphitised cathode samples (Sample D). During the electrolysis experiments, the carbon cathodes were subjected to sodium and bath infiltration and during the sodium expansion experiments the carbon cathodes were subjected to a sodium rich environment. The experimental results are divided into two parts:

Part I – Electrolysis results

- Quantitative XRD results
- Microstructural analysis
- SEM-EDS results

Part II – Rapoport Results

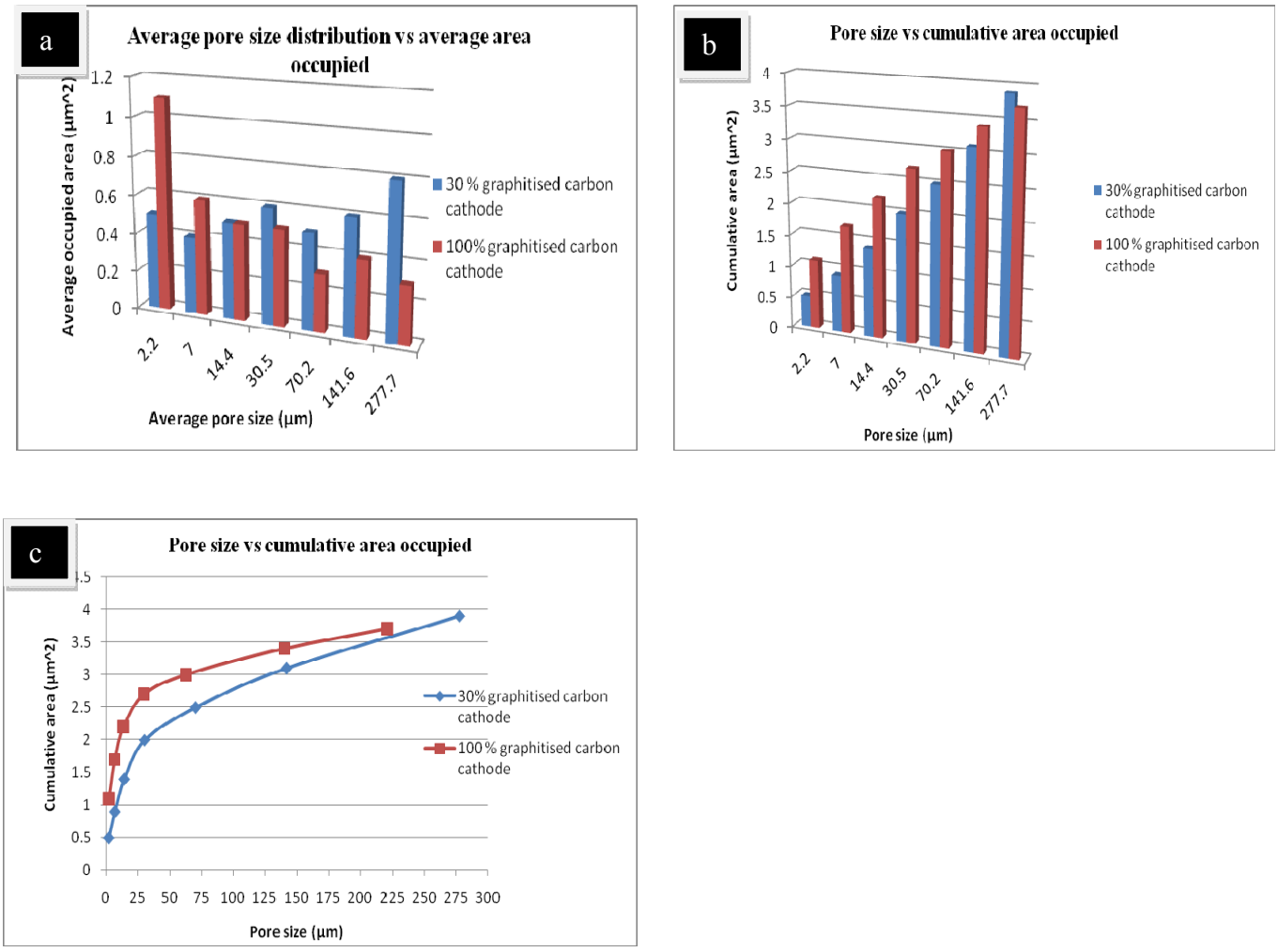

Figure 5.1: *Pore size distribution bar graphs in carbon cathodes (a) average pore size occupying certain area (b) cumulative area occupied at given pore size(c) line graph for pore size vs cumulative area occupied*

5.3. Electrolysis results

5.3.1. Experimental observations

Electrolysis experiments were performed for different time periods. The first experiment was performed for 1hr 30minutes and the second was performed for 3 hours.

Table 5.1 shows the experiment data collected during the 1hr 30 minutes experiment. After 35minutes the current diminished, thus causing the voltage to increase. This was the result of the anode being consumed. At this point the anode was lowered 1mm below the molten bath and the voltage became stable again at 4.5 V. The voltage increased again after 70 minutes, after which the anode was lowered again and the voltage stabilised once more. The anode was adjusted twice during the 1hr30minute experiment.

Table 5.1 *Currrent, voltage and dissociation voltage during the electrolysis process*

Time (min)	Current (Amp)	Voltage (V)	Dissociation Voltage (V)
0	28	4.5	0
5	28	4.5	1.2
10	28	4.5	1.2
15	28	4.5	1.2
20	28	4.5	1.2
25	28	4.5	1.2
30	28	4.5	1.2
35	26	5.0	1.3
40	28	4.5	1.2
45	28	4.5	1.2
50	28	4.5	1.2
55	28	4.5	1.2
60	28	4.5	1.2
65	28	4.5	1.2
70	25	5.1	1.3
75	28	4.5	1.2
80	28	4.5	1.2
85	28	4.5	1.2
90	28	4.5	1.2

The current interrupter method was used to check the dissociation voltage which was found to be 1.2V throughout the experiment. After 1hr 30 minutes the furnace was cooled to 420ºC. After removing the experimental setup from the furnace, it was observed that approximately 20% (by mass) of the carbon anode was consumed. The inlet gas pipe was broken, and the alumina tube was slightly consumed (approximately 1% by mass). The carbon crucible was not oxidised as expected. The molten bath bubbled into the carbon crucible holder. A hammer was used to break the carbon crucible. After removing the solidified molten cryolite bath, aluminium metal pieces were observed on the surface of the sample. The aluminium metal pieces weighed approximately 4g. During the 3hr experiment the same observation was made except that the anode was adjusted four times and the anode was 60% consumed (by mass). The observed aluminium metal pieces weighed approximately 7g.

5.3.2. Analysis of cathode samples

X-ray diffraction analysis (XRD), scanning electron microscopy (SEM/EDS), reflected light and stereo microscopy were used to analyse the electrolysed carbon cathode samples.

5.3.2.1. X-ray diffraction analysis

The diffractograms of only the two virgin materials are given in this chapter (Figures 5.2 and 5.3). The rest of the diffractograms are given in Appendix A. The semi-quantitative XRD results of all the samples are given in Table 5.2. The 30% graphitised carbon has more amorphous concentration as compared to the 100% graphitised cathode. Profiles of the amount of each phase as a function of the depth at which this phase was detected in the cathode, were drawn. Phase profiles were drawn on the same figure in circumstances where the same phase was detected in both carbon grades after the same electrolysis period.

Only two phases (graphite and silicon) were identified in the virgin materials. The silicon is from the added standard for the semi-quantification of the phases. A d-spacing value for the graphite peak (Figure 5.2 and 5.3) of 3.37Å was calculated for both materials from Bragg's law and a $\lambda_{Co\text{-}K\alpha}$ of 1.7902Å.

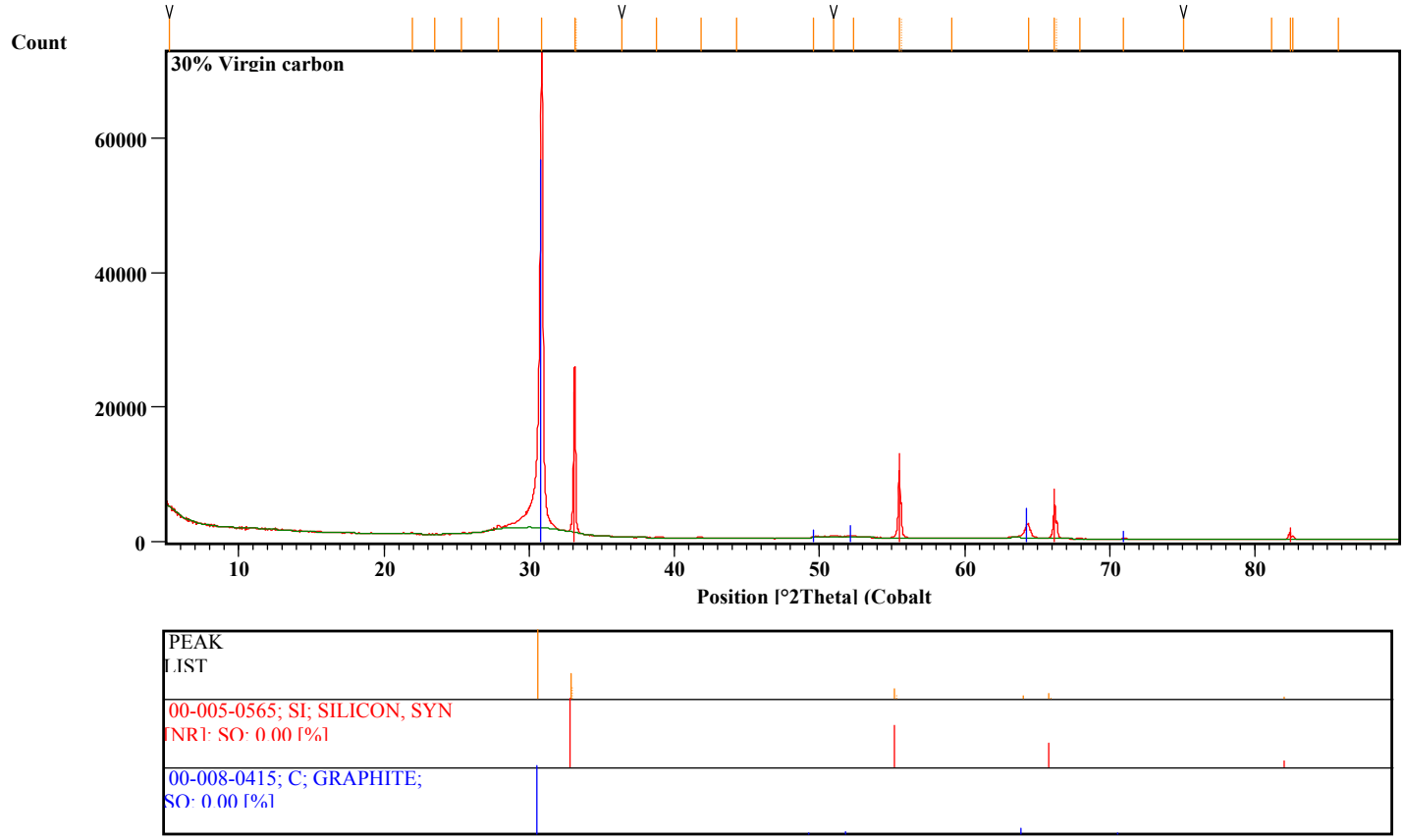

Figure 5.2: *Diffractogram of 30% graphitised virgin carbon cathode material*

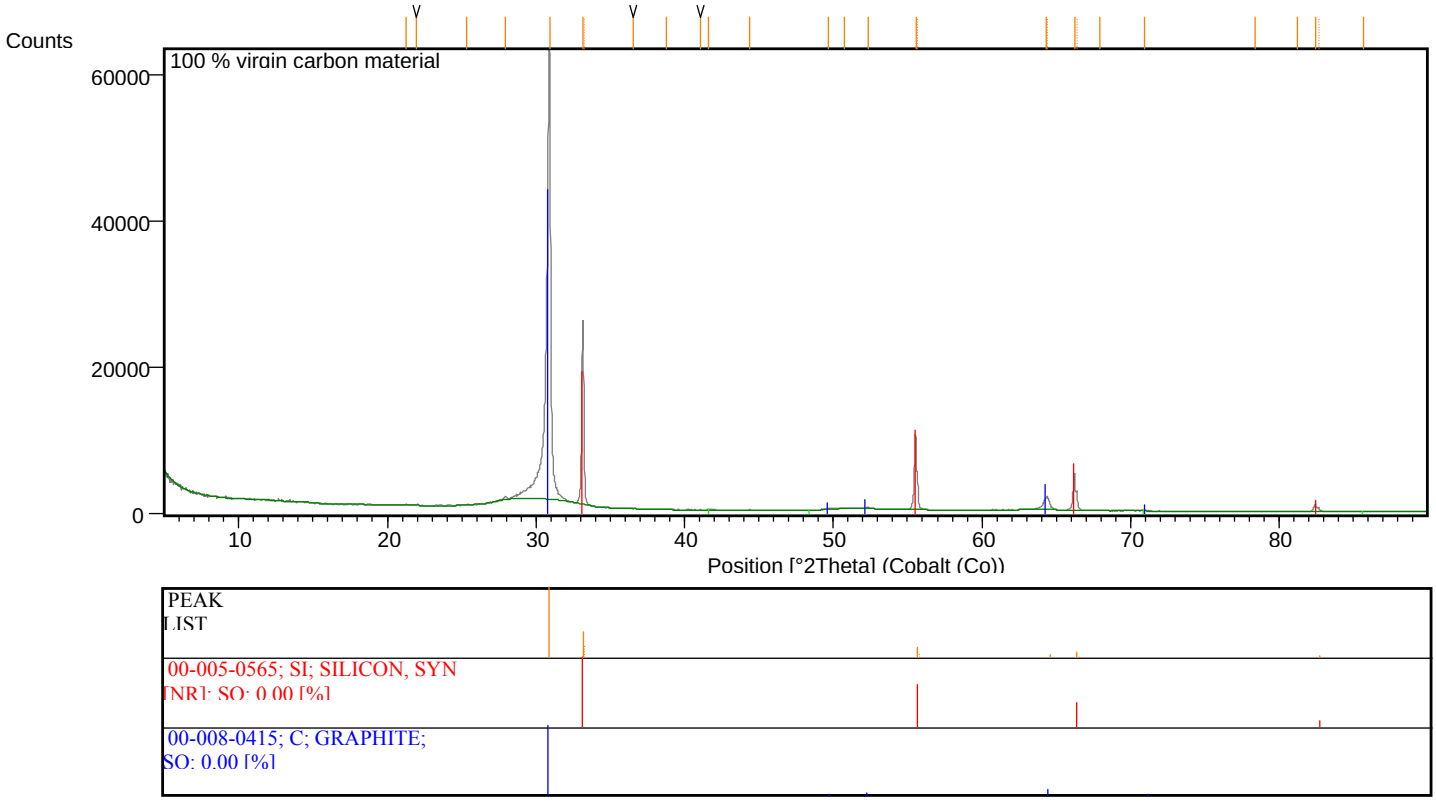

Figure 5.3: *Diffractogram of 100% graphitised virgin carbon cathode material*

The XRD analysis of the virgin carbon cathode of different grades is given in Table 5.2. It is evident that the d-spacing, peak position and FWHM is not different from the two grades.

Table 5.2: *Quantitative XRD results of the virgin carbon cathode materials*

Carbon cathode virgin materials					
30 % graphitised carbon cathode	Wt %	Wt % error	**100 % graphitised carbon cathode**	Wt %	Wt % error
Amorphous	56.5	2.23	Amorphous	2.2	0.58
Graphite	43.5	0.95	Graphite	97.8	2.64
Position (2θ)	31.21		31.20		
d-spacing (Å)	3.37		3.37		
FWHM [2θ]	0.221		0.223		

The cylindrical electrolysed sample was cut as shown in Figure 5.4. The part labelled 2 was sectioned to 2mm thick samples. These samples were cut into half, of which one half was used for XRD analysis and the other half was mounted and polished for microstructure and SEM/EDS analyses. The two diffractograms that are displayed are from sub-samples taken respectively 2mm and 4mm (Figure 5.4) below the carbon-electrolyte interface of the sample.

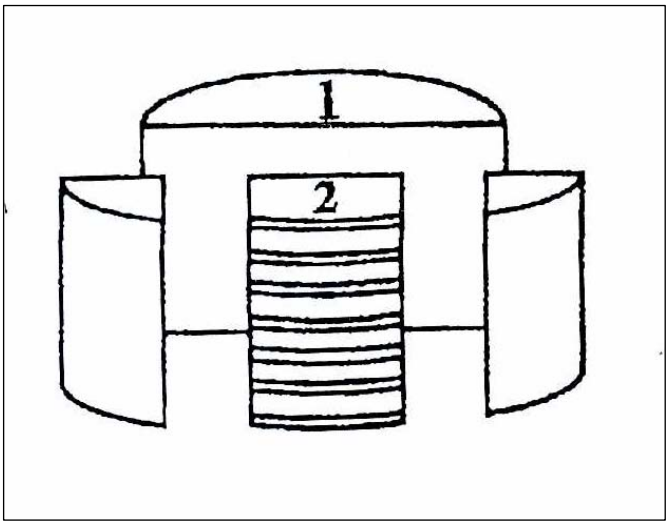

Figure 5.4: *Sectional cuts for XRD and SEM/EDS analyses*

Results

The quantitative XRD results of the sub-sections of sample "C" and sample "D" are given in Table 5.3. The data given in Table 5.3 and Table 5.4 shows the concentration of each detected phase in each specimen at given depth.

***Table 5.3**: Quantitative XRD results of the electrolysed 30% graphitised carbon cathode using the Rietveld method **

Sample C 1hr 30 minutes		**Na_3AlF_6 Cryolite**		**CaF_2 Fluorite**		**2H-Graphite**		**$NaAl_{11}O_{17}$ beta-Diaoyudaoite**		**NaF Villiaumite**	
		Wt %	Err	Wt %	Err	Wt %	Err	Wt %	Err	Wt %	Err
	Distance from hot zone (mm)										
1	2	8.2	1.14	X	X	32	1.61	0.18	0.001	12.4	1.09
2	4	9.2	0.98	X	X	38.15	1.72	0.52	0.002	5.4	0.84
3	6.2	9.4	1.11	X	X	37.50	1.73	0.56	0.001	11.6	1.03
4	8.2	6.1	1.21	X	X	37.6	1.25	0.02	0.001	12.4	1.01
Sample C 3hrs											
	Distance from hot zone (mm)										
1	2	17	1.12	2.4	0.11	32.1	1.37	2.2	0.04	X	X
2	4	16.2	1.08	2.2	0.12	33.4	1.61	2.8	0.01	X	X
3	6.2	19.95	1.15	2.5	0.11	34.8	1.82	0.12	0.05	X	X
4	8.0	X	X	1.8	0.01	40.2	1.08	X	X	X	X

*: Balance includes the amorphous phase in the samples
X=Not detected

Table 5.4: *Quantitative XRD results of the electrolysed 100% graphitised carbon cathode, using the Rietveld method**

Sample D 1hr 30 minutes		**Na_3AlF_6 Cryolite**		**CaF_2 Fluorite**		**2H-Graphite**		**$NaAl_{11}O_{17}$ beta-Diaoyudaoite**		**NaF Villiaumite**		**$Na_5Al_3F_{14}$ Chiolite**	
		Wt %	Err	Wt %	Err	Wt %	Err	Wt %	Err	Wt %	Err	Wt %	Err
	Distance from hot zone (mm)												
1	2	2.5	0.81	9.7	0.52	87.6	1.02	X	X	0.22	0.01	X	X
2	4	2.0	0.79	7.8	0.88	90.0	0.41	X	X	0.21	0.02	X	X
3	6.2	1.42	0.88	12.35	0.69	86.0	0.33	X	X	0.22	0.01	X	X
4	8.2	X	X	X	X	91.33	0.38	X	X	X	X	X	X
Sample D 3hrs													
	Distance from hot zone (mm)												
1	2	13.8	1.07	X	X	73.86	0.82	4.1	0.66	5.2	0.58	3.04	0.01
2	4	11.6	1.03	X	X	75.28	0.49	3.9	0.54	6.2	0.76	3.02	0.01
3	6.2	13.2	1.10	X	X	71.7	0.52	3.7	0.90	9.3	0.63	2.08	0.02
4	8.0	12.2	1.09	X	X	72.15	0.46	1.8	0.88	X	X	X	X

*: Balance includes the amorphous content of the samples

X=Not Identified

Table 5.5 shows the full width half maximum results that were obtained using the X'Pert data Viewer software. There is no difference between the two carbon grades, this shows that there was no peak broadening during the electrolyte penetration in the carbon sample during the

laboratory electrolysis. Therefore it shows that there is no lattice or structural change due to phase or electrolyte penetration into the carbon cathode.

***Table 5.5**: The effect of electrolyte penetration on the graphite peak of the laboratory samples.*

	Sample number				
Sample	1	2	3	4	5
C					
Position (2θ)	31.42	31.41	31.42	31.42	31.42
d-spacing (Å)	3.37	3.37	3.37	3.37	3.37
FWHM [2θ]	0.230	0.231	0.230	0.230	0.231
D					
Position (2θ)	31.11	31.21	31.11	31.11	31.41
d-spacing (Å)	3.37	3.37	3.37	3.37	3.37
FWHM [2θ]	0.229	0.228	0.229	0.229	0.229

Graphs of the concentration profiles in the two different types of carbon cathodes are given in Figures 5.9 - 5.19. This is to establish a penetration trend associated with these two different carbon grades.

5.3.2.2. Stereo microscopy analysis (1 hr 30 minutes)

The two electrolysed carbon cathode grades (30% and 100% graphitised) were investigated under a stereo microscope for phase formation on the surface or inside the pores. The stereo micrographs of the electrolysed cathode samples “C1” and “D1” after 1 hr 30 minutes of electrolysis are shown in Figures 5.5 and 5.6.

In sample “C1” (30% graphitised carbon grade), the degree of alteration decreased with increasing distance from the carbon-electrolyte interface. Sample $C1_5$ shows less bath penetration than the other C1 specimens. Bath penetration decreased with increasing distance from the carbon-electrolyte interface.

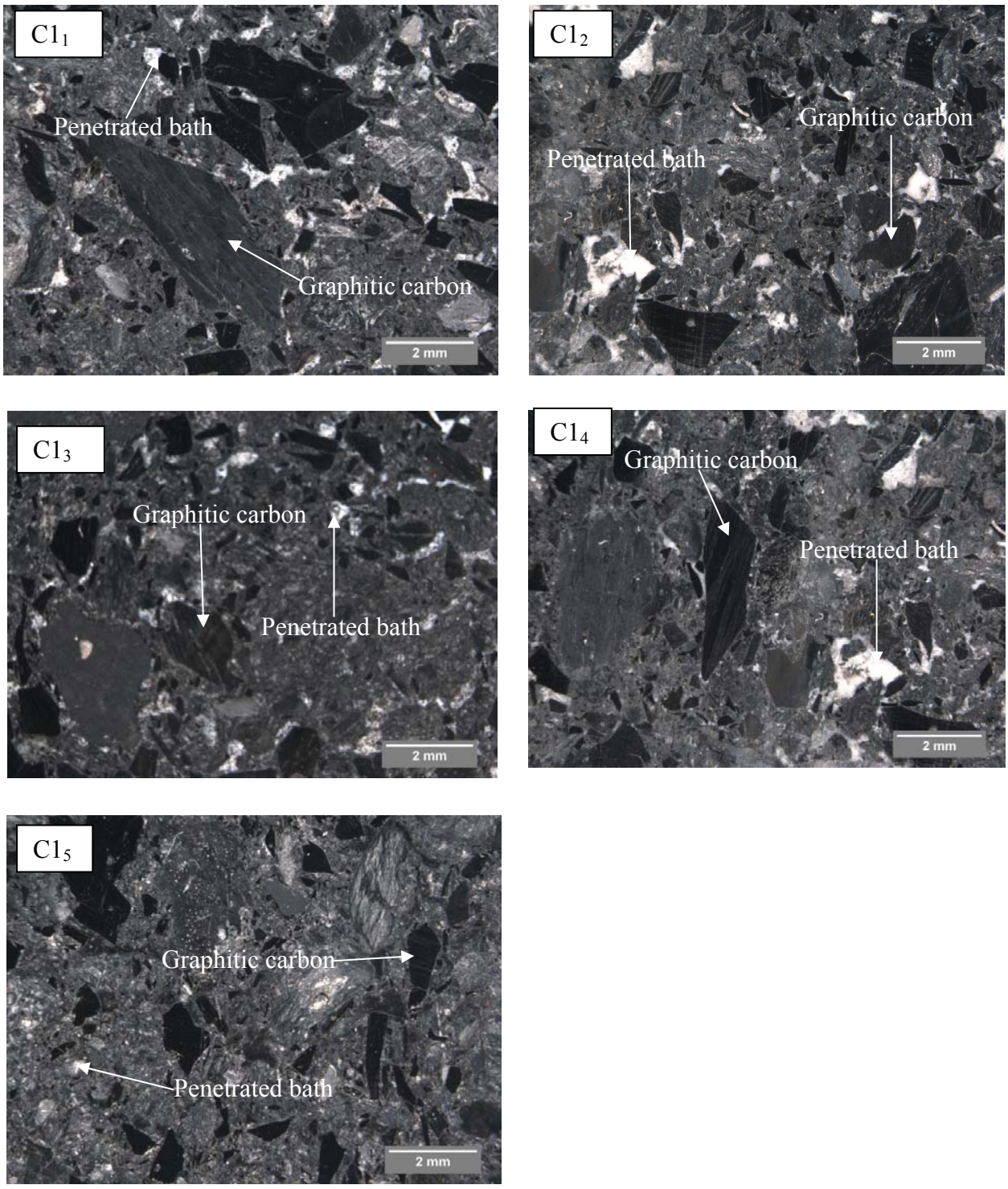

Figure 5.5: *Stereo microscope images of sample "C1" electrolysed for 1hr 30 minutes*

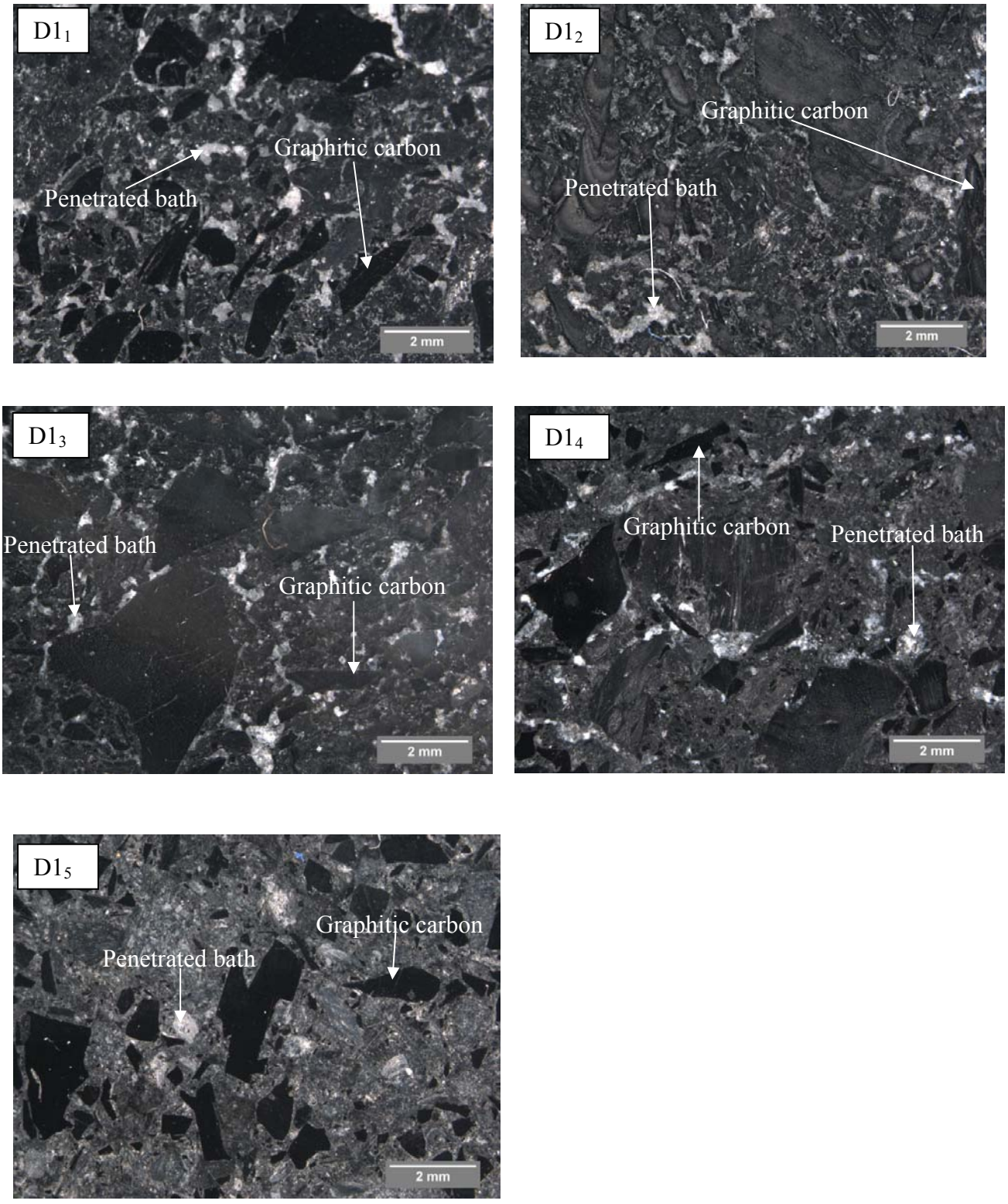

Figure 5.6: *Stereo microscope images of sample "D1" electrolysed for 1hr 30 minutes*

The 30% graphitised carbon cathode has large graphite grains as compared to the 100% graphitised carbon cathode and the post-mortem samples.

Comparison of samples "C1" and "D1"

There are traces of electrolyte in both samples "C1" and "D1". The bath penetrated only the non-graphitic sections in the sample. In both sample "C1" and "D1", the bath penetration decreased with increasing the distance from the carbon-electrolyte interface.

5.3.2.3. Stereo microscope analysis (3hrs)

Sample "C2" (30% graphitised carbon) and sample "D2" (100% graphitised carbon) were taken from the same carbon block as "C1" and "D1". The difference is that samples "C2" and "D2" were electrolysed for a longer period (3 hours) than samples "C1" and "D1" (1hr 30 min). The samples were analysed using the stereo microscope.

Stereo microscope images of the laboratory electrolysed samples (3 hour experiment) are given in Figures 5.7 and 5.8. Traces of electrolyte and graphitic carbon regions can be distinguished.

Sample "C2" contains bath penetrated and graphitic carbon regions as shown in Figure 5.7. High concentrations of electrolyte were observed in sample $C2_1$, which is closer to the carbon-electrolyte interface. This means the bath penetration decreased with increasing the distance from the carbon-electrolyte interface. Not all the sections contained electrolyte.

Bigger grains of graphitic carbon are visible in Figure 5.7. The bath contents were observed in the non-graphitic parts of the carbon. The concentration of bath contents in the carbon cathode decreased with increasing distance from the carbon-electrolyte interface.

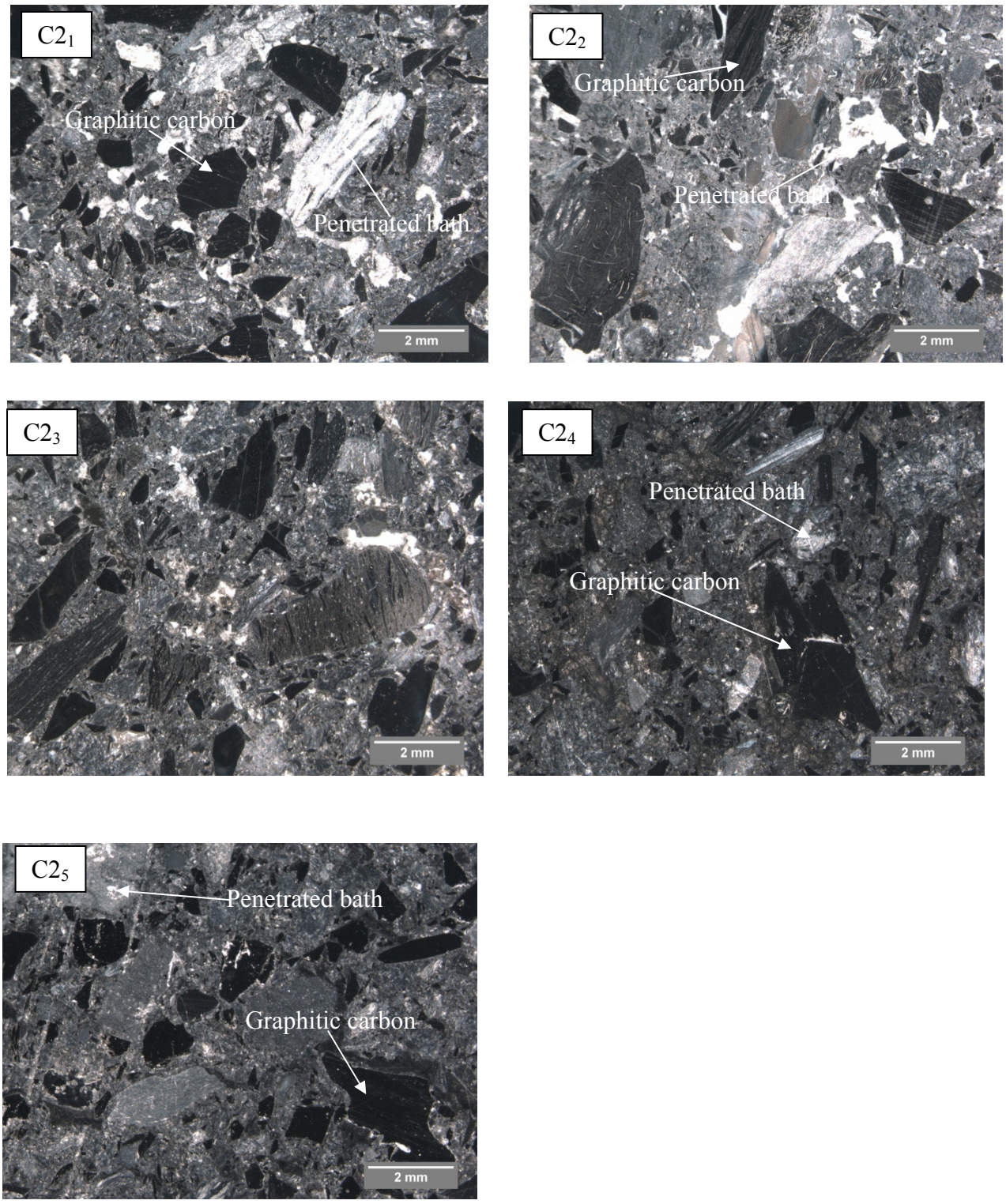

***Figure 5.7**: Stereo microscope images of sample "C2" electrolysed for 3 hours*

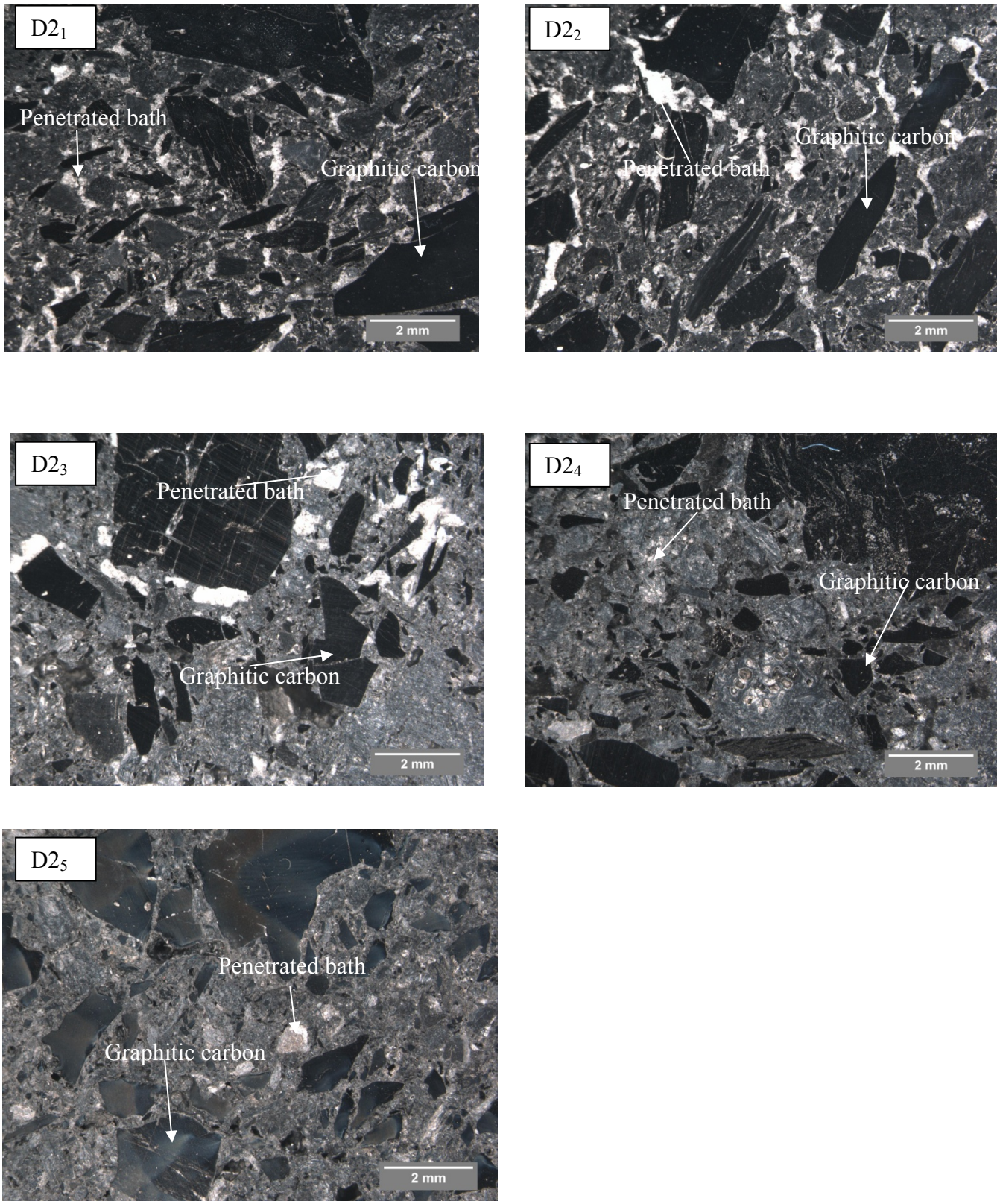

Figure 5.8: *Stereo microscope images of sample "D2" electrolysed for 3 hours*

Comparison of samples "C2" and "D2"

The identification of phases/electrolytes by XRD on both the samples leads to a conclusion that there is bath penetration during the electrolysis process after 3 hours. The quantification by the Rietveld method revealed that there is more phases/electrolyte constituents detected in the 30% graphitised carbon than it is in the 100% graphitised carbon. Therefore the 30% graphitised carbon is more susceptible to electrolyte penetration than the 100% graphitised carbon. The degree of graphitisation is the main factor that determines the degree of bath penetration. Bath penetration decreased with increasing distance from the carbon-electrolyte interface in both samples.

Time dependence of bath penetration into the carbon cathode

The laboratory electrolysis experiments were run at two different periods, namely 1hr 30 minutes and 3 hours. The stereo microscope micrographs showed that the longer the experiment the more the bath penetrated into the carbon cathode. This holds for both the 30% graphitised carbon and the 100% graphitised carbon.

5.3.2.4. The 30 % graphitised carbon cathode

The semi-quantitative XRD analysis identified the following phases in the 1hr30minutes electrolysed sample (Appendix D): Graphite (C), Villiaumite (NaF), Cryolite (Na_3AlF_6), and the beta-Diayudaoite ($NaAl_{11}O_{17}$). Fluorite (CaF_2) was only detected in the 3hr experiment with 30% graphitised carbon cathode, but NaF was then not detected. An amorphous phase was also detected. The 3hr electrolysis experiment has a high concentration of the penetrated phases, and there is no NaF phase detected.

5.3.2.5. The 100 % graphitised carbon cathode

The following phases were identified by XRD: Graphite (C), fluorite (CaF_2), Cryolite (Na_3AlF_6), and Villiaumite (NaF), as well as an amorphous phase. Two additional phases could be identified in the 3 hour experiment namely chiolite ($Na_5Al_3F_{14}$) and beta-Diaoyudaoite ($NaAl_{11}O_{17}$). Fluorite (CaF_2) could not be detected after 3hrs. The common identified penetrated phase is cryolite. The concentration of cryolite in the carbon increased with increasing time of electrolysis.

5.3.2.6. Comparison between 30% and 100% graphitised carbon cathodes

1hr 30 minutes of electrolysis

Only NaF and Na_3AlF_6 are the common phases that were identified in both the 30% and 100% graphitised carbon cathode samples. Concentrations of the common penetrated phases that were identified after 1hr 30 minutes of electrolysis are higher in the 30% graphitised carbon cathode than in the 100% graphitised carbon cathode.

3 hours of electrolysis

The penetrated phases that are common to both carbon grades are $NaAl_{11}O_{17}$ and Na_3AlF_6. The 30% graphitised carbon shows a higher degree of $NaAl_{11}O_{17}$ penetration than the 100% graphitised carbon.

Phase concentrations of the identified phases as a function of penetration depth are given in Figures 5.9-5.19. In some graphs the error bars on either the depth or concentration axis can not be seen. This is because the error associated with the analyses results is very small.

Cryolite was observed in all the carbon cathode materials (30 and 100 % graphitised carbon). More cryolite penetrated the 30% graphitised carbon cathode than the 100% graphitised carbon cathode (Figures 5.9 and 5.10). In the 1hr 30 minute experiments the cryolite penetration decreased with increasing distance from the carbon-electrolyte interface, while in the 3 hour experiment there is no distinct trend. The cryolite concentration increased with increasing time of electrolysis as shown in Figures 5.9 and 5.10.

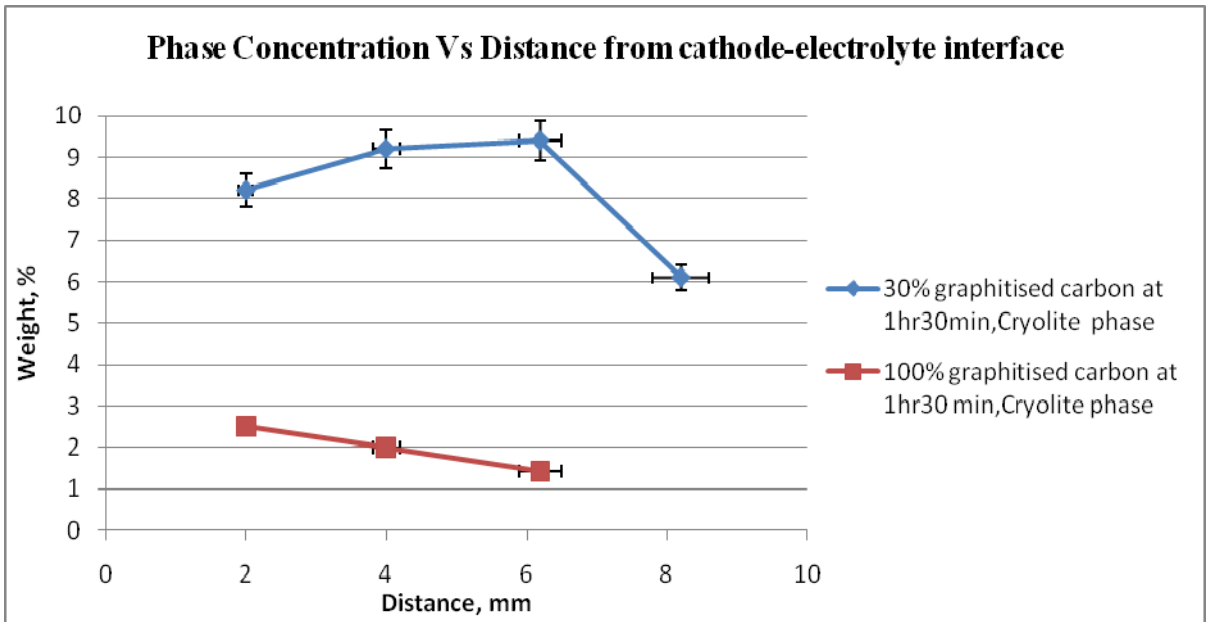

Figure 5.9: *Comparison of cryolite phase profiles in samples C and D, 1hr30 min of electrolysis.*

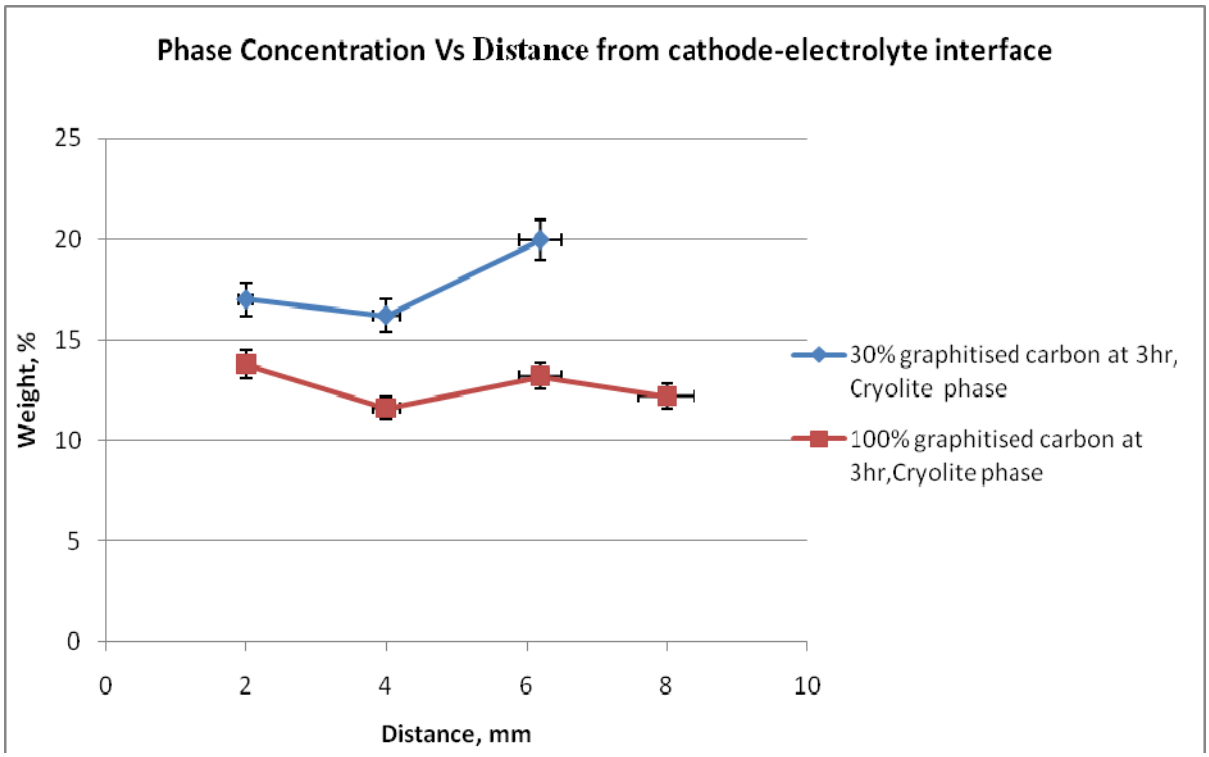

Figure 5.10: *Comparison of cryolite phase profiles in samples C and D, 3hr of electrolysis.*

The concentration of villiaumite (NaF) does not follow a clear trend with increasing depth into the 30% graphitised carbon cathode, while it remained constant in the 100% graphitised carbon cathode after 1hr 30 minutes (Figure 5.11). The concentration of villiaumite is very low in the 100% graphitised carbon cathode as compared to the 30% graphitised cathode. The NaF content increased with increasing depth into the 30% graphitised carbon cathode, while no NaF could be detected in the 100% graphitised carbon after 3hr of electrolysis (Figure 5.12).

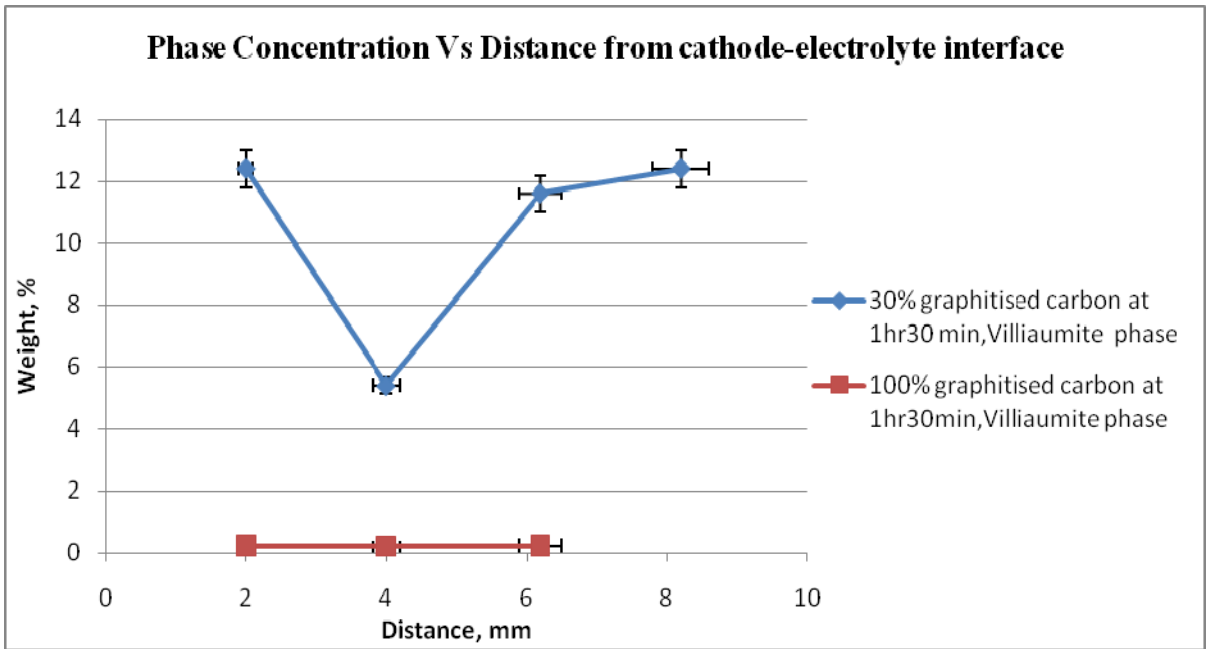

***Figure 5.11**: Comparison of Villiaumite phase profiles in samples C and D, 1hr30 min of electrolysis.*

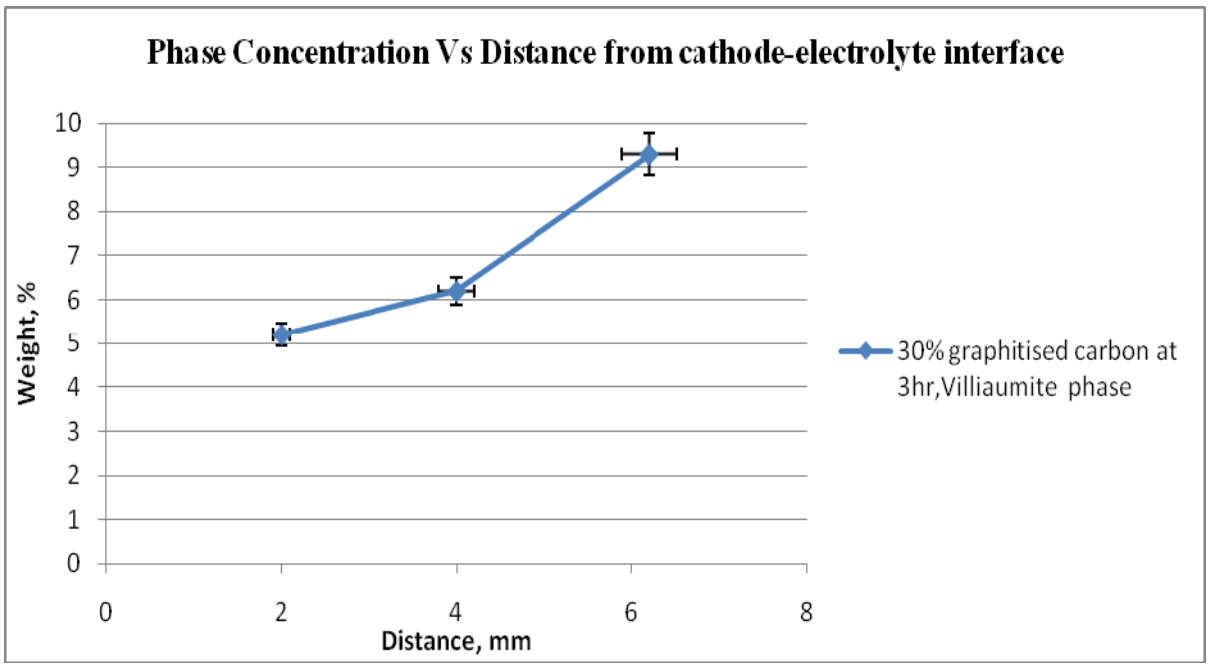

***Figure 5.12**: Villiaumite phase profile in sample C, 3hrs of electrolysis.*

The graphite concentration increases with increasing distance from cathode-electrolyte interface.

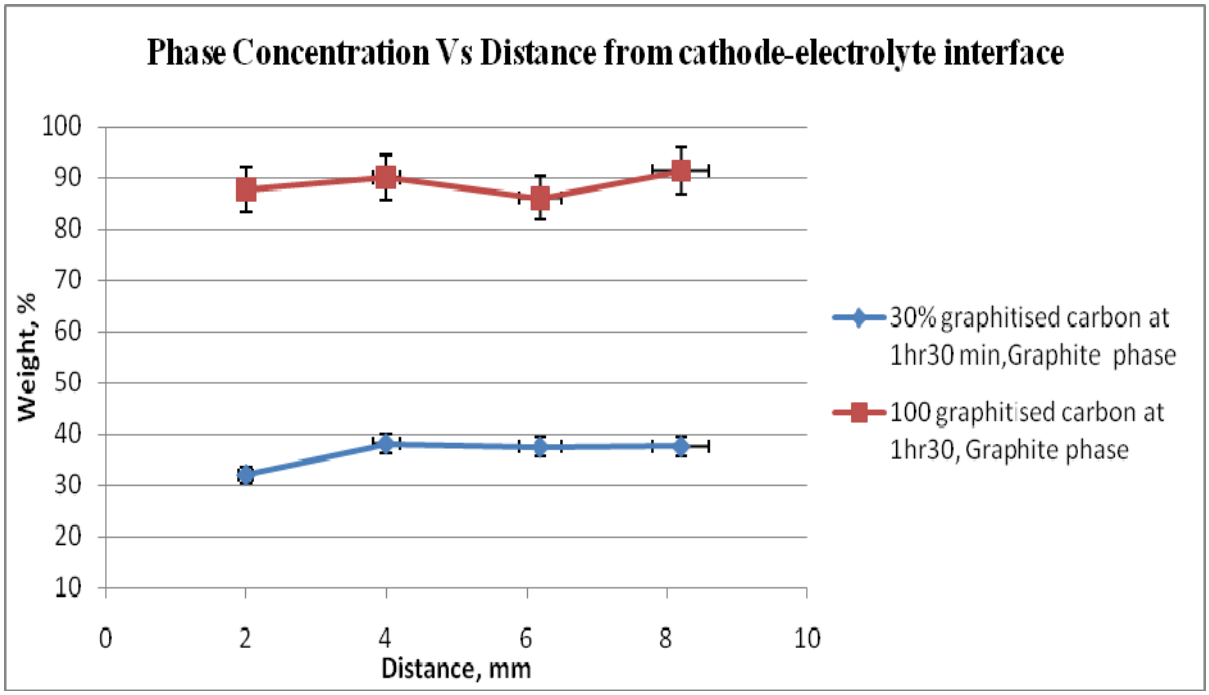

***Figure 5.13:** Comparison of graphite phase profiles in samples C and D, 1hour 30 minutes of electrolysis.*

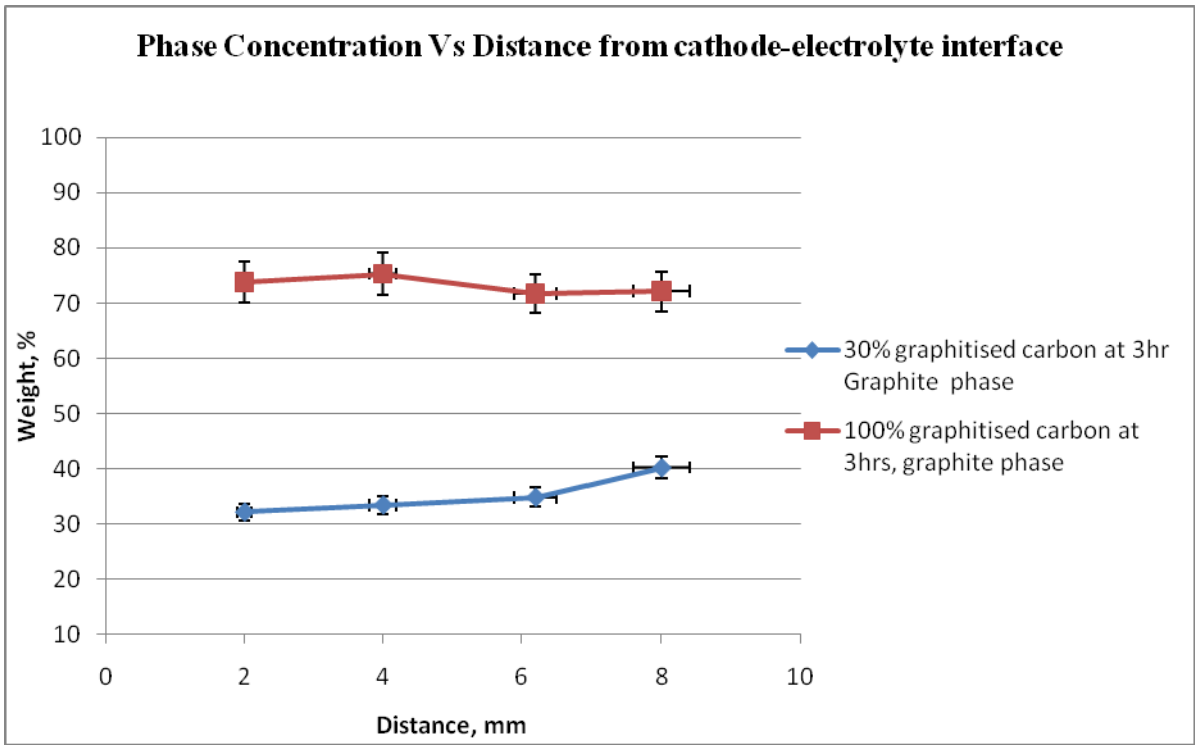

Figure 5.14: *Comparison of graphite phase profiles in samples C and D, 3hour of electrolysis.*

Low concentrations of beta-diayudaoite ($NaAl_{11}O_{17}$) were only identified in the 30% graphitised carbon after 1 hr 30 minutes of electrolysis (Figure 5.15). Higher concentrations of beta-diayudaoite could be detected in the 100% graphitised carbon than in the 30% graphitised carbon after 3hours of electrolysis. There is a decrease in concentration of beta-diayudaoite in both carbon cathode grades as the distance from the carbon-electrolyte interface increased.

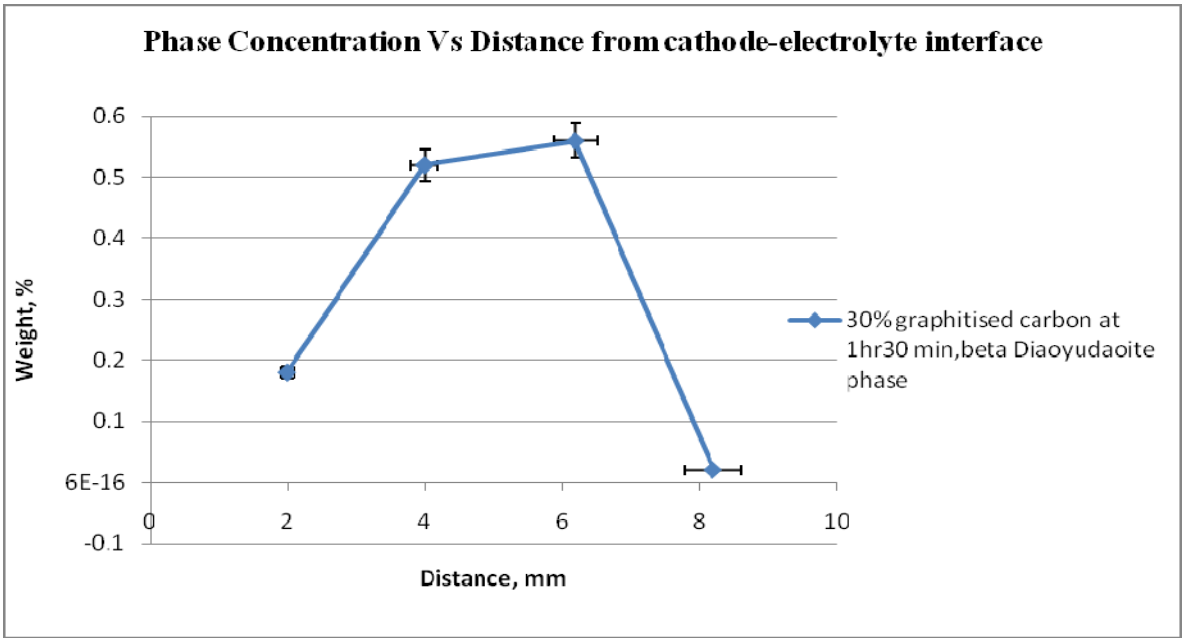

Figure 5.15: *Beta-diayudaoite phase profile of sample C, 1hr30 min of electrolysis.*

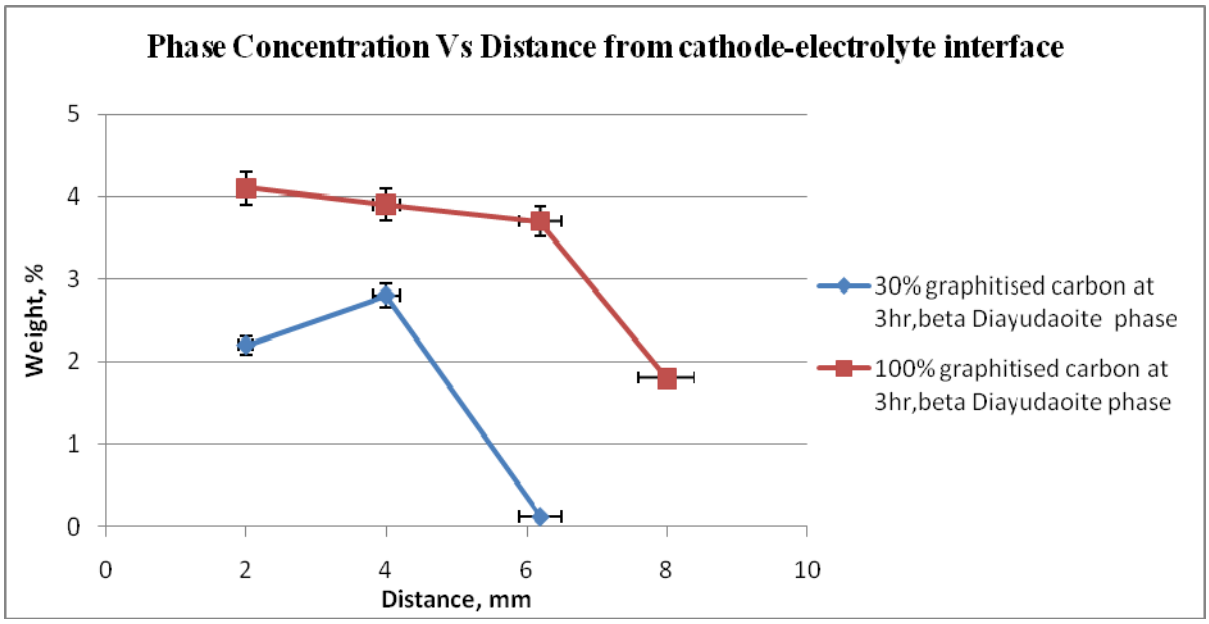

Figure 5.16*: Comparison of beta-diayudaoite phase profiles in samples C and D, 3hr of electrolysis.*

Fluorite was only identified in the 100% graphitised carbon cathode after 1hr 30 min of electrolysis (Figure 5.17), and in the 30% graphitised carbon cathode after 3 hours of electrolysis (Figures 5.18).

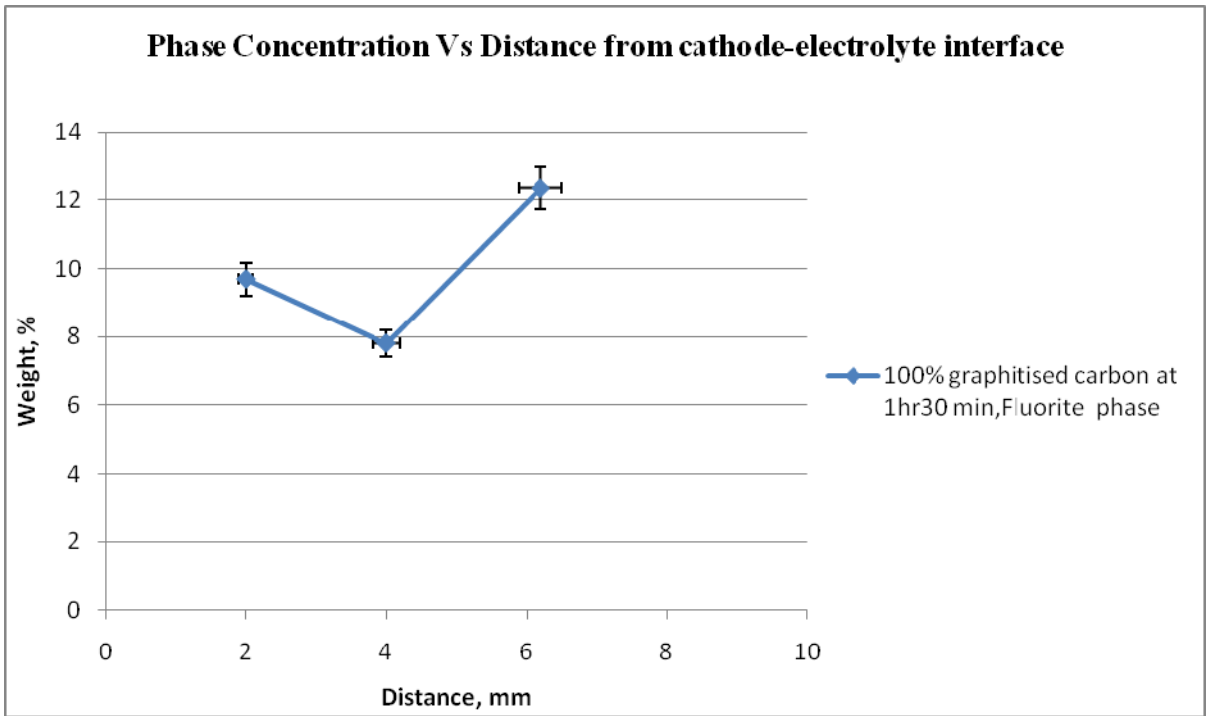

***Figure 5.17**: Fluorite phase profiles of sample D, after 1hr30 min of electrolysis.*

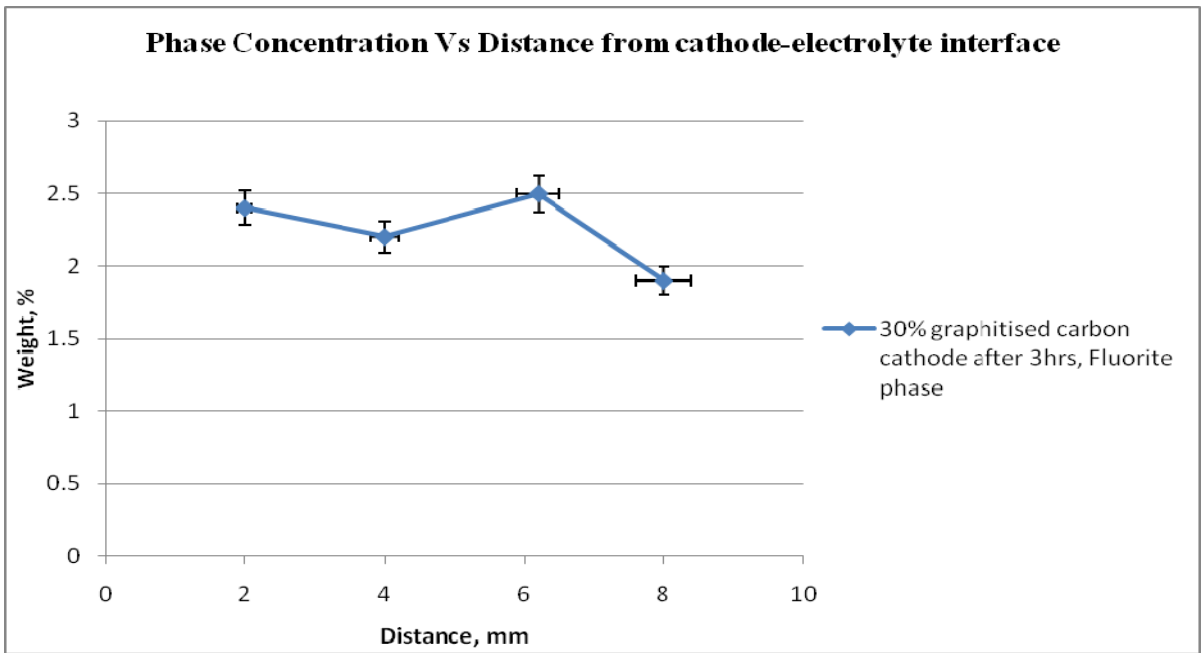

***Figure 5.18:** Fluorite phase profiles of sample C, after 3hours of electrolysis.*

The concentration profile of chiolite ($Na_5Al_3F_{14}$) is shown in Figure 5.19. Chiolite was only detected in the 100% graphitised carbon after 3hours of electrolysis. The concentration decreases with increasing the distance from the carbon-electrolyte interface.

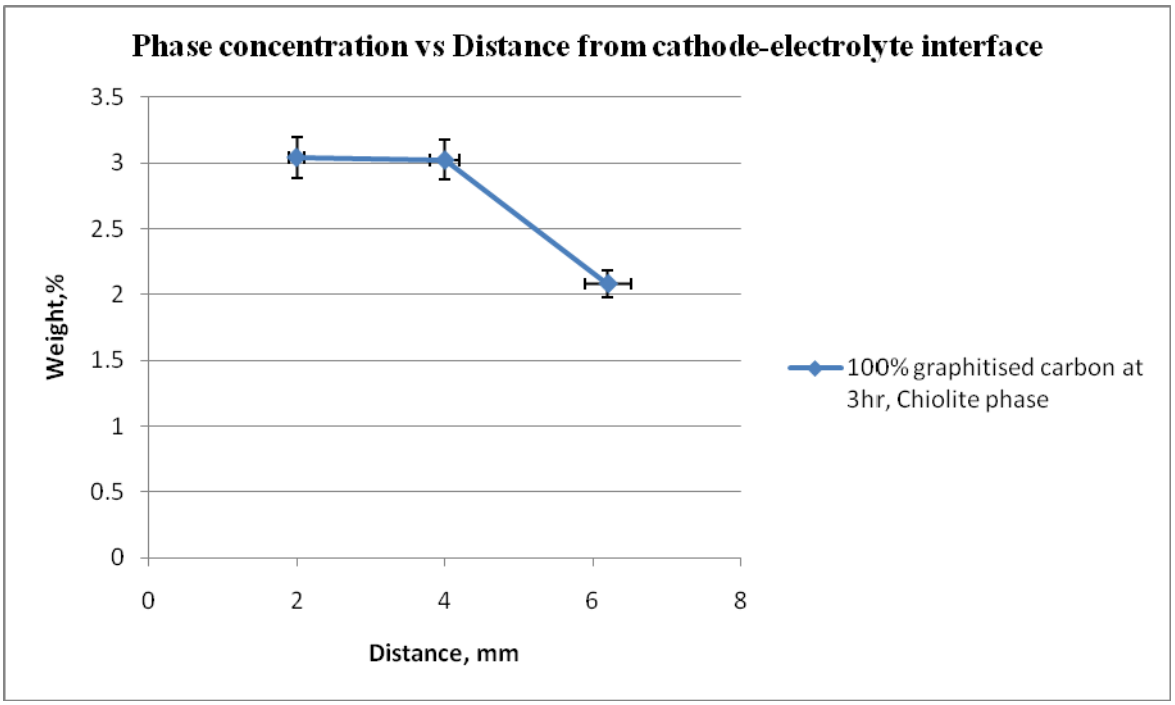

***Figure 5.19**: Chiolite phase profile sample D, after 3hrs of electrolysis.*

5.4. Scanning electron microscopy (SEM)

The same samples used for the reflected light microscopy analysis were taken for scanning electron microscopy (SEM) analysis. Phases of different grey intensities could be distinguished in the carbon cathode samples (Figures 5.20 - 5.23). These phases were analysed by SEM-EDS and their compositions are given in Tables 5.7-5.10. Bulk analysis of the two grades at different electrolysis time is given in Table 5.6.

***Table 5.6:** SEM-EDS elemental analysis of the two carbon grades at different electrolysis period.*

	C	O	F	Na	Al	Ca
C1 (1hr30)	52.75±0.40	2.62±0.23	17.17±0.23	10.79±0.14	10.08±0.14	3.59±0.02
C2 (3 hrs)	50.30±0.38	3.12±0.23	18.25±0.38	13.81±0.20	11.94±0.12	1.58±0.08
D1(1hr30)	62.04±0.16	2.13±0.09	24.38±0.14	6.04±0.05	4.26±0.03	1.15±0.03
D2 (3 hrs)	61.38±0.34	1.17±0.12	2.72±0.17	28.74±0.28	5.53±0.13	0.46±0.08

5.4.1. 30% graphitised carbon after 1hr 30 minutes

$C1_1$ is used as the representative sample of all the 30% graphitised carbon cathode samples after 1hour 30 minutes of electrolysis (Figure 5.20, Table 5.7). $NaAl_{11}O_{17}$, NaF and Na_3AlF_6 are the dominant phases.

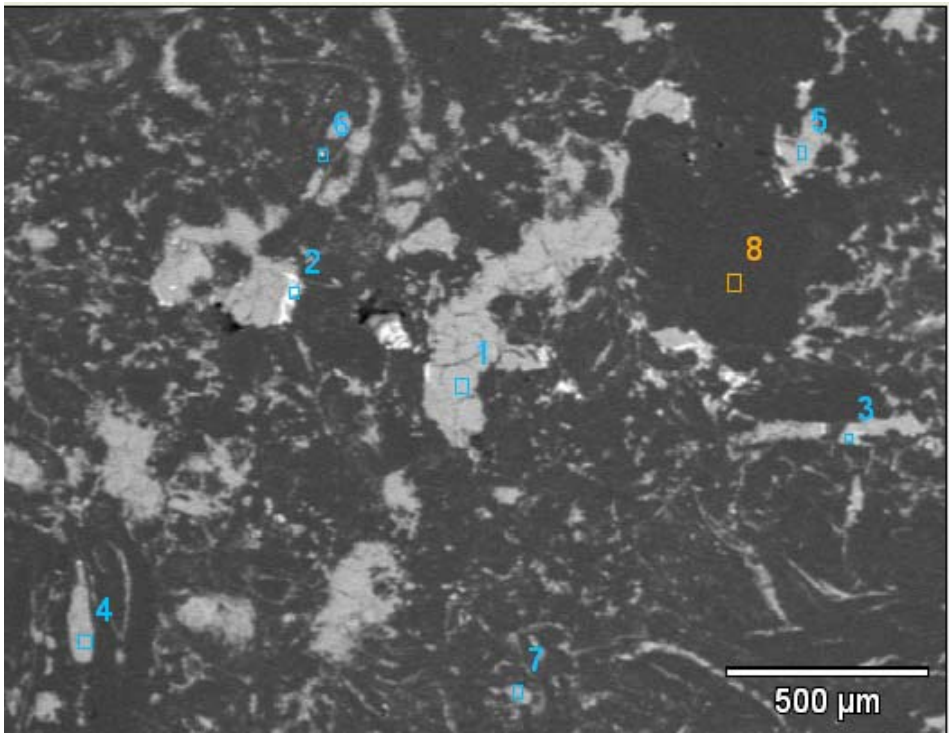

Figure 5.20: *Backscattered electron image of sample $C1_1$ (30% graphitised carbon after 1hour 30 minutes experiment) showing penetrated bath and analysed points.*

***Table 5.7**: EDS results of possible phases that could be distinguished in Sample $C1_1$ (30 % graphitised carbon after 1hr 30 minutes electrolysis)*

Point	**Detected elements in at%**							
	Carbon (C)	Nitrogen (N)	Oxygen (O)	Fluorine (F)	Sodium (Na)	Aluminium (Al)	Calcium (Ca)	Phase or Phases
1	0.63	0.03	57.16	N/d	3.48	38.67	0.03	$NaAl_{11}O_{17}$
2	0.26	N/d	N/d	49.68	49.62	0.38	0.06	NaF
3	0.38	0.10	N/d	49.17	49.88	0.46	0.01	NaF
4	0.86	N/d	0.16	60.08	29.78	9.12	N/d	Na_3AlF_6
5	0.19	0.06	N/d	58.56	33.86	7.18	0.14	Na_3AlF_6 and NaF
6	0.06	N/d	N/d	63.18	27.89	9.87	N/d	Na_3AlF_6
7	99.14	N/d	N/d	0.28	0.52	0.06	N/d	Graphite
8	99.22	N/d	N/d	0.16	0.59	0.02	0.03	Graphite

N/d=Not detected

5.4.2. 100% graphitised carbon after 1hr 30 minutes

Sample $D1_1$ represents the 100% graphitised samples that were electrolysed for 1hour 30 minutes. All the electrolyte constituents were detected (i.e. $NaAl_{11}O_{17}$, Na_3AlF_6, NaF and CaF_2) except Al_2O_3 (Figure 5.21, Table 5.8).

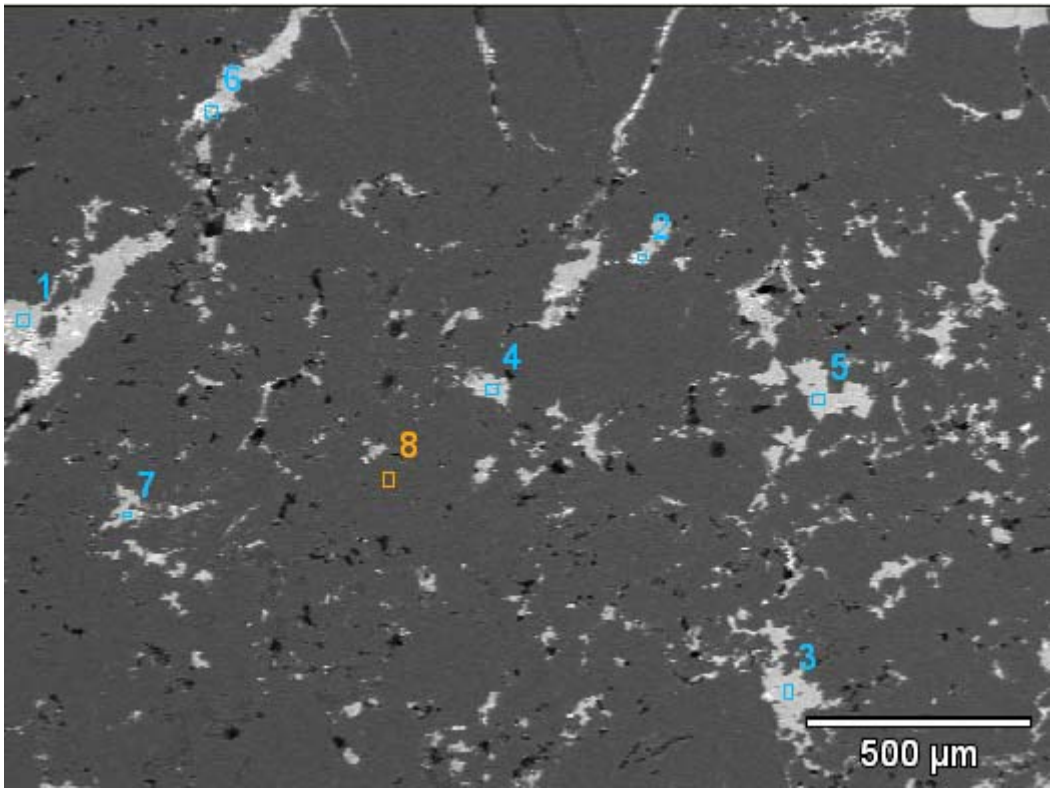

Figure 5.21: *Backscattered electron image of sample $D1_1$ (100% graphitised carbon after 1hour 30 minutes of electrolysis) showing penetrated bath and the analysed points*

Table 5.8: *EDS results of possible phases that could be distinguished in Sample $D1_1$ (10 % graphitised carbon after 1hr30 minutes electrolysis)*

Point	**Detected elements in at%**							
	Carbon (C)	Nitrogen (N)	Oxygen (O)	Fluorine (F)	Sodium (Na)	Aluminium (Al)	Calcium (Ca)	Phase or Phases
1	0.14	N/d	58.74	0.26	4.88	35.98	N/d	$NaAl_{11}O_{17}$
2	0.68	N/d	0.04	62.81	23.94	12.38	0.15	Na_3AlF_6
3	1.04	N/d	N/d	49.08	49.17	0.64	0.07	NaF
4	1.22	N/d	N/d	64.18	0.82	0.11	33.67	CaF_2
5	1.78	N/d	58.07	N/d	4.63	35.52	N/d	$NaAl_{11}O_{17}$
6	0.23	0.13	N/d	47.89	51.68	0.07	N/d	NaF
7	0.76	N/d	N/d	54.78	21.78	0.05	22.63	CaF_2 and NaF
8	98.25	N/d	N/d	N/d	0.01	0.25	1.49	Graphite

N/d=Not detected

5.4.3. Comparison of 30% graphitised carbon and 100% graphitised carbon electrolysed for 1hour 30 minutes.

In both carbon grades bath constituents (Na_3AlF_6, CaF_2) were detected. This showed that bath constituents penetrated the carbon cathode during the electrolysis process. The electrolyte reaction product that penetrated the carbon cathode was $NaAl_{11}O_{17}$, which could be detected in both the carbon grades. CaF_2 could be identified in the 100% graphitised carbon grade and not in the 30% graphitised carbon for the same experimental period.

5.4.4. 30% graphitised carbon after 3hrs of electrolysis

The following phases were detected in the 30% graphitised carbon sample after 3hours of electrolysis: Na_3AlF_6 (cryolite), $NaAl_{11}O_{17}$ (Diaoyudaoite), CaF_2 (Fluorite) and graphite (Figure 5.22 and Table 5.9).

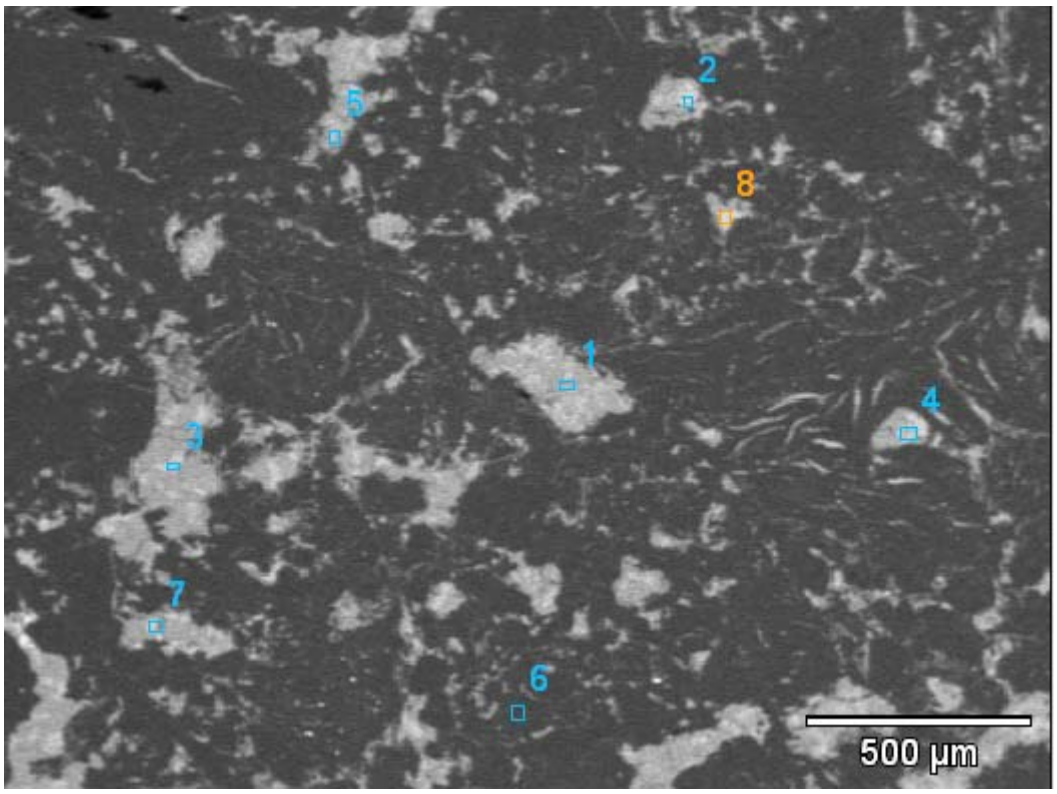

Figure 5.22: *Backscattered electron image of sample $C2_1$ (30% graphitised carbon after 3hours of electrolysis) showing penetrated bath and the analysed points*

Table 5.9: *EDS results of possible phases that could be distinguished in Sample $C2_1$ (30 % graphitised carbon after 3hours of electrolysis)*

Point	**Detected elements in at%**							
	Carbon (C)	Nitrogen (N)	Oxygen (O)	Fluorine (F)	Sodium (Na)	Aluminium (Al)	Calcium (Ca)	Phase or Phases
1	0.14	N/d	58.74	0.26	4.88	35.98	N/d	$NaAl_{11}O_{17}$
2	0.68	N/d	0.04	62.81	23.94	12.38	0.15	Na_3AlF_6
3	0.23	N/d	60.74	0.19	5.88	32.96	N/d	$NaAl_{11}O_{17}$
4	1.22	N/d	N/d	64.18	0.82	0.11	33.67	CaF_2
5	1.78	N/d	58.07	N/d	4.63	35.52	N/d	$NaAl_{11}O_{17}$
6	97.62	N/d	0.01	0.03	0.52	0.23	1.62	Graphite
7	0.28	N/d	0.24	65.81	21.94	11.38	0.35	Na_3AlF_6
8	0.22	N/d	N/d	64.18	0.82	0.11	34.67	CaF_2

N/d=Not detected

5.4.5. The 100% graphitised carbon after 3hours of electrolysis

The following phases were detected in the 100% graphitised carbon cathode after the 3hour electrolysis period: Na_3AlF_6 (cryolite), NaF (Villiaumite), $Na_5Al_3F_{14}$ (chiolite), $NaAl_{11}O_{17}$ (beta-Diaoyudaoite) and graphite (Figure 5.23 and Table 5.10).

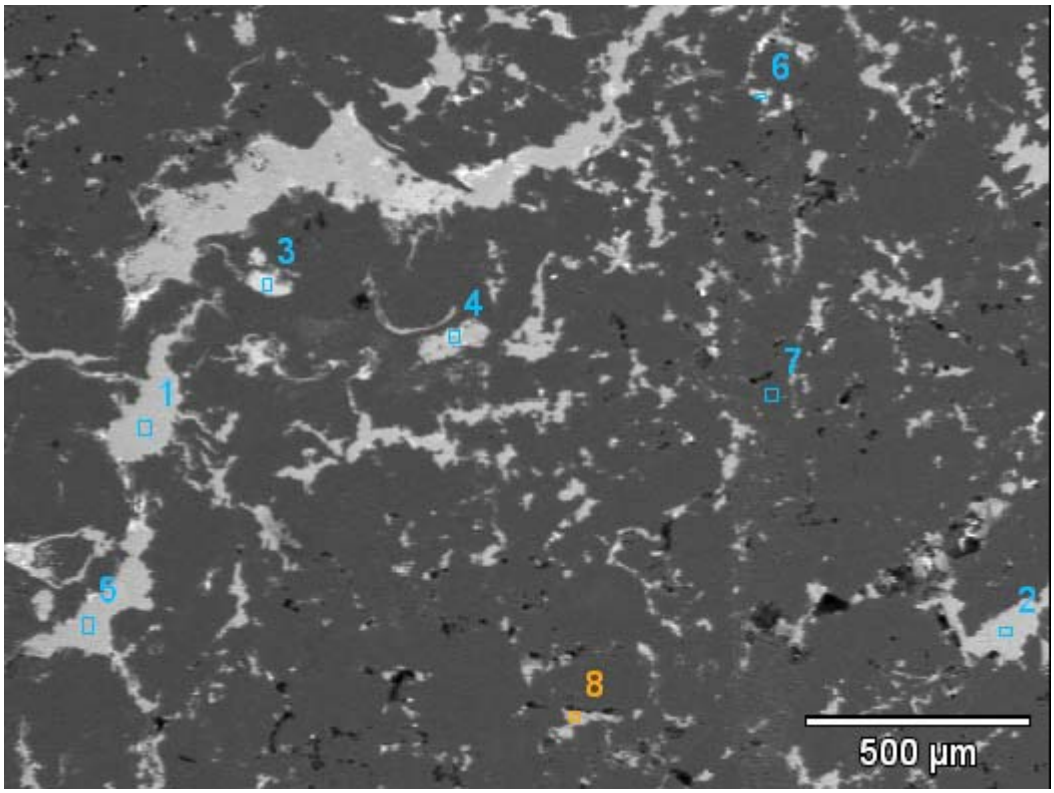

Figure 5.23: *Backscattered electron image of sample $D2_1$ (100% graphitised carbon after 3hour experiment) showing penetrated bath and the analysed points*

Table 5.10: *EDS results of possible phases that could be distinguished in Sample $D2_1$ (100 % graphitised carbon after 3hours of electrolysis)*

Point	**Detected elements in at%**							
	Carbon (C)	Nitrogen (N)	Oxygen (O)	Fluorine (F)	Sodium (Na)	Aluminium (Al)	Calcium (Ca)	Phase or Phases
1	0.21	N/d	60.56	0.15	3.43	35.65	N/d	$NaAl_{11}O_{17}$
2	0.88	N/d	61.74	0.96	4.23	32.19	N/d	$NaAl_{11}O_{17}$
3	0.18	N/d	0.25	61.79	25.32	12.23	0.23	Na_3AlF_6
4	0.01	N/d	N/d	48.92	51.07	N/d	N/d	NaF
5	0.04	N/d	N/d	65.59	20.25	14.12	N/d	$Na_5Al_3F_{14}$
6	0.05	0.01	N/d	58.26	27.82	13.28	0.58	Na_3AlF_6
7	99.32	N/d	0.32	N/d	0.14	0.21	N/d	Graphite
8	0.04	N/d	N/d	47.74	52.06	0.16	N/d	NaF

N/d=Not detected

5.4.6. Comparison of 30% graphitised and 100% graphitised carbon electrolysed for 3 hours

Na_3AlF_6 (cryolite) and $NaAl_{11}O_{17}$ (Diaoyudaoite) were observed in both the 30% and 100% graphitised carbon cathodes. The CaF_2 phase was only detected in the 30% graphitised carbon, while NaF (Villiaumite) and $Na_5Al_3F_{14}$ (chiolite) were detected in the 100% graphitised carbon only.

Figure 5.24 shows a phase diagram of the NaF-AlF_3-Al_2O_3 (Na_3AlF_6-Al_2O_3) obtained using the cryoscopy and emf measurements [39].

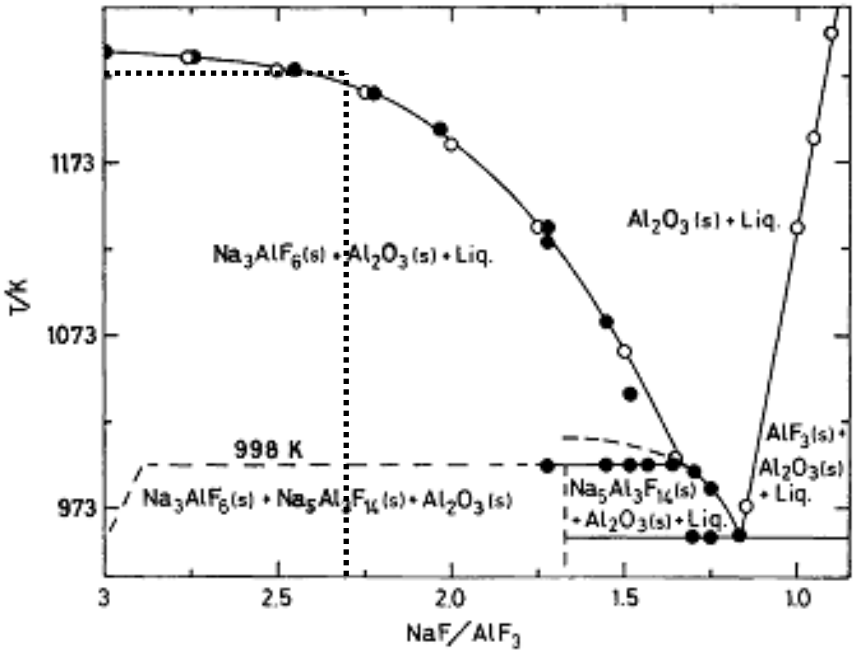

***Figure 5.24**: Crystallisation fields of the NaF-AlF_3 system saturated with alumina in the acidic region [39].*

The composition of interest at cryolite ratio of 2.29 is shown by means of the inserted dotted vertical line on the phase diagram. The experiment was carried out at 960°C (1233K) as shown by the inserted dotted horizontal line. At this temperature and composition there is solid Al_2O_3 and liquid. That means if composition analysis was carried out at this temperature there should only be solid Al_2O_3 and liquid only according to the phase diagram. There was no means of doing composition analysis at these conditions and there was no design of equipment that would allow for the quenching of the products which freeze the experiment and therefore the samples that were analysed were furnace cooled. The results of the analysis show equilibrium products from furnace cooling the samples from 1233K. Room temperature analysis data cannot necessarily be used to predict the reaction. Analysis at the temperature of interest or quenching the sample from the temperature to freeze the products would be the most appropriate.

5.5. Rapoport tests

5.5.1. Experimental observations

Two samples of each carbon grade were tested for percentage expansion during electrolysis. After removing the sample from the furnace, it was observed that 5% of the 20mm of the carbon sample that was not immersed in the molten salt was oxidised. The carbon crucible was also slightly oxidised at the top. There were traces of molten salt that spilled or bubbled into the stainless crucible holder.

5.5.2. Results

Two sets of results for each sample are reported (Table 5.11-5.18) and show good repeatability (Figures 5.25-5.28). The first two graphs are for the 30% graphitised carbon (Figure 5.25 and 5.26) followed by the graphs for the 100% graphitised carbon cathode (Figure 5.27 and Figure 5.28). The percentage expansion was calculated from the measured (experimental) expansion divided by the expansion length (expansion length = length of the small hole – length of the bigger hole of the sample) (Figure 3.9).

5.5.2.1. The 30% graphitised carbon results

Figure 5.25 is the graph of the 2 hour Rapoport experiment while Figure 5.25 is of the 8 hour experiment. It is evident that exposing the 30% graphitised carbon cathode to a sodium rich environment results in an average expansion of 0.77% after 2 hours and an average of 0.80% after 8 hours (Tables 5.11 and 5.12 vs. Tables 5.13 and 5.14).

Table 5.11: *Rapoport data of the 1st test on the 30% graphitised carbon cathode (2 hours).*

Time (minutes)	Expansion (µm)	Expansion (mm)	Temp (ºC)	Expansion Length (mm)	Calculated expansion (%)
1	16	0.016	985	57	0.03
2	35	0.035	985	57	0.06
3	47	0.047	985	57	0.08
4	83	0.083	985	57	0.14
5	130	0.13	985	57	0.23
6	161	0.161	985	57	0.28
7	183	0.183	985	57	0.32
8	198	0.198	985	57	0.35
9	211	0.211	985	57	0.37
10	219	0.219	985	57	0.38
11	232	0.232	985	57	0.41
15	273	0.273	985	57	0.48
20	308	0.308	985	57	0.54
25	319	0.319	985	57	0.56
30	337	0.337	985	57	0.59
40	351	0.351	985	57	0.61
50	352	0.352	985	57	0.62
60	363	0.363	985	57	0.64
70	386	0.386	985	57	0.68
80	404	0.404	985	57	0.71
90	417	0.417	985	57	0.73
100	424	0.424	985	57	0.74
110	431	0.431	985	57	0.76
120	433	0.433	985	57	0.76

Table 5.12: *Rapoport data of the 2nd test on the 30% graphitised carbon cathode (2 hours).*

Time (minutes)	Expansion (µm)	Expansion (mm)	Temp (ºC)	Expansion Length (mm)	Calculated expansion (%)
0					
1	14	0.014	985	57	0.03
2	35	0.035	985	57	0.06
3	47	0.047	985	57	0.08
4	83	0.083	985	57	0.14
5	130	0.13	985	57	0.22
6	161	0.161	985	57	0.28
7	183	0.183	985	57	0.32
8	198	0.198	985	57	0.34
9	211	0.211	985	57	0.35
10	219	0.219	985	57	0.38
11	232	0.232	985	57	0.42
15	273	0.273	985	57	0.48
20	308	0.308	985	57	0.54
25	319	0.319	985	57	0.56
30	337	0.337	985	57	0.58
40	351	0.351	985	57	0.62
50	352	0.352	985	57	0.65
60	363	0.363	985	57	0.65
70	386	0.386	985	57	0.69
80	404	0.404	985	57	0.72
90	417	0.417	985	57	0.73
100	424	0.424	985	57	0.74
110	431	0.431	985	57	0.76
120	433	0.433	985	57	0.78

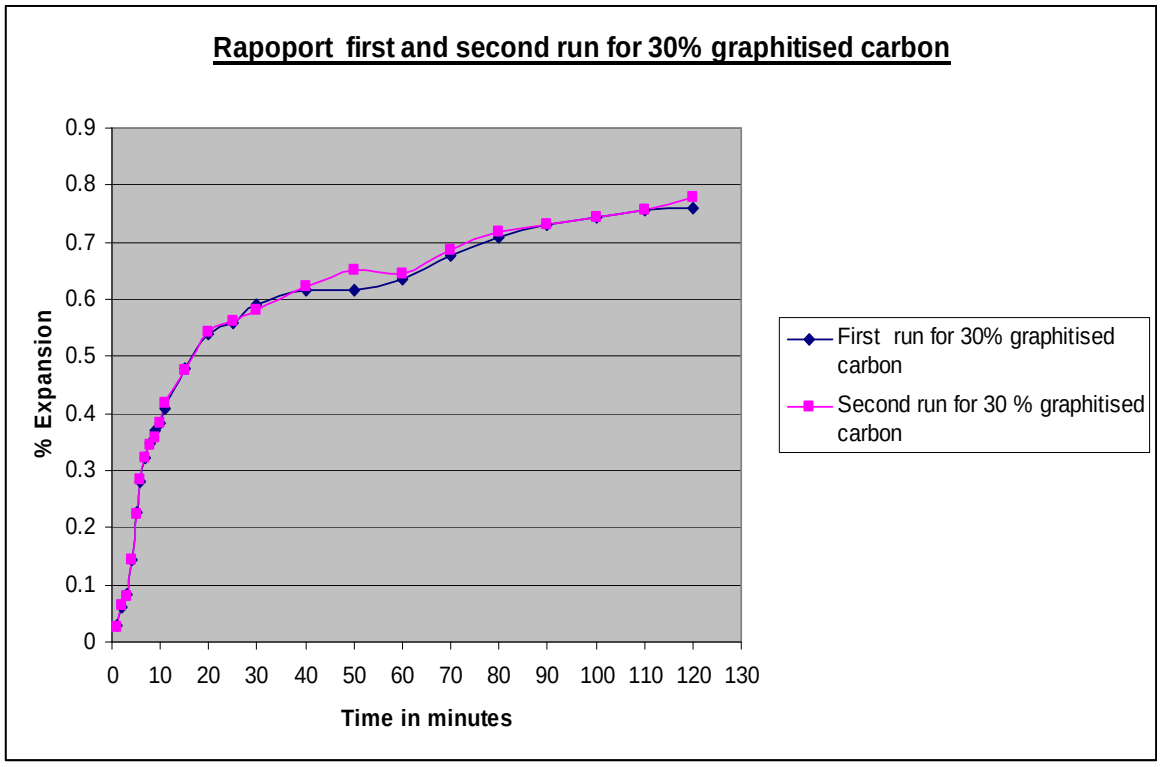

Figure 5.25: *Rapoport graphs of the first and second tests (2 hour experiments) on the 30% graphitised carbon*

Table 5.13: *Rapoport data of the 1st test on the 30% graphitised carbon cathode (8 hours)*

Time (minutes)	Expansion (µm)	Expansion (mm)	Temp (ºC)	Expansion Length(mm)	Calculated Exp %
0	0	0	990	57.25	0
1	15	0.015	990	57.25	0.03
2	36	0.036	990	57.25	0.06
3	46	0.046	990	57.25	0.08
4	80	0.08	990	57.25	0.14
5	125	0.125	990	57.25	0.22
6	159	0.159	990	57.25	0.28
7	186	0.186	990	57.25	0.32
8	200	0.2	990	57.25	0.35
9	214	0.214	990	57.25	0.37
10	225	0.225	990	57.25	0.39
15	235	0.235	990	57.25	0.41
20	275	0.275	990	57.25	0.48
25	310	0.31	990	57.25	0.54
30	341	0.341	990	57.25	0.60
40	353	0.353	990	57.25	0.62
50	360	0.36	990	57.25	0.63
60	367	0.367	990	57.25	0.64
70	388	0.388	990	57.25	0.68
80	402	0.402	990	57.25	0.70
90	419	0.419	990	57.25	0.73
100	425	0.425	990	57.25	0.74
110	429	0.429	990	57.25	0.75
120	435	0.435	990	57.25	0.76
130	436	0.436	990	57.25	0.76
140	438	0.438	990	57.25	0.76
150	440	0.44	990	57.25	0.77
160	441	0.441	990	57.25	0.77
170	441	0.441	990	57.25	0.77
180	443	0.443	990	57.25	0.77
190	444	0.444	990	57.25	0.77
200	447	0.447	990	57.25	0.78
210	450	0.45	990	57.25	0.79
220	450	0.45	990	57.25	0.79
230	450	0.45	990	57.25	0.79
240	450	0.45	990	57.25	0.79
250	450	0.45	990	57.25	0.79
260	451	0.451	990	57.25	0.79
270	451	0.451	990	57.25	0.79
280	452	0.452	990	57.25	0.79
290	453	0.453	990	57.25	0.79
300	453	0.453	990	57.25	0.79

Table 5.13 *Rapoport data of the 1st test on the 30% graphitised carbon cathode (8 hours) (Continued)*

Time (minutes)	Expansion (µm)	Expansion (mm)	Temp (ºC)	Expansion Length(mm)	Calculated Exp %
310	454	0.454	990	57.25	0.79
320	454	0.454	990	57.25	0.79
330	455	0.455	990	57.25	0.79
340	455	0.455	990	57.25	0.79
350	456	0.456	990	57.25	0.80
360	456	0.456	990	57.25	0.80
370	457	0.457	990	57.25	0.80
380	457	0.457	990	57.25	0.80
390	458	0.458	990	57.25	0.80
400	459	0.459	990	57.25	0.80
410	459	0.459	990	57.25	0.80
420	459	0.459	990	57.25	0.80
430	460	0.46	990	57.25	0.80
440	460	0.46	990	57.25	0.80
450	461	0.461	990	57.25	0.80
460	462	0.462	990	57.25	0.80
470	462	0.462	990	57.25	0.80
480	462	0.462	990	57.25	0.80

Table 5.14: *Rapoport data of the 2nd test on the 30% graphitised carbon cathode (8 hours)*

Time (minutes)	Expansion (µm)	Expansion (mm)	Temp (ºC)	Expansion Length(mm)	Calculated Exp %
0	0	0	990	58.23	0
1	16	0.016	990	58.23	0.03
2	38	0.038	990	58.23	0.06
3	50	0.05	990	58.23	0.09
4	85	0.085	990	58.23	0.15
5	134	0.134	990	58.23	0.23
6	167	0.167	990	58.23	0.29
7	185	0.185	990	58.23	0.32
8	198	0.198	990	58.23	0.34
9	213	0.213	990	58.23	0.37
10	221	0.221	990	58.23	0.38
15	278	0.278	990	58.23	0.48
20	305	0.305	990	58.23	0.52
25	319	0.319	990	58.23	0.55
30	340	0.34	990	58.23	0.58
40	353	0.353	990	58.23	0.61
50	362	0.362	990	58.23	0.62
60	370	0.37	990	58.23	0.63
70	389	0.389	990	58.23	0.67

Table 5.14: *Rapoport data of the 2nd test on the 30% graphitised carbon cathode (8 hours) (Continued)*

Time (minutes)	Expansion (µm)	Expansion (mm)	Temp (ºC)	Expansion Length(mm)	Calculated Exp %
80	403	0.403	990	58.23	0.69
90	418	0.418	990	58.23	0.72
100	428	0.428	990	58.23	0.73
110	430	0.43	990	58.23	0.74
120	431	0.431	990	58.23	0.74
130	434	0.434	990	58.23	0.74
140	435	0.435	990	58.23	0.75
150	435	0.435	990	58.23	0.75
160	436	0.436	990	58.23	0.75
170	436	0.436	990	58.23	0.75
180	436	0.436	990	58.23	0.75
190	438	0.438	990	58.23	0.75
200	438	0.438	990	58.23	0.75
210	443	0.443	990	58.23	0.76
220	444	0.444	990	58.23	0.76
230	448	0.448	990	58.23	0.77
240	449	0.449	990	58.23	0.77
250	452	0.452	990	58.23	0.78
260	453	0.453	990	58.23	0.79
270	453	0.453	990	58.23	0.78
280	454	0.454	990	58.23	0.78
290	454	0.454	990	58.23	0.78
300	454	0.454	990	58.23	0.78
310	454	0.454	990	58.23	0.78
320	456	0.456	990	58.23	0.78
330	456	0.456	990	58.23	0.78
340	457	0.457	990	58.23	0.78
350	458	0.458	990	58.23	0.79
360	458	0.458	990	58.23	0.79
370	459	0.459	990	58.23	0.79
380	460	0.46	990	58.23	0.79
390	461	0.461	990	58.23	0.79
400	461	0.461	990	58.23	0.79
410	463	0.463	990	58.23	0.79
420	463	0.463	990	58.23	0.79
430	465	0.465	990	58.23	0.79
440	466	0.466	990	58.23	0.80
450	467	0.467	990	58.23	0.80
460	467	0.467	990	58.23	0.80
470	467	0.467	990	58.23	0.80
480	468	0.468	990	58.23	0.80

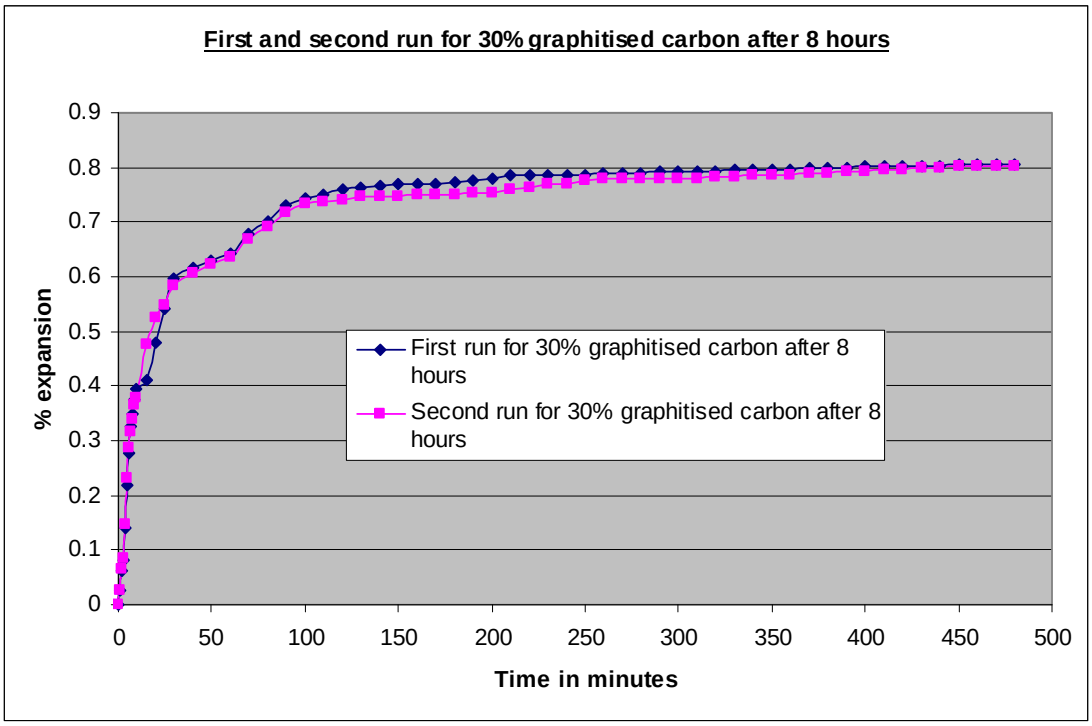

Figure 5.26: *Rapoport graphs of the first and second tests (8 hour experiments) on the 30% graphitised carbon.*

5.5.2.2. The 100% graphitised carbon results

Graphite has a hexagonal close packed structure of carbon. A 100% graphitised carbon material has the most homogeneous structure [3].

When 100% graphitised carbon is exposed to a sodium rich environment, the expansion is very limited. Figure 5.27 is the graph of the 2 hour Rapoport experiment while Figure 5.28 is that of the 8 hour experiment that was performed on the 100% graphitised sample. It is evident that exposing the 100% graphitised carbon cathode to a sodium rich environment results in an average expansion of 0.28% after 2 hours and an average of 0.34% after 8 hours. Running the experiment for 8 hours increased the expansion with about 4% as compared to the 2 hour period.

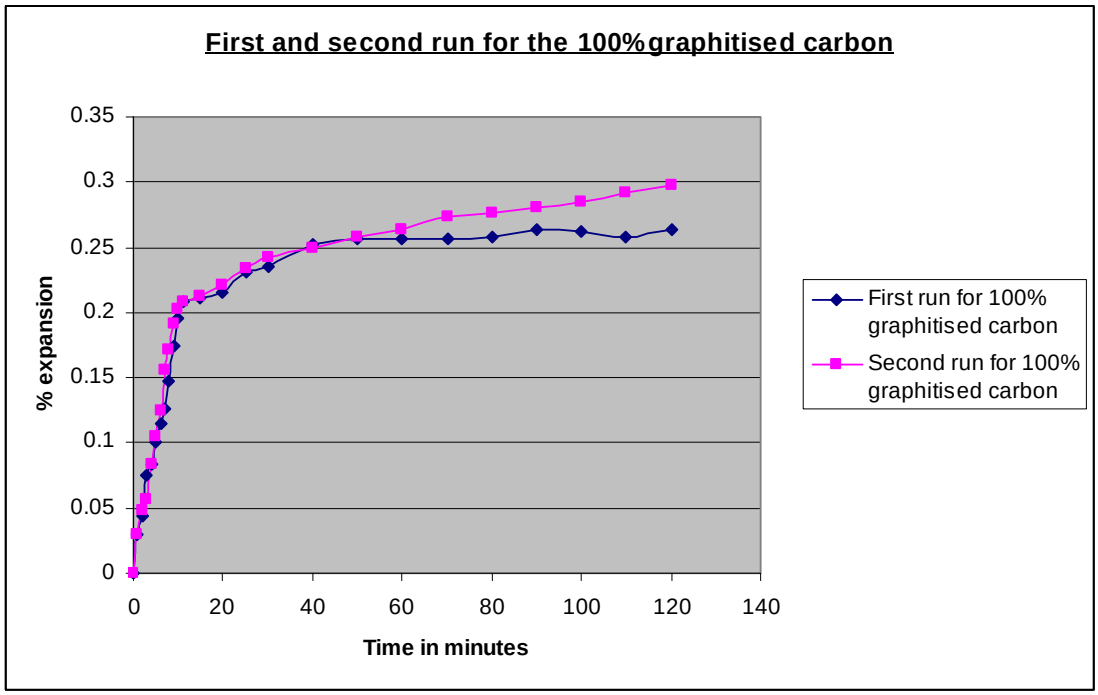

Figure 5.27: *Rapoport graphs of the first and second tests (2 hour experiments) on the 100% graphitised carbon.*

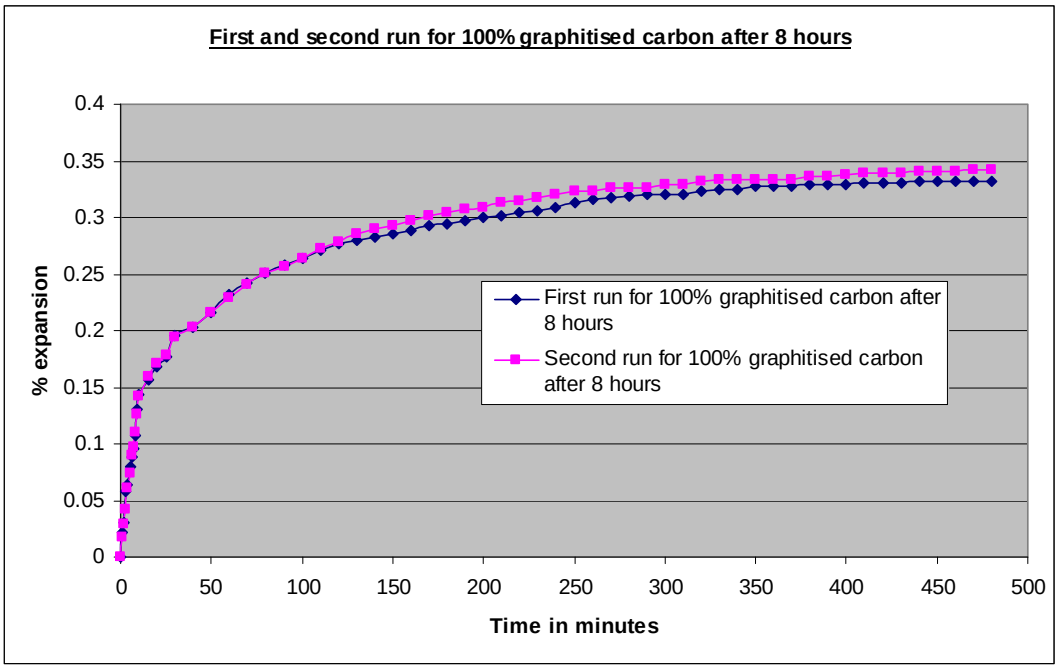

Figure 5.28: *Rapoport graphs of the first and second tests (8 hour experiments) on the 100% graphitised carbon.*

Table 5.15: *Rapoport data of the 1st test on the 100% graphitised carbon (2hours)*

Time (minutes)	Expansion (µm)	Expansion (mm)	Temp (ºC)	Expansion Length (mm)	Calculated Exp %
0	0	0		49.16	0
1	15	0.015	1000	49.16	0.03
2	22	0.022	1000	49.16	0.04
3	37	0.037	1000	49.16	0.07
4	41	0.041	1000	49.16	0.08
5	50	0.05	1000	49.16	0.10
6	57	0.057	1000	49.16	0.11
7	62	0.062	1000	49.16	0.13
8	73	0.073	1000	49.16	0.15
9	86	0.086	1000	49.16	0.17
10	96	0.096	1000	49.16	0.19
15	104	0.104	1000	49.16	0.21
20	106	0.106	1000	49.16	0.21
25	114	0.114	1000	49.16	0.23
30	116	0.116	1000	49.16	0.23
40	124	0.124	1000	49.16	0.25
50	126	0.126	1000	49.16	0.26
60	126	0.126	1000	49.16	0.26
70	126	0.126	1000	49.16	0.26
80	127	0.127	1000	49.16	0.26
90	130	0.13	1000	49.16	0.26
100	129	0.129	1000	49.16	0.26
110	127	0.127	1000	49.16	0.26
120	130	0.13	1000	49.16	0.26

Table 5.16: *Rapoport data of the second test on the 100% graphitised carbon (2hours)*

Time (minutes)	Expansion (µm)	Expansion (mm)	Temp (ºC)	Expansion Length (mm)	Calculated % Expansion
0	0	0	1000	59.62	0
1	18	0.018	1000	59.62	0.03
2	35	0.035	1000	59.62	0.06
3	48	0.048	1000	59.62	0.08
4	58	0.058	1000	59.62	0.10
5	69	0.069	1000	59.62	0.11
6	82	0.082	1000	59.62	0.14
7	92	0.092	1000	59.62	0.15
8	103	0.103	1000	59.62	0.17
9	112	0.112	1000	59.62	0.19
10	117	0.117	1000	59.62	0.20
11	126	0.126	1000	59.62	0.21
15	127	0.127	1000	59.62	0.21
20	130	0.130	1000	59.62	0.22
25	139	0.139	1000	59.62	0.23
30	145	0.145	1000	59.62	0.24
40	148	0.148	1000	59.62	0.25
50	153	0.153	1000	59.62	0.26
60	158	0.158	1000	59.62	0.26
70	163	0.163	1000	59.62	0.27
80	165	0.165	1000	59.62	0.28
90	167	0.167	1000	59.62	0.28
100	172	0.172	1000	59.62	0.29
110	174	0.174	1000	59.62	0.29
120	178	0.178	1000	59.62	0.30

Table 5.17: *Rapoport data of the 1st test on the 100% graphitised carbon cathode (8 hours)*

Time (minutes)	Expansion (µm)	Expansion (mm)	Temp (ºC)	Expansion Length(mm)	Calculated Exp %
0	0	0	0	0	0
1	14	0.014	985	59.62	0.02
2	20	0.02	985	59.62	0.03
3	38	0.038	985	59.62	0.06
4	42	0.042	985	59.62	0.07
5	52	0.052	985	59.62	0.09
6	58	0.058	985	59.62	0.10
7	63	0.063	985	59.62	0.10
8	70	0.07	985	59.62	0.12
9	86	0.086	985	59.62	0.14
10	94	0.094	985	59.62	0.16
15	103	0.103	985	59.62	0.17
20	110	0.11	985	59.62	0.18
25	116	0.116	985	59.62	0.19
30	128	0.128	985	59.62	0.21
40	133	0.133	985	59.62	0.22
50	142	0.142	985	59.62	0.24
60	152	0.152	985	59.62	0.25
70	159	0.159	985	59.62	0.27
80	165	0.165	985	59.62	0.28
90	169	0.169	985	59.62	0.28
100	173	0.173	985	59.62	0.29
110	178	0.178	985	59.62	0.30
120	182	0.182	985	59.62	0.30
130	184	0.184	985	59.62	0.31
140	185	0.185	985	59.62	0.31
150	187	0.187	985	59.62	0.31
160	189	0.189	985	59.62	0.32
170	192	0.192	985	59.62	0.32
180	193	0.193	985	59.62	0.32
190	195	0.195	985	59.62	0.33
200	197	0.197	985	59.62	0.33
210	198	0.198	985	59.62	0.33
220	200	0.2	985	59.62	0.33
230	201	0.201	985	59.62	0.34
240	203	0.203	985	59.62	0.34
250	203	0.203	985	59.62	0.34
260	203	0.203	985	59.62	0.34
270	203	0.203	985	59.62	0.34
280	203	0.203	985	59.62	0.34
290	203	0.203	985	59.62	0.34
300	203	0.203	985	59.62	0.34

Table 5.17: *Rapoport data of the 1st test on the 100% graphitised carbon cathode (8 hours) (Continued)*

Time (minutes)	Expansion (µm)	Expansion (mm)	Temp (ºC)	Expansion Length(mm)	Calculated Exp %
310	203	0.203	985	59.62	0.34
320	203	0.203	985	59.62	0.34
330	203	0.203	985	59.62	0.34
340	203	0.203	985	59.62	0.34
350	203	0.203	985	59.62	0.34
360	203	0.203	985	59.62	0.34
370	203	0.203	985	59.62	0.34
380	203	0.203	985	59.62	0.34
390	203	0.203	985	59.62	0.34
400	203	0.203	985	59.62	0.34
410	203	0.203	985	59.62	0.34
420	203	0.203	985	59.62	0.34
430	203	0.203	985	59.62	0.34
440	203	0.203	985	59.62	0.34
450	203	0.203	985	59.62	0.34
460	203	0.203	985	59.62	0.34
470	203	0.203	985	59.62	0.34
480	203	0.203	985	59.62	0.34

Table 5.18: *Rapoport data of the 2nd test on the 100% graphitised carbon cathode (8 hours)*

Time (minutes)	Expansion (µm)	Expansion (mm)	Temp (ºC)	Expansion Length(mm)	Calculated Exp %
0	0	0	0	0	0
1	12	0.012	995	66.63	0.02
2	19	0.019	995	66.63	0.03
3	28	0.028	995	66.63	0.04
4	41	0.041	995	66.63	0.06
5	49	0.049	995	66.63	0.07
6	60	0.06	995	66.63	0.09
7	65	0.065	995	66.63	0.10
8	73	0.073	995	66.63	0.11
9	84	0.084	995	66.63	0.13
10	95	0.095	995	66.63	0.14
15	106	0.106	995	66.63	0.16
20	114	0.114	995	66.63	0.17
25	119	0.119	995	66.63	0.18
30	129	0.129	995	66.63	0.19
40	135	0.135	995	66.63	0.20
50	144	0.144	995	66.63	0.22
60	153	0.153	995	66.63	0.23
70	160	0.16	995	66.63	0.24
80	167	0.167	995	66.63	0.25

Table 5.18: *Rapoport data of the 2nd test on the 100% graphitised carbon cathode (8 hours) (Continued)*

90	171	0.171	995	66.63	0.26
100	176	0.176	995	66.63	0.26
110	182	0.182	995	66.63	0.27
120	185	0.185	995	66.63	0.28
130	190	0.19	995	66.63	0.28
140	193	0.193	995	66.63	0.29
150	195	0.195	995	66.63	0.29
160	198	0.198	995	66.63	0.30
170	201	0.201	995	66.63	0.30
180	203	0.203	995	66.63	0.30
190	205	0.205	995	66.63	0.31
200	206	0.206	995	66.63	0.31
210	209	0.209	995	66.63	0.31
220	210	0.21	995	66.63	0.31
230	211	0.211	995	66.63	0.32
240	213	0.213	995	66.63	0.32
250	215	0.215	995	66.63	0.32
260	215	0.215	995	66.63	0.32
270	217	0.217	995	66.63	0.32
280	217	0.217	995	66.63	0.33
290	217	0.217	995	66.63	0.33
300	219	0.219	995	66.63	0.33
310	219	0.219	995	66.63	0.33
320	221	0.221	995	66.63	0.33
330	222	0.222	995	66.63	0.33
340	222	0.222	995	66.63	0.33
350	222	0.222	995	66.63	0.33
360	222	0.222	995	66.63	0.33
370	222	0.222	995	66.63	0.33
380	224	0.224	995	66.63	0.34
390	224	0.224	995	66.63	0.34
400	225	0.225	995	66.63	0.34
410	226	0.226	995	66.63	0.34
420	226	0.226	995	66.63	0.34
430	226	0.226	995	66.63	0.34
440	227	0.227	995	66.63	0.34
450	227	0.227	995	66.63	0.34
460	227	0.227	995	66.63	0.34
470	228	0.228	995	66.63	0.34
480	228	0.228	995	66.63	0.34

The percentage expansion of the carbon cathode versus time (Figure 5.25-5.28) shows parabolic rate behaviour. During the first 20 minutes of the experiment, electrolyte penetrates rapidly into the carbon cathode, after which penetration slows down.
The period of electrolysis has an influence on the percentage expansion of the carbon cathode. The experiments that were run for long periods (8 hours) exhibited a high percentage of expansion as compared to the shorter electrolysis periods (2 hours) (Figures 5.25-5.28).

Another factor that has an influence on the penetration of the electrolyte into the carbon is the pore size distribution of the carbon cathode material. The electrolyte penetrates the larger pores first, thus having an intial high penetration rate as shown in Figures 5.25-5.28. As the large pores are filled, the electrolyte starts to penetrate the smaller pores at a slower rate, thus resulting in the flat shape of the graphs.

During the aluminium electrolysis process, the side walls of the cell have low temperature as compared to the internal part of the cell. Due to this temperature gradient associated with the side walls, the electrolyte that is closer to the side wall solidifies to form the so called “frozen ledge”. The frozen ledge protects the cell from further penetration by the extremely corrosive molten cryolite [9].

During the laboratory aluminium electrolysis experiments, the temperature was distributed uniformly in the furnace. Due to the homogeneous distribution of temperature in the furnace, it is therefore not easy to evaluate the effect of temperature during the laboratory aluminium electrolysis experiments.

Comparing the two graphitised carbon cathodes (30% and 100% graphitised carbon), it is evident that their expansion behaviour is different. The 30% graphitised carbon expands more (0.78% after 2 hours and 0.80% after 8 hours) as compared to the 100% graphitised carbon cathode which showed an average expansion of 0.27% after 2 hours and 0.34% after 8 hours.

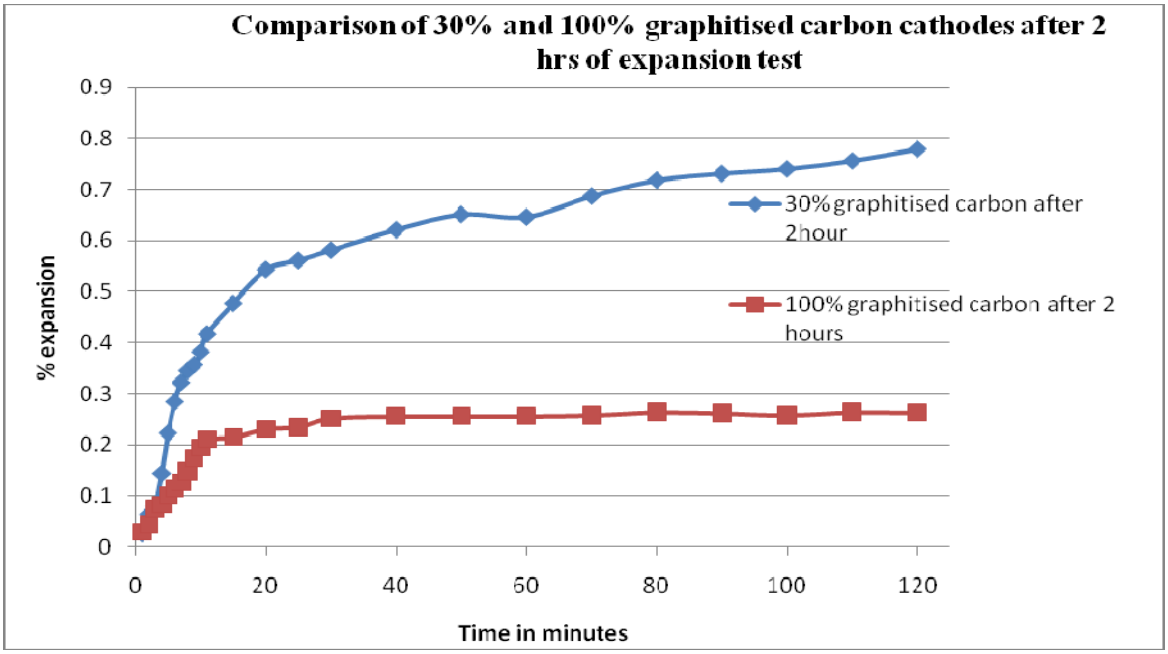

Figure 5.29: *Graphical data comparison of 30% and 100% graphitised carbon after 2 hrs of expansion test.*

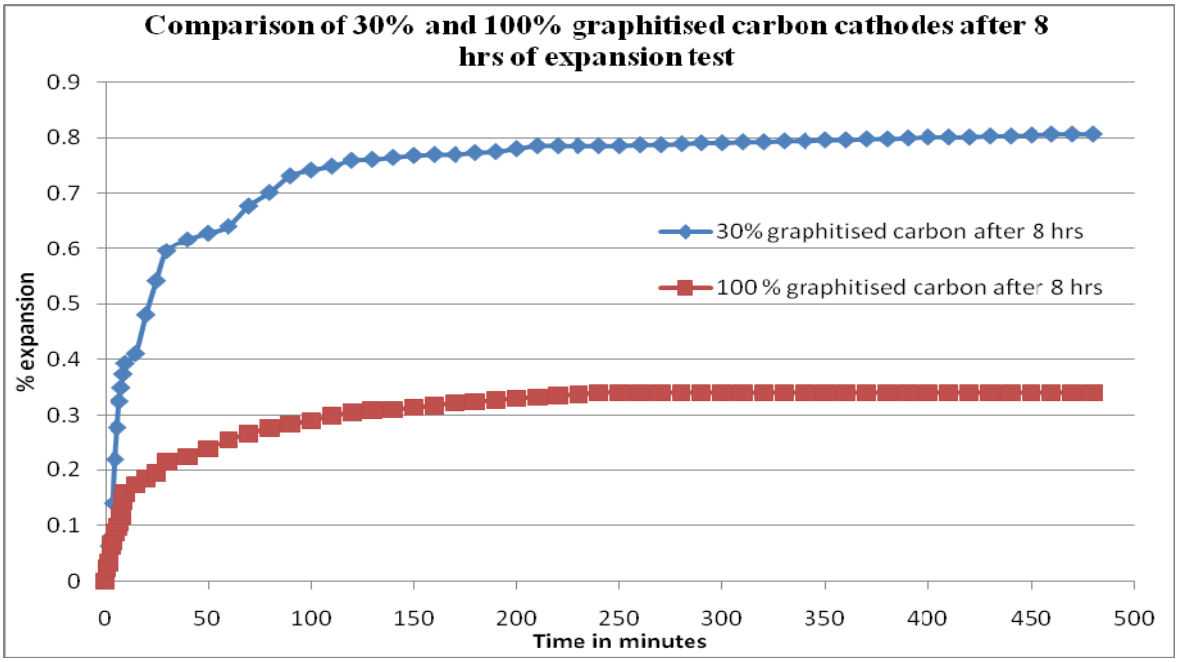

Figure 5.30: *Graphical data comparison of 30% and 100% graphitised carbon after 8 hrs of expansion test.*

The data obtained shows that 30% graphitised carbon has higher expansion than the 100% graphitised carbon. This data agrees with the literature data obtained by A.Zlochvisky et al [35][36].

Chapter 6: Conclusions

6.1. Introduction

The carbon cathode lining is in contact with the electrolyte during the aluminium electrolysis process. The primary aim of the study was to identify phases that penetrate, react and cause expansion of carbon cathode lining during the electrolytic production of aluminium.

Phases that form as the electrolyte penetrates the carbon cathode lining were identified using XRD, and quantifying them using the Rietveld (Autoquan) method. Response of different graphitised carbon cathode during electrolytic production of aluminium was evaluated. Rapoport (sodium expansion) experiments were used to investigate the degree of expansion of different carbon grades when exposed to a sodium and fluorine rich environment.

In the quest to achieve the project objectives, post mortem and virgin carbon cathode samples were obtained from a South African smelting plant. The virgin carbon cathode materials that were examined were respectively 30% and 100% graphitised. The post-mortem data was compared to the laboratory data.

6.2. Post-Mortem analysis

Two plant samples that were in operation for respectively 1944 (sample "A") and 1644 (sample "B") days were obtained and investigated. The following phases were detected in the two samples: NaF, Na_3AlF_6, $NaAl_{11}O_{17,}$ CaF_2 and graphite. NaCN was only detected in sample "A", while AlN and $Na_5Al_3F_{14}$ were only detected in sample "B".

In order to distinguish between phases that form due to electrolyte reacting with carbon cathode and those due to chemical reaction in the electrolyte, a solidified bath was analysed. The following phases were identified from the solidified bath Na_3AlF_6, NaF, CaF_2, Al_2O_3 and $NaAl_{11}O_{17}$. Only Diaoyudaoite ($NaAl_{11}O_{17}$) is the phase that was identified from the solidified bath that was not in the initial bath constituents, therefore this means $NaAl_{11}O_{17}$ is the only chemical reaction product from the solidified bath.

Analysis of the two carbon cathode and the solidified bath confirmed the penetration of the bath electrolyte into the carbon cathode. The penetration of bath electrolyte causes expansion and swelling of the carbon cathode, as this was shown to be the wear mode of the carbon cathode from the literature, therefore it could be concluded that electrolyte penetration causes wear/failure of the carbon cathode during the electrolytic production of aluminium. Three phases were identified that are the product of the reaction between the carbon cathode, electrolyte and the atmosphere. The three phases are NaCN, AlN and NaF. These three phases presumable formed through reaction of electrolyte (that penetrated into the carbon structure) with nitrogen and cryolite according to the following two reactions [10]:

$$3/2N_2(g) + 3C(s) + 3Na(in\ C) = 3NaCN(l) \quad \text{6.1}$$

$$1/2N_2(g) + Na_3AlF_6(l) + 3Na(in\ C) = AlN(s) + 6NaF(l) \quad \text{6.2}$$

Chiolite ($Na_5Al_3F_{14}$) could also be detected in the carbon cathodes. It is assumed that chiolite formed through reaction of the cryolite (Na_3AlF_6) and aluminium fluoride (AlF_3) above 734°C, according to the following reaction [36]:

$$5\ Na_3AlF_6 + 4\ AlF_3 = 3\ Na_5Al_3F_{14} \quad \text{6.3}$$

The phase distribution in the “A” and “B” samples are quite similar, except the detection of the NaCN in sample “A” only and AlN and $Na_5Al_3F_{14}$ in sample “B” only. There is Na intercalation in the carbon cathode during the electrolytic production of aluminium.

6.3. Laboratory scale electrolysis experiment.

Two experimental periods (1hours 30minutes and 3hours) were used to investigate bath penetration into the carbon cathodes and phases that formed during the laboratory aluminium electrolysis process. The following phases were detected in both the 30% and 100% graphitised carbon cathodes after 1hr 30 minute of electrolysis: Na_3AlF_6, NaF and graphite. $NaAl_{11}O_{17}$ was only detected in the 30% graphitised carbon, while CaF_2 was only found in the 100% graphitised carbon cathode.

After the 3hour experiments the following phases were detected in both the 30% graphitised and the 100% graphitised carbon cathodes: Na_3AlF_6, $NaAl_{11}O_{17}$ and graphite. NaF and CaF_2 were only found in the 30% graphitised carbon cathode.

It is evident that the bath did penetrate both carbon cathode grades during the laboratory aluminium electrolysis process. Neither graphite peak shift, nor peak broadening or peak splitting was observed from the XRD patterns. Sodium intercalation into the carbon could therefore not be confirmed. The NaF that formed in the laboratory experiments presumably formed according to the following equations:

It formed due to the reaction of cryolite with sodium vapour as given in equation 6.4 [10].

$$6Na\ (vapour) + 2Na_3AlF_6 \longrightarrow 12NaF + 2Al \quad \text{.....6.4.}$$

The NaF can also form according to equation 6.5 [10]:

$$Na_3AlF_6\ (l) + 3Na\ (in\ C) = 0.25\ Al_4C_3\ (s) + 6NaF \quad \text{.....6.5.}$$

There is different phase distribution from the two analysed carbon cathode graphites. There is no Na intercalation that could be confirmed during the laboratory scale process.

The results of the analysis show equilibrium products from furnace cooling the samples from 1233K. Room temperature analysis data cannot necessarily be used to predict the reaction. Analysis at the temperature of interest or quenching the sample from the temperature to freeze the products would be the most appropriate.

The pore size distribution and the degree of graphitisation of a carbon cathode grade have a direct influence on the penetration of electrolyte into the carbon cathode. Bath penetrated more into the 30% graphitised carbon cathode than the 100% graphitised carbon cathode. The less graphitised carbon cathode (30% graphitised) was found to be more susceptible to bath penetration than the more graphitised carbon cathode (100% graphitised).

6.4. Rapoport experiment

The Rapoport (sodium expansion) experiment was used to investigate the expansion of carbon cathodes in a sodium rich environment. The experiments were done on the same carbon grades (30 % and 100% graphitised carbon) as the electrolysis experiments.

The carbon cathode lining expands when exposed to the sodium rich environment at 960°C. Expansion is dependent on the degree of graphitisation of the carbon cathode: the less graphitised (30%) grade expands more than the grade that is more graphitised (100%). In this study the 30% graphitised grade expanded 0.78% after 2 hours of exposure and 0.80% after 8 hours of exposure to the sodium rich environment, while the 100% graphitised carbon expanded only 0.27% after 2 hours and 0.34% after 8 hours. Expansion occurred rapidly with the onset of the tests, and then slowed down after approximately one hour.

6.5. Comparison between laboratory scale tests and Post-Mortem results

Virgin and post-mortem (from failed cells) carbon cathode samples were received from a South African aluminium smelter. Bath constituents were identified in all carbon cathode samples. The post-mortem samples have more reaction products (phases that did not originate from the bath constituents) than the laboratory scale results. Reaction products that were identified in the post-mortem samples are $NaAl_{11}O_{17}$ and NaCN in the sample A (1944 life span), and $Na_5Al_3F_{14}$ and AlN in sample B (1644 life span). Of these reaction products only $NaAl_{11}O_{17}$ was identified in the laboratory scale experiment on the 30% graphitised carbon sample after both experimental periods tested (1hour 30 minutes and 3 hours) but was only identified after 3hours in the 100% graphitised carbon.

The electrolyte penetration depends on the degree of graphitisation (heat treatment temperature) of the carbon cathode. Carbon cathode that are heat treated at higher temperature (3000°C) has more graphitised and low porous structure as compared to the carbon cathode heat treated al low temperature (1200°). Therefore the 30% graphitised carbon cathode is more vulnerable to electrolyte penetration than the 100% graphitised carbon cathode

The 30% graphitised carbon has larger graphite grains as compared to both 100% and the post-mortem samples. Using the FWHM to investigate peak broadening showed that there is no peak broadening due to electrolyte penetration and Na intercalation. It was further revealed that there in lattice constant change during the penetration of the electrolyte into the carbon cathode lining.

The study was successful in its aim of identifying phases that forms, react and cause the failure of the carbon cathode lining during the electrolytic production of aluminium. The possible penetrating mechanism that could have taken place is the interface mass transfer where sodium penetrates the carbon due to chemical potential gradient. Otherwise the electrolyte penetrated the carbon through the porous regions of the carbon cathode. The post-mortem data gave more conclusive information about phases penetrating the carbon cathode and sodium intercalation than the laboratory experiments. The laboratory experiment periods has to be longer in order to give conclusive information about phases and reaction of the bath electrolyte with carbon cathode. Wear of the carbon cathode lining is due to electrolyte penetration and sodium intercalation.

Chapter 7: Future work on this topic.

Though extensive work has been done on this subject, there is still more work that still need to be investigated. To consolidate this study a more advanced/sensitivy technique such as Transmission Electron Microscope method can be applied to do the elemental mapping and determine the depth of penetration of the electrolyte. Computational simulation of the penetration behaviour of the bath contents still need an investigation, the study of different materials that can be used and perform the same as the carbon cathode also needs to be looked at.

References:

1. Search for Hall-Heroult process, http//en.wikipedia.org/wiki/hall-H%3A9roult_process (last accessed 12/08/2011).
2. J.G. Hop, "Sodium Expansion and Creep of cathode", Thesis submitted to Institute of Materials Technology, Norwegian University of Science and Technology, 2003, 1-176.
3. P.Y.Brisson, G. Soucy, M. Fafard and M. Dionne, "The effect of sodium on carbon lining of the aluminium electrolysis cell-A Review", Canadian Metallurgical Quarterly, 2002, volume 44 (no 2), pp265-279.
4. N. Adhoum, J. Bouteillon, D. Dumasand and J. Claude Poignet, "Electrochemical insertion of sodium into graphite in molten sodium at 1025°C" electrochemical acta, 2008, volume 58, pp5402-5406.
5. A. Zlochevsky, J.G.Hop, T.Foosnaes and H.A.Oye, "Rapoport-Samoilenko test for cathode materials-I, experimental results and constitutive modelling", Carbon, 2003, volume 41, pp497-505.
6. http//sam.davson.com/as/physical/aluminium/site/abundance.html, (last accessed 22/12/2011).
7. A.R.Burkin, John Wiley and sons, "production of aluminium and alumina", 1987, volume 20, pp11-15.
8. www.chemistrydaily.com (last accessed 27/08/2011).
9. B.Droy, and D.Michaux, "Bauxite ore digestion in Bayer process" US Patent 65550761, 2003, pp1-34.
10. K. Gtjotheim and H.Kvande, "Introduction to aluminiumelectrolysis" Aluminium Verlag, 2nd edition, 1993, pp40-41.
11. J.Hope, A. Store, T. Foosnaes and H.A.Oye, "Chemical and physical changes of cathode carbon by aluminium electrolysis" South African Institute of Mining and Metallurgy, 2004, pp775-782.
12. Richerson and Association, "Aluminium industry", Chapter 7, 1998. Pp1-13.
13. M. Sorlie and H.A.Oye, Cathodes in aluminium electrolysis", Aluminium Verlag, 2nd edition, 1994, pp127-129.
14. J. xue, Q. Liu, J. Zhu and w. Ou, "Sodium penetration into carbon-based cathodes during aluminium electrolysis", Light Metals, 2006, pp651-654.
15. W. Wayne and R.Hale "Improving the useful life of aluminium industry cathodes", Journal of Metals, 1998, pp20-25.
16. M. Imris, G. Soucy and M. Fafard, "Carbon cathode resistance against sodium penetration during aluminium electrolysis-An Overview", Acta Metallurgical slovaka, 2005, volume 11 (no2), pp231-243.
17. P.Y.Brisson, H. Darmstadt, M. Fafard, A. Adnot, G. Servant and G. Soucy, "X-ray photoelectron spectroscopy study of sodium reaction in carbon cathode blocks of aluminium oxide reduction cell", Carbon, 2006, volume 44, pp1438-1447.

18. P. Brilloit, L.P. Lossius and H.A.Oye, "Melt penetration and chemical reactions in carbon during aluminium electrolysis, I, Laboratory experiments" Light Metals, 1993, pp321-330.
19. G. Yuanling, X.Jilai, J. Zhu, K. Jiao and J. Gangqin, "Characterization of sodium and fluoride penetration into carbon cathodes by image analysis and SEM-EDS Techinques", The minerals, Metals and Materials Science, Light Metals, 2011, pp1103-1107.
20. P.Brilloit, L.P.Lossius and H.A.Oye, "Penetration and chemical reactions in carbon cathodes during aluminium electrolysis, Part I, laboratory experiments", Metallurgical Transactions B, 1993, volume 24, pp75-89.
21. S. Zhang, Q. Han and Z. Liu, "Thermodynamic modelling of the Al-Mg-Na system", Journal of alloys And compounds, 2006, volume 419 (no 2), pp91-97.
22. E. Scheuer, "Study of the solubility of sodium in aluminium", Metall Kd, 1935, volume 27, pp83-85.
23. W.L. Fink, L.A. Willey and H.C.Stumpf, "Equilibrium relation in aluminium-sodium alloy of high puriy", Transition AIME, 1948, volume 175, pp364-371.
24. C.E.Ransley and H. Neufeld, "The solubility relationship in the aluminium-sodium and aluminium silicon system" Journal of Interaction Metallurgy, 1950, volume 28, pp25-46.
25. S.G. Hansen, J.K.Tuset and G.M.Haarberg, "Thermodynamics of liquid Al-NA alloys determined by using CaF2 solid electrolyte", Metallurgy Transition B, 2002, volume 33B, pp577-588.
26. P. Fellner, M. Korenko and V. Danielik, "Comments on solubility and activity of sodium in molten aluminium", The International Jomar Thonstad Symposium Trongheim, 2002, pp199-206.
27. J. Thonstad, " The solubility of aluminium in NaF-AlF_3-Al_2O_3 melts", 1965, volume 43, pp3429-3432.
28. J.L.Murray, "Alloy phase diagram" 1993, volume 5, pp536-540.
29. J.C. Mitchel and C.S. Samis, "Activity of sodium in Na-Al system and NaF and AlF3 activities in NaF-AlF3 melts", 1969, volume 245, pp1227-1284.
30. Gang Xei and Shiyin Shen, "Sodium activity in molten aluminium measured with a solid electrolyte", Journal of Materials Science Technology, 1993, volume 9, pp388-390.
31. E.W.Dewing, "Thermodynamic of the system NaF-AlF3, I: The equilibrium 6NaF+Al=Na_3AlF_6 +3Na", Metallurgical Transitions, 1970, volume 1, pp1691-1694.
32. R.J.Brisley and D.J.Fray, "Determination of sodium activity in aluminium silicon alloys using sodium beta alumina", Metallurgical and Materials, Transactions B, 1998, volume 14, pp435-440.
33. T. Foosnaes, G.M.Harberg, A.P.Ratvik and E.Skybakmoen, "Wear of carbon cathodes in cryolite-alumina melts", Light Metals, 2007, pp820-826.
34. Y.Mikhalev and H.A.Oye, "Absorption of Metallic sodium in carbon cathode materials", Carbon, 1996, volume 34, pp37-41.

35. A. Zlochvisky, J.G.Hop, T. Foosnaes, and H.A.Oye", Rapoport-Samailenko test for cathode materials-II swelling with external pressure and effect of creep", Carbon Journal, 2005, volume 43, pp1222-1230.
36. A.Zlochvisky, J.G.Hop, G. Servant, T. Foosnaes and H.A.Oye, "Creep and sodium expansion in semigraphitic cathode carbon", The Minerals, Metals and Materials Society, Light metals, 2003, pp595-602.
37. http://en.wikipedia.org/wiki/SGL_Carbon.
38. G. Scholz, M. Feist and E. Kermitz, "On the influence of humidity in the mechanochemical reactions between NaF and AlF_3", Solid State Science, 2008, volume 10, pp1640-1650.

APPENDIX

Appendix A: Diffractograms of the solidified bath samples taken from a South African smelting plant

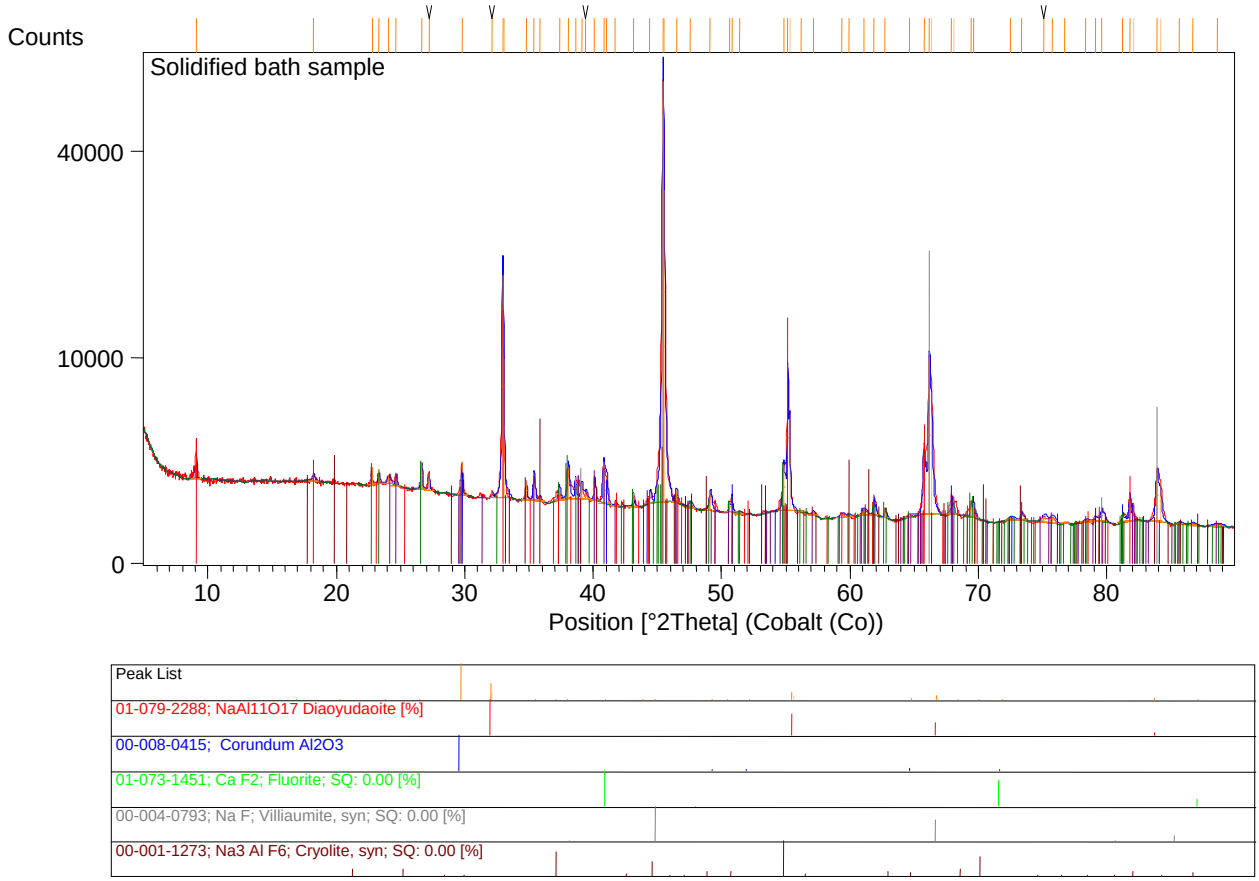

Appendix B: Diffractograms of the post-mortem samples"A"

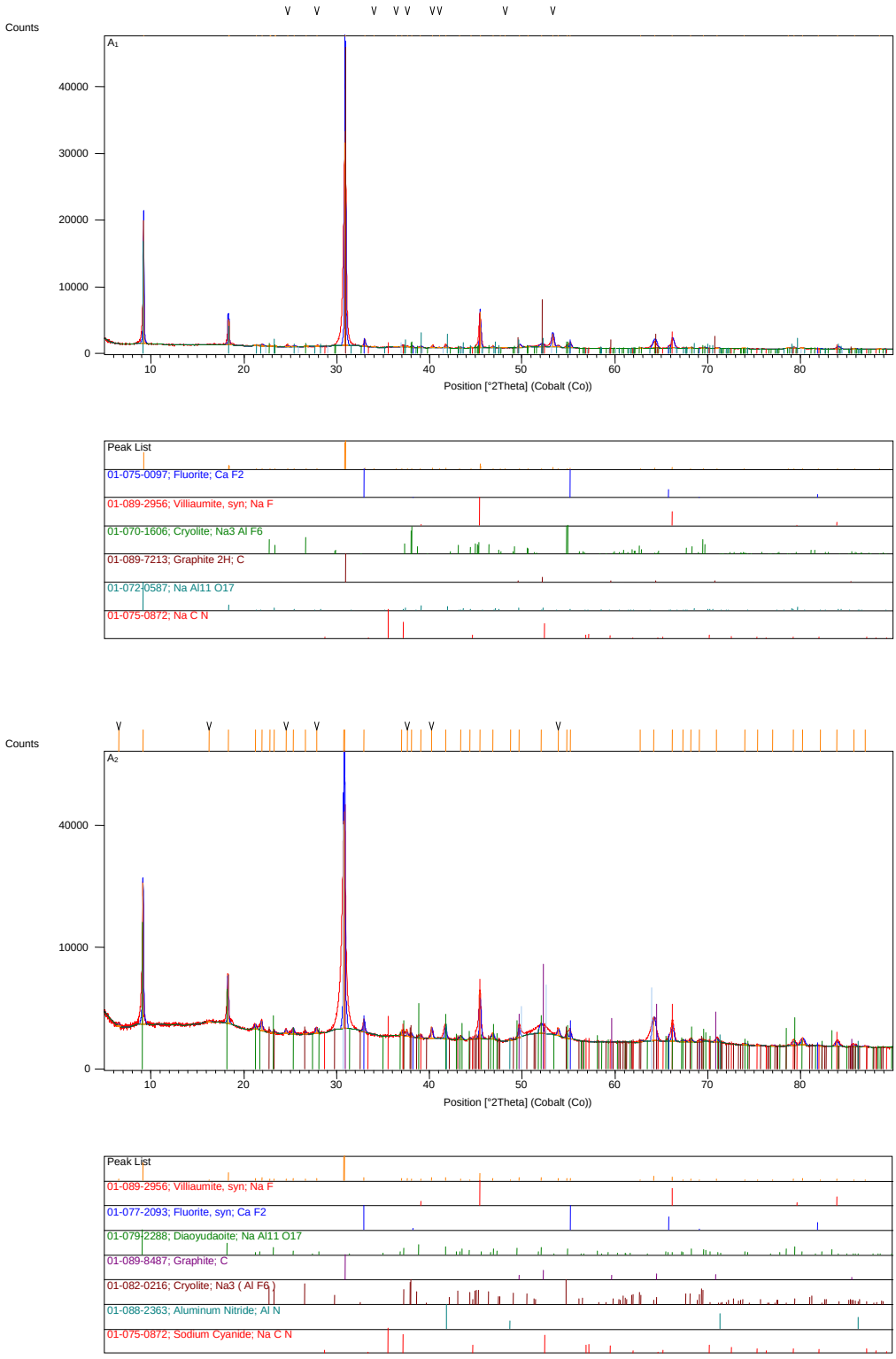

REACTIVITY OF CARBON CATHODE MATERIALS WITH ELECTROLYTE BASED ON PLANT AND LABORATOTY DATA

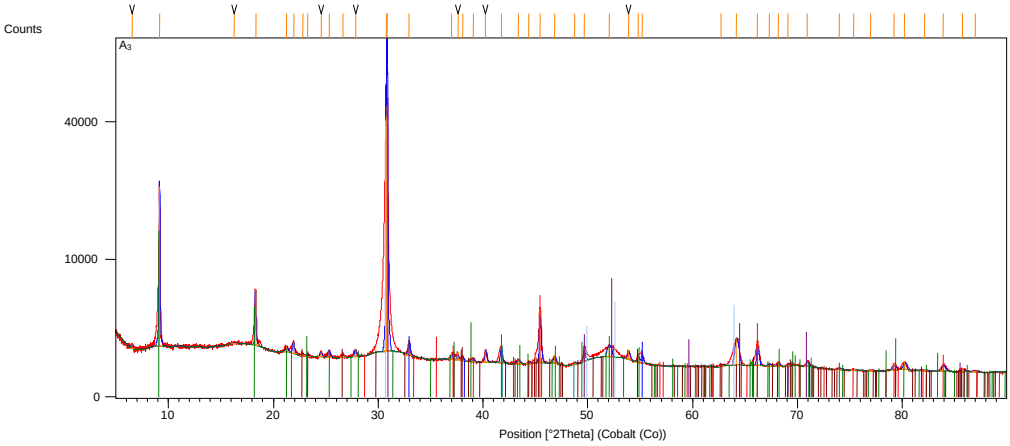

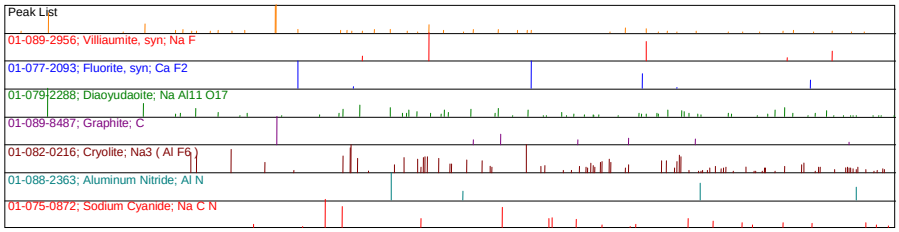

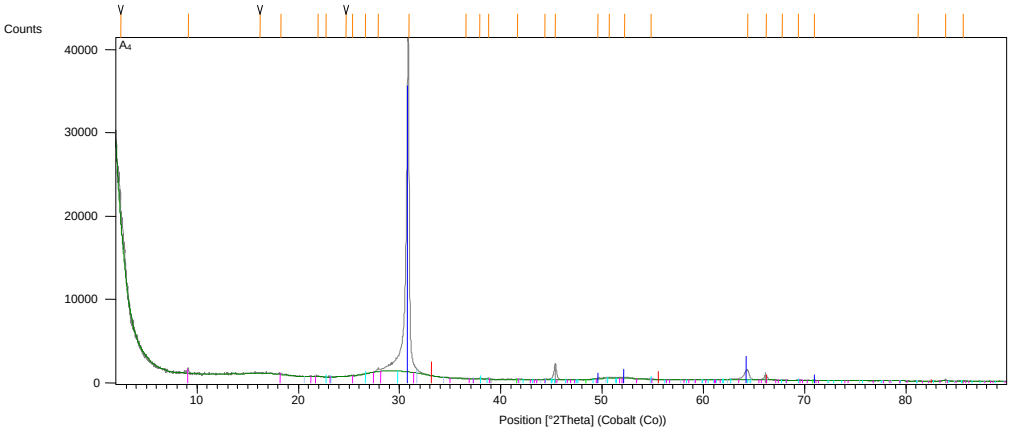

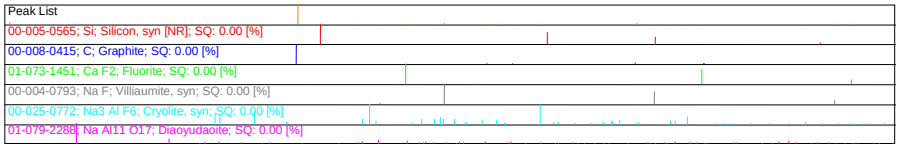

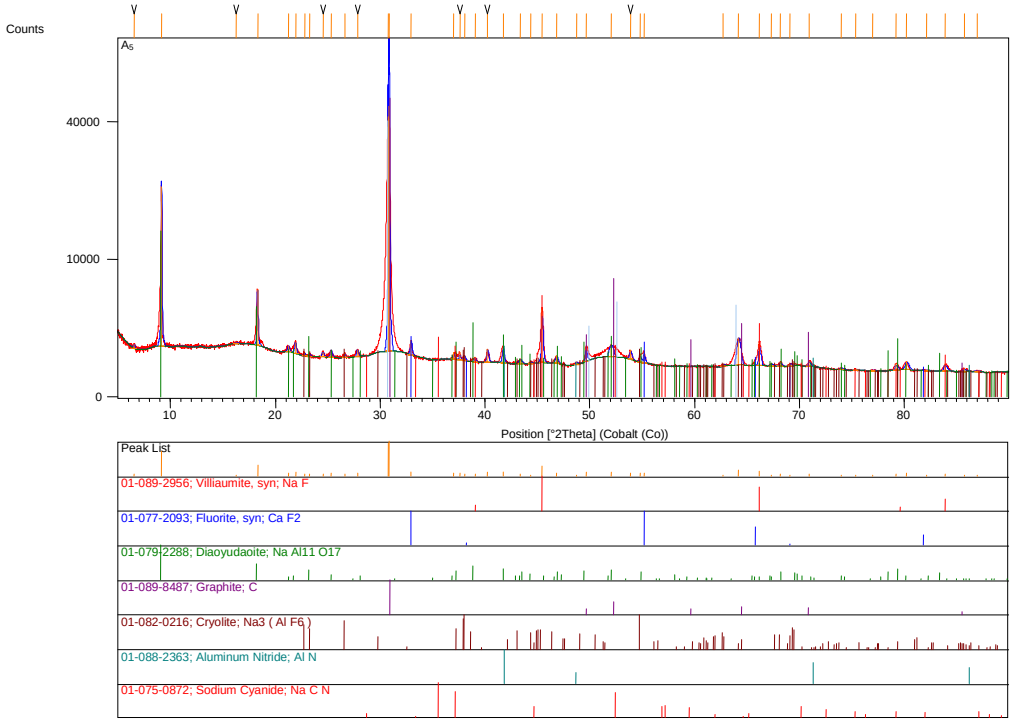

Appendix C: Diffractograms of the post-mortem samples"B"

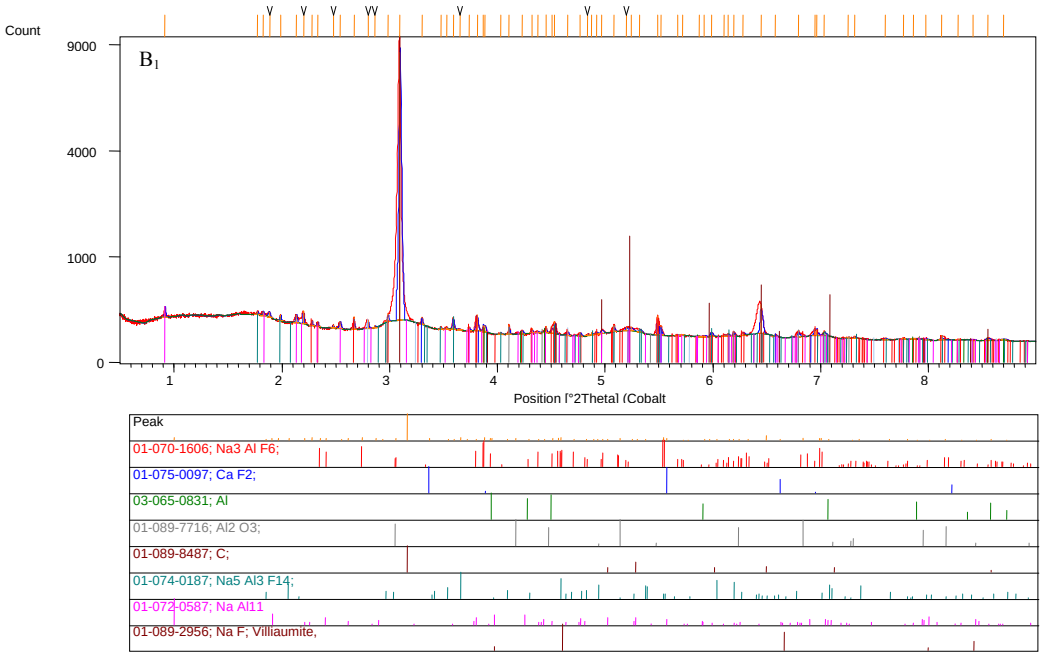

REACTIVITY OF CARBON CATHODE MATERIALS WITH ELECTROLYTE BASED ON PLANT AND LABORATOTY DATA

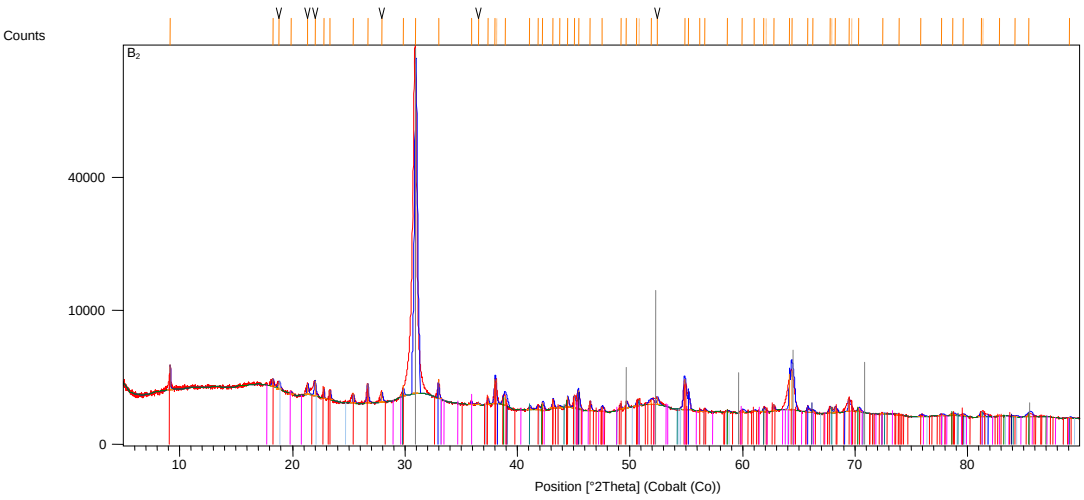

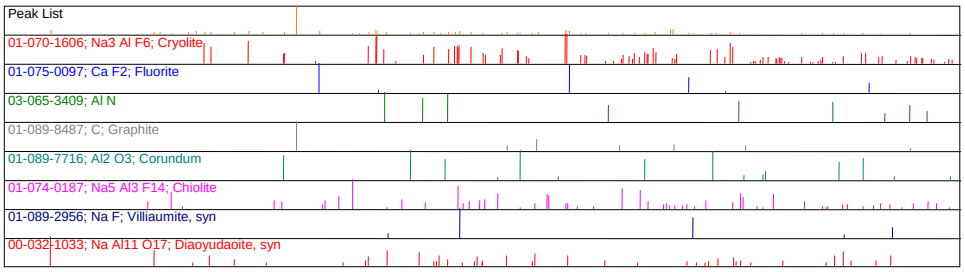

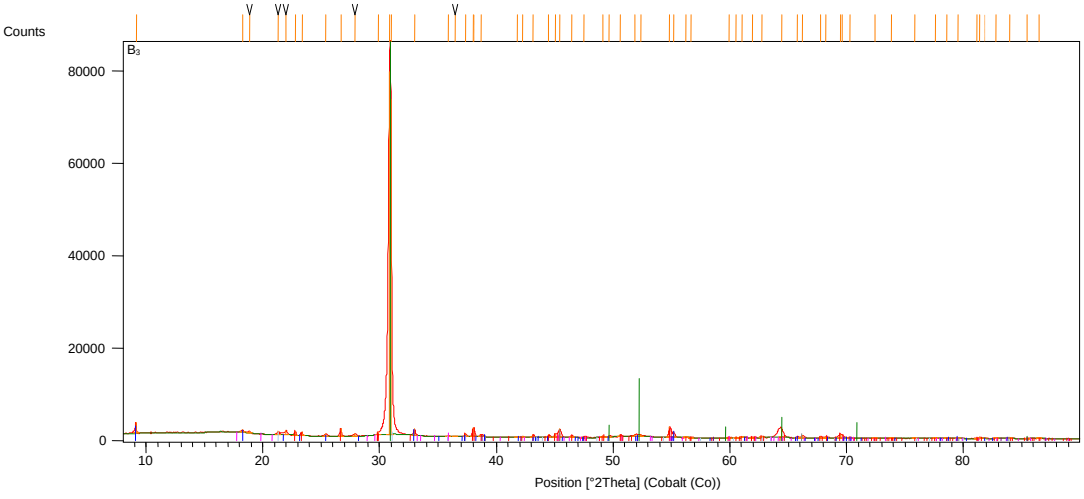

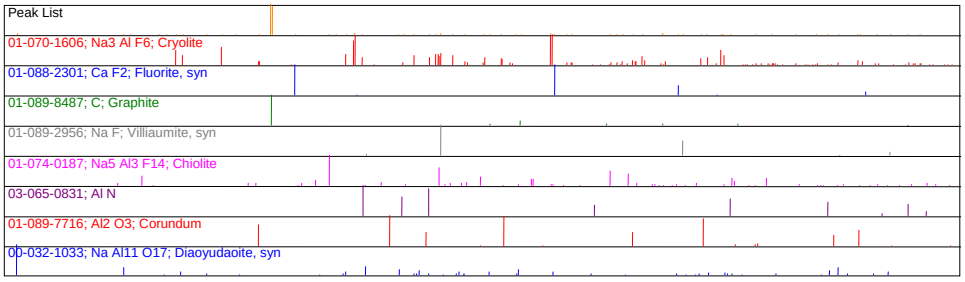

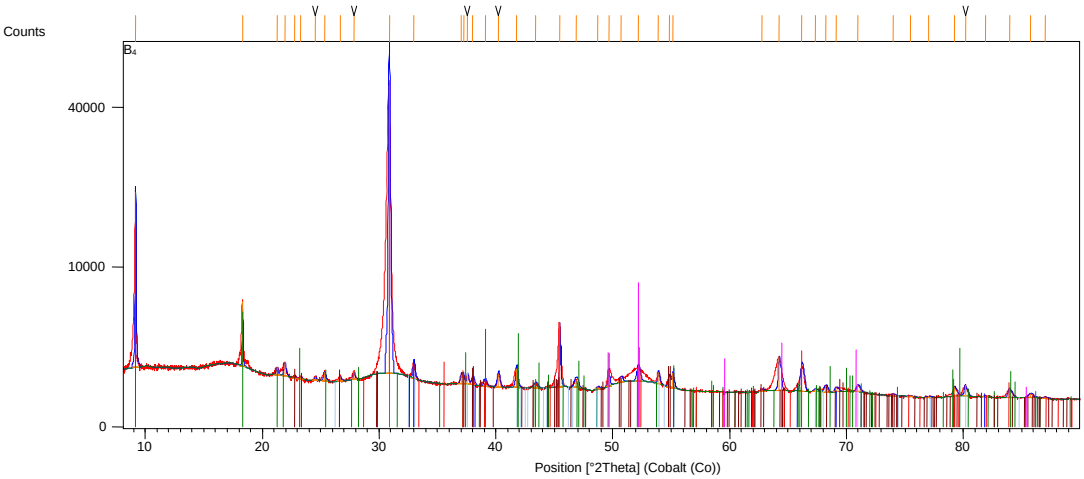
Counts
B4
40000
10000
0
10
20
30
40
50
60
70
80
Position [°2Theta] (Cobalt (Co))

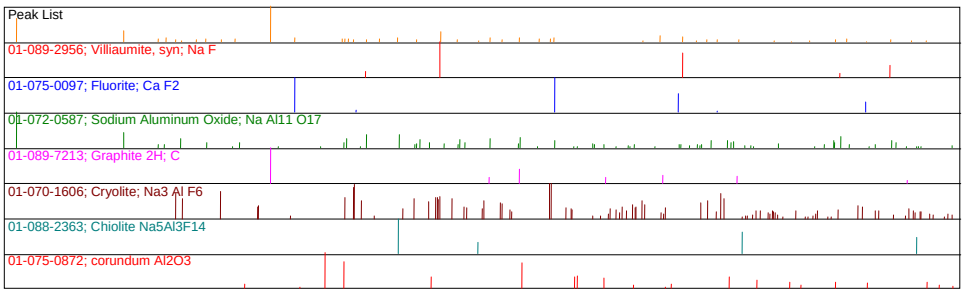
Peak List
01-089-2956; Villiaumite, syn; Na F
01-075-0097; Fluorite; Ca F2
01-072-0587; Sodium Aluminum Oxide; Na Al11 O17
01-089-7213; Graphite 2H; C
01-070-1606; Cryolite; Na3 Al F6
01-088-2363; Chiolite Na5Al3F14
01-075-0872; corundum Al2O3

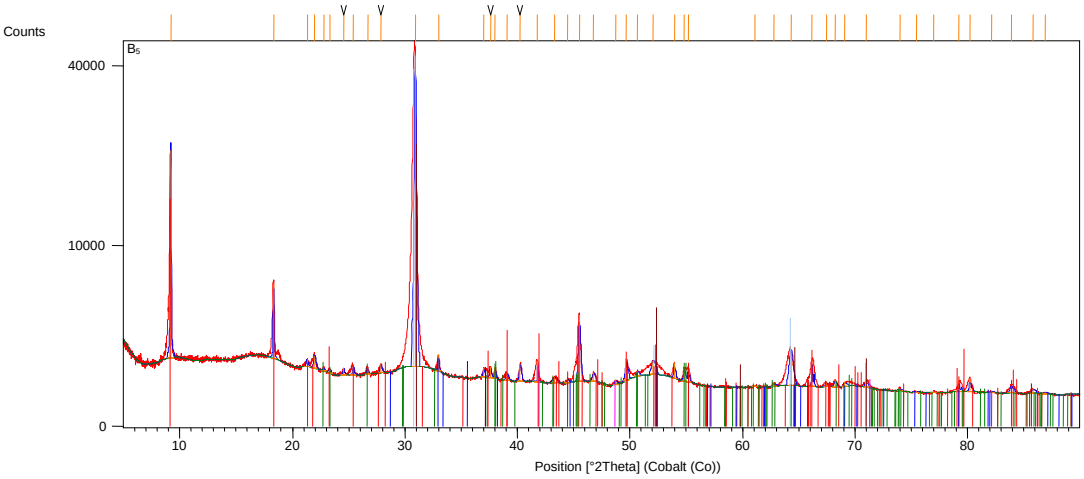
Counts
B5
40000
10000
0
10
20
30
40
50
60
70
80
Position [°2Theta] (Cobalt (Co))

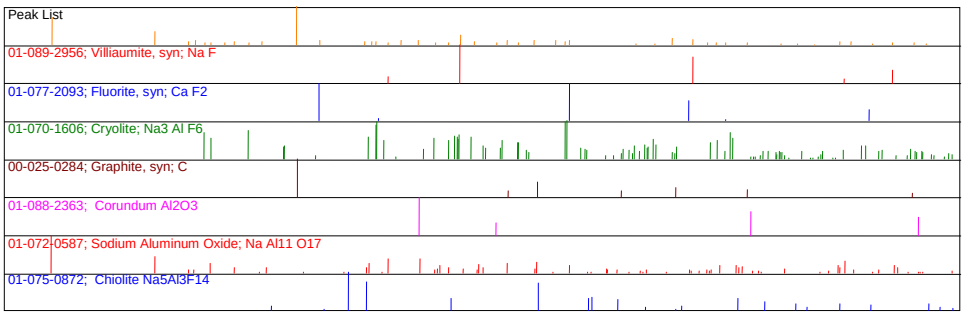
Peak List
01-089-2956; Villiaumite, syn; Na F
01-077-2093; Fluorite, syn; Ca F2
01-070-1606; Cryolite; Na3 Al F6
00-025-0284; Graphite, syn; C
01-088-2363; Corundum Al2O3
01-072-0587; Sodium Aluminum Oxide; Na Al11 O17
01-075-0872; Chiolite Na5Al3F14

Appendix D: Diffractograms of the laboratory electrolysed samples

Since the phases are common in all the diffractograms of the same carbon grade at given electrolysis period only one diffractogram is given for each electrolysis period on each carbon grade.

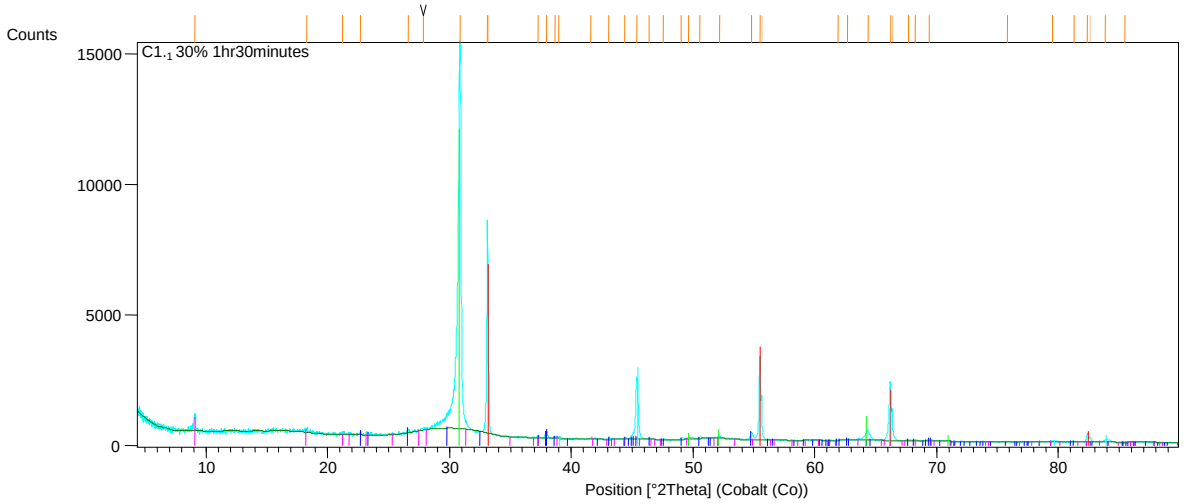

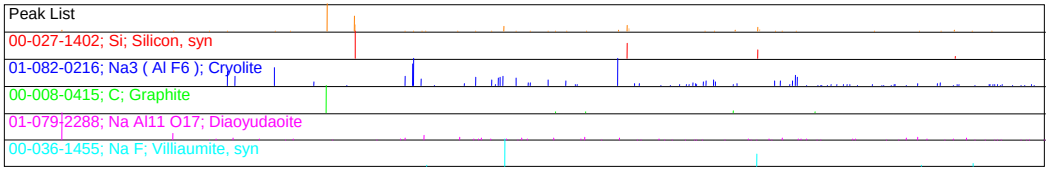

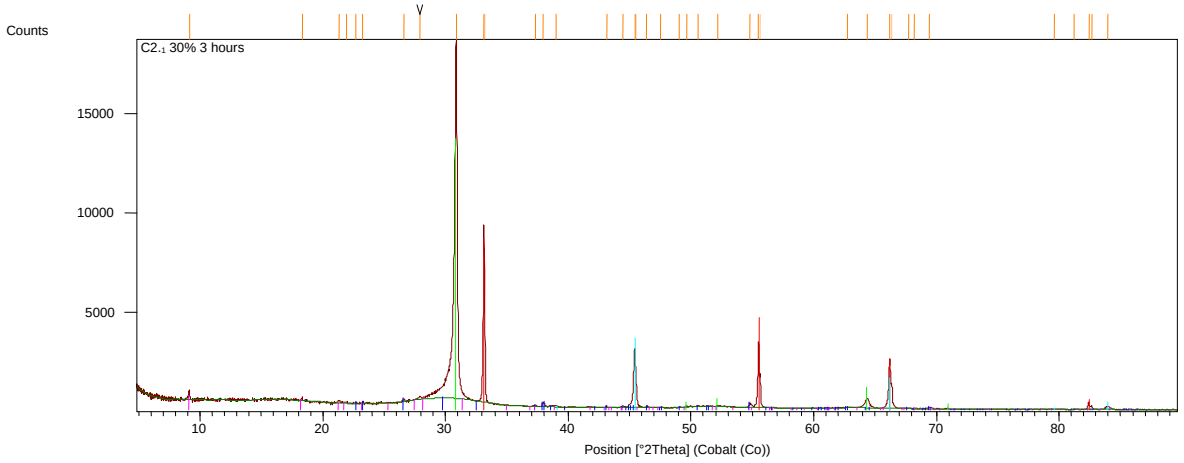

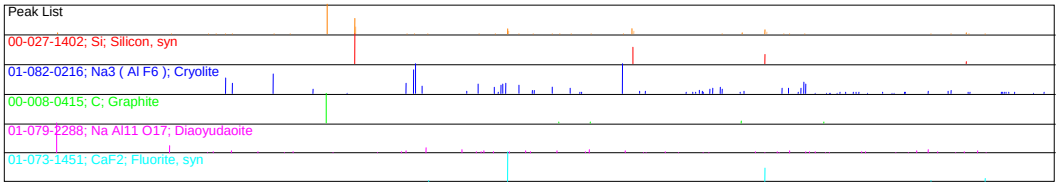

REACTIVITY OF CARBON CATHODE MATERIALS WITH ELECTROLYTE BASED ON PLANT AND LABORATOTY DATA